J. Fluid Mech., page 1 of 53
doi:10.1017/S0022112010002533

Planar inviscid flows in a channel of finite length: washout, trapping and self-oscillations of vorticity

V. N. GOVORUKHIN[1], A. B. MORGULIS[1,2] AND V. A. VLADIMIROV[3]†

[1]Department of Mathematics and Mechanics, Southern Federal University, Melchakova Street 8a, 344090 Rostov-on-Don, Russia

[2]Southern Institute of Mathematics, Russian Academy of Sciences, Marcus Street 22, 362027 Vladikavkaz, Russia

[3]Department of Mathematics, University of York, Heslington, York YO10 5DD, UK

(Received 17 October 2006; revised 25 April 2010; accepted 26 April 2010)

The paper addresses the nonlinear dynamics of planar inviscid incompressible flows in the straight channel of a finite length. Our attention is focused on the effects of boundary conditions on vorticity dynamics. The renowned Yudovich's boundary conditions (YBC) are the normal component of velocity given at all boundaries, while vorticity is prescribed at an inlet only. The YBC are fully justified mathematically: the well posedness of the problem is proven. In this paper we study general nonlinear properties of channel flows with YBC. There are 10 main results in this paper: (i) the trapping phenomenon of a point vortex has been discovered, explained and generalized to continuously distributed vorticity such as vortex patches and harmonic perturbations; (ii) the conditions sufficient for decreasing Arnold's and enstrophy functionals have been found, these conditions lead us to the washout property of channel flows; (iii) we have shown that only YBC provide the decrease of Arnold's functional; (iv) three criteria of nonlinear stability of steady channel flows have been formulated and proven; (v) the counterbalance between the washout and trapping has been recognized as the main factor in the dynamics of vorticity; (vi) a physical analogy between the properties of inviscid channel flows with YBC, viscous flows and dissipative dynamical systems has been proposed; (vii) this analogy allows us to formulate two major conjectures (C1 and C2) which are related to the relaxation of arbitrary initial data to C1: steady flows, and C2: steady, self-oscillating or chaotic flows; (viii) a sufficient condition for the complete washout of fluid particles has been established; (ix) the nonlinear asymptotic stability of selected steady flows is proven and the related thresholds have been evaluated; (x) computational solutions that clarify C1 and C2 and discover three qualitatively different scenarios of flow relaxation have been obtained.

Key words: application, general fluid mechanics, vortex dynamics

1. Introduction

The inviscid flows through a given two- or three-dimensional domain $\mathscr{D}$ with the boundary $\partial\mathscr{D}$ consisting of the inlet $\partial\mathscr{D}^{in}$, the outlet $\partial\mathscr{D}^{out}$ and the solid walls

† Email address for correspondence: vv500@york.ac.uk
(This paper is dedicated to the memory of Victor Yudovich)

$\partial\mathscr{D}^{solid}$ arise in many applications. Relevant examples include the weather forecast in dynamical meteorology (Haltiner & Williams 1980), the circulation of blood in large vessels (Pedley 1980), any computational models of flows that use the artificially introduced boundaries of computational domains and the vortex breakdown in swirling flows (Benjamin 1967; Batchelor 1987; Brown & Lopez 1990; Lopez 1990; Lopez & Perry 1992; Saffman 1992; Wang & Rusak 1997; Rusak, Wang & Whiting 1998; Gallaire & Chomaz 2004; Martemianov & Okulov 2004). The studies of all these problems require to set up some boundary conditions (BC) on all parts of $\partial\mathscr{D}$. There are different types of BC used in the literature. Different BC related to our research can be found in Batchelor (1987), Pedley (1980), Antontsev, Kazhikhov & Monakhov (1990), Chwang (1983), Wang & Rusak (1997), Morgulis & Yudovich (2002), Beavers & Joseph (1967), Goldshtik & Javorsky (1989), Cox (1991), Berdichevskiy (1983) and Wei (2004). It is not simple to choose the appropriate BC on $\partial\mathscr{D}^{in}$ and $\partial\mathscr{D}^{out}$ for each particular problem. The difficulties are often caused by the absence of answers to key questions: (Q1) Which physical fields can be prescribed at $\partial\mathscr{D}^{in}$ and $\partial\mathscr{D}^{out}$ (one may consider velocity, vorticity, pressure, their various derivatives, combinations, integrals, etc.)? (Q2) Is the choice of BC unique for the selected class of flows? If not, then what advantage one can obtain from the description of the same flows with two or more different sets of BC? (Q3) How to select BC that are well posed mathematically and, in particular, how to avoid underdetermined or overdetermined problems? (Q4) If the particular type of BC is selected, then what are the qualitative properties of the corresponding flows? (Q5) How sensitive is a channel flow to the change of boundary data on different parts of $\partial\mathscr{D}$? All these questions are difficult to answer due to the multiplicity of available BC and the lack of available qualitative results for each type of BC.

A significant progress has been achieved in the studies related to Q3: it is known that some BC deliver the mathematically correct setting of a problem. A short survey of such BC is given by Morgulis & Yudovich (2002). The most celebrated are Yudovich's boundary conditions (YBC) for planar flows: the normal velocity v_n is prescribed everywhere at $\partial\mathscr{D}$ and the vorticity ω is given at $\partial\mathscr{D}^{in}$. Yudovich (1963) proved that YBC led to the mathematically well-posed problem for Euler's equations; moreover, every solution of this problem was well defined in an arbitrarily long time interval. Later on, Alekseev (1972) considered planar steady flows with YBC for a curvilinear channel and proved that every set of steady boundary data produced at least one steady solution. Finally, Kazhikhov (1981) extended YBC to three-dimensional flows: he proved that in addition to v_n on $\partial\mathscr{D}$ one could prescribe only a tangential vorticity component on $\partial\mathscr{D}^{in}$. The natural way to complement this outstanding mathematical progress in Q3 is to concentrate efforts on Q4 and Q5, i.e. on the fluid dynamics of flows with YBC. It is also clear that the study of YBC represents a necessary precursor to a rigorous treatment of other BC.

This paper is devoted to the studies of planar inviscid flows with YBC in the straight channel of a finite length. All presented results are strictly nonlinear. The attention is concentrated on two key features of related vortex dynamics: the washout of vorticity and the trapping of vorticity. We demonstrate how the counterbalance between these two factors leads to different flow structures. The paper can be divided into two parts: analytical (§§ 2–8) and computational (§§ 9–11). The analytical part is entirely devoted to understanding of the mechanisms of vorticity trapping and washout, to studying the most important flow properties, and to introducing two central physical conjectures C1 and C2. All our analytical results represent mathematical theorems proven for the exact Euler's equations with YBC. However, our intention is to build a

much-needed bridge between the mathematical and physical efforts in this fascinating research area where major previous publications are mathematical. Therefore, all our theorems are deliberately presented very briefly, in the physical style of exposition and rigour, with the use of standard calculus only, and with comments on their physical meaning. The computational part is aimed to illustrate the conjectures C1 and C2, and to clarify the conditions when three different flow scenarios take place, hence this part is composed as a number of specially selected examples. Their presentation is also extremely brief: we outline the computational methods used, present only few key figures and graphs, and give comments on the results directly linked to C1 and C2. Any systematic computational studies of planar inviscid channel flows lay far outside of the scope of this paper.

Since our presentation is very brief and compressed, we have provided more details in §§ 2–12.

In § 2 we set up the mathematical problem of planar inviscid flows through a straight channel of a finite length, so that the flow domain $\mathscr{D}$ is a rectangle. Here we present the governing equations, the formulation of YBC, the exact solutions, the additional restrictions, the terminology used, and the dimensionless formulation of the problem.

In § 3 we consider a point vortex as a perturbation of a channel flow with YBC. Here we discover a novel phenomenon of vortex dynamics: the trapping of a point vortex. We prove that a point vortex of any circulation Γ initially placed in any point inside $\mathscr{D}$ cannot escape from $\mathscr{D}$. The proof is based on the fact that the equations of motion for a single vortex represent a one-dimensional Hamiltonian system whose trajectories represent the level curves of the Hamiltonian function. We show that none of these trajectories crosses the inlet or outlet. Our proof exploits the explicit form of Green's function in a rectangular box (Villat 1930).

Section 4 is devoted to the washout of smooth perturbations. Our consideration is based on the calculation of the time evolutions of Arnold's functional $\mathscr{W}_\alpha$ (Arnold 1966) and the enstrophy functional $\mathscr{I}$. The related divergent forms and fluxes lead us to the discovery that $\mathscr{W}_\alpha$ or $\mathscr{I}$ always decrease (or at least non-increase) by virtue of YBC. It creates a basis for introducing the key notion of the washout for both $\mathscr{W}_\alpha$ and $\mathscr{I}$. After that we prove nonlinear stability for three classes of steady channel flows with either monotonic changes of vorticity across streamlines or with constant vorticity. The flow stability is defined as $\mathscr{I}(t) \leqslant C\mathscr{I}(0)$ with a constant C. The plane-parallel shear flows with the uniform, linear, and parabolic profiles give us the important examples of stable flows. Another important result of this section is that YBC represent the only physically reasonable BC which provide the decrease of Arnold's functional.

Section 5 is both physical and heuristic. Here we formulate our qualitative understanding that vortex dynamics in a channel with YBC is determined by two factors: the washout of vorticity and the trapping of vorticity. Using this qualitative idea we propose to consider a physical analogy between inviscid channel flows, viscous flows, and finite-dimensional non-conservative dynamical systems. We also introduce the notion of dissipative YBC, which admits a decreasing Lyapunov functional. That allow us to formulate two major conjectures (C1 and C2). Conjecture C1 proposes that any flow with dissipative YBC must eventually (for $t \to \infty$) relax to a steady state, which depends on the chosen boundary data, channel geometry, and on the initial shape of a perturbation. It comprises the existence of a non-trivial attractor in the phase space of Euler's equation with YBC. C2 assumes that any YBC that does not admit a decreasing Lyapunov functional eventually produces a steady, self-oscillating,

or chaotic flow. The appearance of self-oscillations is well established for viscous flows but it is novel and highly unusual for inviscid flows.

In § 6 we analytically study the washout phenomenon by obtaining a sufficient condition for the complete washout of fluid particles (CWOF) that is defined as the property of a flow when all material (fluid) particles, which are initially in $\mathscr{D}$, go out of $\mathscr{D}$ in finite time. In other words, CWOF means that no material particle can stay in $\mathscr{D}$ forever and the formation of recirculation zones is impossible. The main result of § 6 is the proof of conditions sufficient for the CWOF. These conditions are written explicitly and can be easily checked for particular flows. It is remarkable that these conditions impose restrictions on both initial enstrophy and the initial amplitude of perturbations.

In § 7 the consideration of the previous section is extended to the complete washout of perturbations (CWOP). The CWOP imply that the full decay of perturbations is the same as the asymptotic stability. A specific feature of CWOP is: the lifespan of perturbations can be finite, that is known as the nilpotent stability (see Morgulis & Yudovich 2002). For the sake of simplicity, we consider CWOP only for a plane-parallel basic flow with a quadratic (Poiseuille-type) velocity profile. The main result here is the proof of sufficient conditions which guarantee at least the exponential decay of perturbations. Once again (like for CWOF) these conditions have an explicit form and impose restrictions on both initial enstrophy and the initial amplitude of perturbations.

In § 8 we consider the simpler cases of linear and uniform velocity profiles of basic flow. Here vorticity perturbations play a part of a passive admixture, therefore both CWOF and CWOP take place simultaneously in finite time, so we always get the nilpotent stability. Using the results of § 6, we obtain the explicit domain of parameters (on the plane of enstrophy versus vorticity amplitude), where both CWOF and CWOP are always valid.

In § 9 we build up several computational examples. First, we briefly describe the employed computational method of particles (or the vortex method). Then we compute the time-evolution of flows with three different sets of initial data. In the first set, the basic flow is quadratic with the strongly localized initial perturbation of vorticity. In the second set, the basic flow is homogeneous where a perturbation represents a circular vortex patch of the amplitude A and the initial position of its centre (x_c, y_c). In the third set, we take three types of a basic flow (quadratic, linear and uniform), while the initial vorticity perturbations represent the Fourier-harmonics of the spatial coordinates with the amplitude A and two scalar wavenumbers. In all three sets, for small A we obtain CWOP in finite time, which supports C1. With the increase of A the phenomenon of vorticity trapping (a partial rejection of vorticity back to $\mathscr{D}$) starts to appear; with the further increase of A the counterbalance between the washout and trapping creates a variety of flow regimes where the amount of trapped vorticity also increases. The most striking result of this section is the observed relaxation of trapped vorticity into almost steady recirculation zones. For the first set, a fast relaxation of all parameters to an almost steady flow takes place (including the formation of a steady flow inside a recirculation zone). We call this flow 'almost steady' since it contains small-scale 'computational turbulence'. For the second set, the relaxation is slow. For the third set, the washout is significant and we observe a fast relaxation in terms of integral parameters (such as the position, geometrical shape, amount of vorticity and enstrophy) while the formation of steady flows in the cores of recirculation zones is much slower. All these results show that the relaxation C1 is different for different flows. However, the presence of such relaxation supports

C1 and can be seen as an evidence towards the existence of an attractor for Euler's equations with YBC.

Section 10 is devoted to computing steady separated flows that are obtained with a very good precision and in a reasonable time. Our computations of § 9 show that 'randomly' chosen initial data relax to steady states only partially, at least for the time of reliable computations. Therefore, in § 10 we additionally apply a filtration procedure at few selected instants (at $t = t_1, t_2$, etc.), while the flow between these instants is computed as in § 9 without use of any filtration. These computations produce steady and apparently stable flows with one, two, three, and four recirculation zones. These examples demonstrate an essential non-uniqueness of solutions, indicate that the computed steady flows belong to some multi-parametric families of solutions, and provide a partial support for C1.

In § 11, we employ the method of § 9 to build an example that supports C2. We use an iteration procedure that allows us to obtain a one-parametric family of flows with the internal shear layer of the 'amplitude' A. This procedure does produce steady flows for $A < A^*$, while for $A > A^*$ we obtain flows with self-oscillations in time and space. With the further increase of A–A^* these self-oscillations change their character from periodic to quasi-periodic and then to chaotic.

Finally, in § 12 we give several comments and mention possible further developments.

2. Equations of planar flows through a finite channel

The governing equations for the planar flows of a homogeneous inviscid incompressible fluid in the $(\boldsymbol{v}, p)$ or (ω, ψ) formulations are

$$\boldsymbol{v}_t + (\boldsymbol{v}\cdot\nabla)\boldsymbol{v} = -\nabla p, \quad \operatorname{div}\boldsymbol{v} = 0 \qquad \text{or} \quad \omega_t + \psi_y\omega_x - \psi_x\omega_y = 0, \tag{2.1}$$

where $\boldsymbol{x} = (x, y)$ and t are Cartesian coordinates and time; $p(\boldsymbol{x}, t)$ and $\boldsymbol{v}(\boldsymbol{x}, t)$ are fields of pressure and velocity; $\boldsymbol{v} = (u, v) = (\psi_y, -\psi_x)$; $\psi(\boldsymbol{x}, t)$ is a streamfunction; the subscripts of independent variables stand for partial derivatives; $\nabla = (\partial/\partial x, \partial/\partial y)$. The vorticity is $\omega \equiv v_x - u_y = -\Delta\psi$ with $\Delta = \partial^2/\partial x^2 + \partial^2/\partial y^2$. The flow domain is a rectangular channel:

$$\mathscr{D} = \{(x, y) : 0 < x < L,\ 0 < y < H\}, \tag{2.2}$$

where L, H are the length and the height of a channel. The additional notations are: $\partial\mathscr{D}$ is the boundary of $\mathscr{D}$; $v_n(\boldsymbol{x}, t) \equiv \boldsymbol{v}\cdot\boldsymbol{n}$ and $\boldsymbol{n}(\boldsymbol{x}, t)$ are the normal velocity and the outer unit normal vector to $\partial\mathscr{D}$. The bottom and top sides of a rectangle are rigid, while the left- and right-hand sides represent the inlet and outlet of a flow:

$$\left.\begin{aligned} v_n = 0 \quad &\text{on} \quad \partial\mathscr{D}^{\pm} = \{(x, y) : 0 < x < L,\ y = H \text{ and } y = 0\}, \\ v_n < 0 \quad &\text{on} \quad \partial\mathscr{D}^{in} = \{(x, y) : x = 0, 0 < y < H\}, \\ v_n > 0 \quad &\text{on} \quad \partial\mathscr{D}^{out} = \{(x, y) : x = L,\ 0 < y < H\}, \end{aligned}\right\} \tag{2.3}$$

where we denote the top solid wall ($y = H$) as $\partial\mathscr{D}^+$ and the bottom one ($y = 0$) as $\partial\mathscr{D}^-$.

Yudovich's boundary conditions prescribe the normal velocity v_n on all parts of $\partial\mathscr{D}$ and, additionally, vorticity ω on $\partial\mathscr{D}^{in}$. It is convenient to formulate YBC in the (ψ, ω) notations with the use of three functions $\psi^{in}(y)$, $\psi^{out}(y)$ and $\omega^{in}(y)$:

$$\psi|_{y=0} = 0,\ \psi|_{y=H} = Q,\ \psi|_{x=0} = \psi^{in}(y),\ \psi|_{x=L} = \psi^{out}(y), \tag{2.4}$$

$$\omega|_{x=0} = \omega^{in}(y), \tag{2.5}$$

where compatibility conditions are $\psi^{in}(0)=\psi^{out}(0)=0$, $\psi^{in}(H)=\psi^{out}(H)=Q$ and $Q>0$ is the total flux of a fluid. Since the locations of $\partial\mathscr{D}^{in}$ and $\partial\mathscr{D}^{out}$ have already been fixed by (2.3), we consider only monotonically increasing functions $\psi^{in}(y)$ and $\psi^{out}(y)$ at $\partial\mathscr{D}^{in}$ and $\partial\mathscr{D}^{out}$:

$$\psi^{in}_y(y)\equiv u^{in}(y)\geqslant U^-,\qquad \psi^{out}_y(y)\equiv u^{out}(y)\geqslant U^-,\qquad U^-=\text{const}>0. \tag{2.6}$$

The agreement between (2.3) and (2.4) is provided by a condition weaker than (2.6), $\psi^{in}_y(y)>0$, $\psi^{out}_y(y)>0$ for $0<y<1$, which includes zero velocities at the vertices of $\mathscr{D}$. For steady non-separated flows it contains the cases of zero boundary velocity at $\partial\mathscr{D}^{\pm}$. Such flows represent a very special case among all inviscid flows, it must be studied separately from the generic flows (2.6) (see § 12). From another side (making a connection to the no-slip condition for a viscous fluid), it is well known that the inviscid limits of viscous flows often violate no-slip conditions at solid boundaries.

We consider only the flows in (2.2) that satisfy YBC with the fixed location of $\partial\mathscr{D}^{in}$ and $\partial\mathscr{D}^{out}$ (see (2.4)–(2.6)). Throughout the paper the width of the channel H and the flux Q are used as the scaling parameters and all independent variables and unknown functions are presented in dimensionless forms. For brevity, we use the same notations for dimensionless variables and functions and for their dimensional counterparts. In particular, we take $H=Q=1$ in (2.1)–(2.6) and everywhere below.

Any steady solution to (2.1)–(2.6) is denoted by capital letters:

$$\boldsymbol{v}=\boldsymbol{V}(\boldsymbol{x})=(U(\boldsymbol{x}),\quad V(\boldsymbol{x})),\quad p=P(\boldsymbol{x}),\quad \psi=\Psi(\boldsymbol{x}),\quad \omega=\Omega(\boldsymbol{x}). \tag{2.7}$$

A fluid flow in $\mathscr{D}$ is called non-separated if every material (fluid) particle leaves $\mathscr{D}$ in finite time. On the contrary, a separated flow contains a material particle that stays in $\mathscr{D}$ forever. Any steady flow (either separated or not) includes a through-flow zone $\mathscr{D}^{tf}\subset\mathscr{D}$ that represents a connected domain and consists of particles that pass through $\mathscr{D}$ in finite time. It is apparent that

$$\Omega=\Omega(\Psi),\quad \Omega(\Psi)\equiv\omega^{in}(y(\Psi))\quad \text{in } \mathscr{D}^{tf}, \tag{2.8}$$

with a single-valued function $\Omega(\Psi)$. Here $y(\Psi)$ is inverse for $\psi^{in}(y)$ which is monotonic by (2.6). If a flow is non-separated, then $\mathscr{D}^{tf}=\mathscr{D}$ and

$$-\Delta\Psi=\Omega(\Psi)\quad \text{in } \mathscr{D}. \tag{2.9}$$

Equation (2.9) and BC (2.4) form the nonlinear Dirichlet's problem in which Ψ is prescribed on the entire $\partial\mathscr{D}$. For the general boundary data (2.4) and (2.5), the existence of the steady solution (2.7) to (2.1)–(2.6) has been proven by Alekseev (1972); his proof does not use the reduction of the problem to (2.9). Several non-separated steady solutions have been found computationally by Moshkin & Mounnamprang (2003). However, the separation is unavoidable for some boundary data. Indeed, the problem (2.9), (2.4) may have no solutions for the given $\mathscr{D}$ and $\Omega(\Psi)$. For example, let $\psi^{in}(y)=\psi^{out}(y)=y$ and $\omega^{in}(y)=\kappa y^2$ where $\kappa>0$ is a constant. One can see that $\Omega(\Psi)=\kappa\Psi^2$, so a plane-parallel shear flow solution does not exist for these boundary data. Moreover, the absence of any solution to (2.9), (2.4) can be proven for sufficiently large $\kappa>0$ (see Gilbarg & Trudinger 1983, § 14.4). At the same time, a steady flow does exist by Alexeev's theorem! Hence, it must be a separated flow. However, the same BC produce a non-separated flow if κ is sufficiently small (Morgulis & Yudovich 2002). Thus, a recirculation (or stagnation) zone in a steady flow can suddenly appear due to the gradual changes of the parameter κ.

A different and instructive example of a separated flow is given by Goldstik (1963) and Goldshtik & Hussain (1998) where its existence is demonstrated for the

steady flows with constant vorticity, provided that vorticity is large enough. It is worth to notice that the analytical extension of $\Omega(\Psi)$ from $\mathscr{D}^{tf}$ to $\mathscr{D}$ is impossible for $\Omega(\Psi)=\kappa\Psi^2$ (and most likely for the flows considered in §§9 and 10 of this paper) while such extension is apparent in this example. One more example of recirculation zones in a shear flow is known as Stuart–Kelvin cat's eyes (Stuart 1971). The mechanism of their formation is purely kinematical and qualitatively different from our case.

In a special case of YBC (2.4), (2.5) with

$$\psi^{in}(y)=\psi^{out}(y) \quad \text{and} \quad \omega^{in}(y)=-\psi^{in}_{yy}(y), \tag{2.10}$$

there exists a shear flow solution:

$$\Psi=\psi^{in}(y), \ (U,V)=(U(y),0)=\big(\psi^{in}_{y}(y),0\big), \ \Omega(y)=-\Psi_{yy}(y)=\omega^{in}(y). \tag{2.11}$$

Three standard shear velocity profiles are Poiseuille $U_p(y)$, Couette $U_c(y)$ and uniform $U_u(y)$ ones; all with unit fluxes and non-negative velocities:

$$U_p=6(y-y^2), \Psi_p=3y^2-2y^3; \quad U_c=2y, \Psi_c=y^2; \quad U_u=1, \Psi_u=y, \tag{2.12}$$

where $U_p(y)\geqslant 0$, $U_c(y)\geqslant 0$, $U_p(0)=U_c(0)=0$ and $\Psi_p(1)=\Psi_c(1)=\Psi_u(1)=1$. The combined shear flow with a unit flux is

$$U(y)=Q_pU_p+Q_cU_c+Q_uU_u, \quad Q_p+Q_c+Q_u=1 \quad \boldsymbol{Q}\equiv(Q_p,Q_c,Q_u), \tag{2.13}$$

where Q_p, Q_c, Q_u are constant partial fluxes that can be positive, zero or negative. We use the terms: quadratic basic flow (QBF) for (2.13) with $Q_p\neq 0$, linear basic flow (LBF) for $Q_p=0$, $Q_c\neq 0$ and uniform basic flow (UBF) for $Q_p=0$, $Q_c=0$ and $Q_u=1$. By virtue of (2.6) every flow (2.13) (as well as any shear flow) obeys the restriction

$$\min_y U(y)=U^->0. \tag{2.14}$$

Since $U(0)=Q_u$, every flow (2.13) includes a non-zero uniform component $Q_u>0$. If both $Q_p\geqslant 0$ and $Q_c\geqslant 0$ then $Q_u=U^-$.

The equations for the finite perturbations of a steady flow are

$$\widetilde{\boldsymbol{v}}_t+(\boldsymbol{v}\cdot\nabla)\widetilde{\boldsymbol{v}}+(\widetilde{\boldsymbol{v}}\cdot\nabla)\boldsymbol{V}=-\nabla\widetilde{p}, \quad \operatorname{div}\widetilde{\boldsymbol{v}}=0 \quad \text{in} \quad \mathscr{D}, \tag{2.15}$$

where $\widetilde{\boldsymbol{v}}(\boldsymbol{x},t)\equiv\boldsymbol{v}(\boldsymbol{x},t)-\boldsymbol{V}(\boldsymbol{x})$, $\widetilde{p}\,(\boldsymbol{x},t)\equiv p\,(\boldsymbol{x},t)-P(\boldsymbol{x})$. They can also be written in the (ω,ψ) form

$$\widetilde{\omega}_t+\psi_y\widetilde{\omega}_x-\psi_x\widetilde{\omega}_y=\widetilde{\psi}_x\Omega_y-\widetilde{\psi}_y\Omega_x, \quad -\Delta\widetilde{\psi}=\widetilde{\omega} \quad \text{in} \quad \mathscr{D}, \tag{2.16}$$

where $\widetilde{\omega}(\boldsymbol{x},t)\equiv\omega(\boldsymbol{x},t)-\Omega(\boldsymbol{x})$, $\widetilde{\psi}(\boldsymbol{x},t)\equiv\psi(\boldsymbol{x},t)-\Psi(\boldsymbol{x})$. Since a perturbed flow obeys the same YBC (2.4) and (2.5) as the main one then

$$\widetilde{v}_n\equiv\widetilde{\boldsymbol{v}}\cdot\boldsymbol{n}=0, \ \widetilde{\psi}=0 \quad \text{on} \quad \partial\mathscr{D}; \quad \widetilde{\omega}=0 \quad \text{on} \quad \partial\mathscr{D}^{in}. \tag{2.17}$$

It is important that all flow perturbations in this paper satisfy (2.17).

We also introduce the enstrophy of perturbations $\mathscr{I}$ as the square of L_2 norm for vorticity perturbations:

$$\mathscr{I}[\widetilde{\omega}]\equiv\int_{\mathscr{D}}\widetilde{\omega}^2(\boldsymbol{x},t)\,\mathrm{d}\boldsymbol{x}\equiv\|\widetilde{\omega}\|_2^2=\mathscr{I}(t), \qquad \mathrm{d}\boldsymbol{x}\equiv\mathrm{d}x\,\mathrm{d}y. \tag{2.18}$$

3. The trapping of a point vortex

In this section we study a singular perturbation of a channel flow that allows us to identify an important feature of related vortex dynamics. Let us consider a steady flow (2.7):

$$\Psi(\boldsymbol{x}),\ \ \Omega(\boldsymbol{x}) = \omega^{in}(y) = \Omega_0 = \text{const} \tag{3.1}$$

with $\psi^{in}(y)$ and $\psi^{out}(y)$ (2.4) prescribed arbitrarily. The existence of such a steady flow is apparent; one can find it by solving Dirichlet's problem for $-\Delta\Psi = \Omega_0$ with the prescribed BC for Ψ; a simple relevant example is LBF (2.13). The initial perturbation of (3.1) is taken in the form of a point vortex.

Proposition 1. *The point vortex of any intensity Γ initially placed at any point $\boldsymbol{x}_0(0) \in \mathscr{D}$ of the flow (3.1) will never leave $\mathscr{D}$. There is at least one point of equilibrium (state of rest) of the vortex.*

The proof of this proposition is given in Appendix A.

The qualitative explanation of the trapping phenomenon of a point vortex is the following. There are two main factors which dominate the motion of a vortex in the vicinity $\partial\mathscr{D}$. In order to describe them, we introduce the distances ρ^{in}, ρ^{out} and $\rho^{\pm}$ between a vortex and the corresponding parts of $\partial\mathscr{D}$. Then, (i) when a vortex approaches any side $\partial\mathscr{D}$ (being far away from vertices, say, $\rho^{out} \ll \rho^{\pm} \sim 1$), its motion is determined mainly by the nearest image across this side; and (ii) when a vortex moves in the vicinity of any vertex (say, $\rho^{out} \sim \rho^{+} \ll 1$) its motion is determined by two nearest images across intersecting sides. Let us first consider a vortex approaching $\partial\mathscr{D}^{out}$ being far away from $\partial\mathscr{D}^{\pm}$ ($\rho^{out} \ll \rho^{\pm} \sim 1$). Then, due to the interaction with the nearest mirror image across $\partial\mathscr{D}^{out}$, the vortex moves tangentially to $\partial\mathscr{D}^{out}$ with such a high speed that it always deviates to a side solid wall (which is $\partial\mathscr{D}^{+}$ for $\Gamma > 0$) where the interaction with the mirror image across this wall moves it back to $\partial\mathscr{D}^{in}$. As a result, the interactions with all walls always produce the periodic motions of the vortex We call this process the vortex–outlet–wall interaction. For the future use we introduce the notions of the trapping-oriented and washing-oriented pairs; each pair consists of a sign of the vortex and a solid wall:

$$\left.\begin{array}{l}(\Gamma > 0, \partial\mathscr{D}^{+}) \text{ and } (\Gamma < 0, \partial\mathscr{D}^{-}) - \text{trapping-oriented pairs,}\\ (\Gamma > 0, \partial\mathscr{D}^{-}) \text{ and } (\Gamma < 0, \partial\mathscr{D}^{+}) - \text{washing-oriented pairs.}\end{array}\right\} \tag{3.2}$$

This terminology reflects the direction of motion of the vortex due to its interaction with the nearest solid wall: the trapping (washing) means the motion towards $\partial\mathscr{D}^{in}$ ($\partial\mathscr{D}^{out}$). One can see that the vortex–outlet–wall interaction always produces the motion of the vortex of any sign towards the trapping-oriented wall that makes the trapping inevitable.

Our comments on these results are:

(i) A single vortex placed in a channel flow represents the Hamiltonian system despite the open boundaries. The related Hamiltonian is given in Appendix A. Note that (A 4) is the Hamiltonian system with one degree of freedom that is always integrable; hence both the quasi-periodic and chaotic motions of the vortex are impossible. The selected trajectories of a point vortex (i.e. the level contours for its Hamiltonian) are given in figure 1. The equilibrium position is shown by a circle sign. The particular trajectory that is shown in bold and the chosen value of $\Gamma = 3.134$ will be used in § 9.

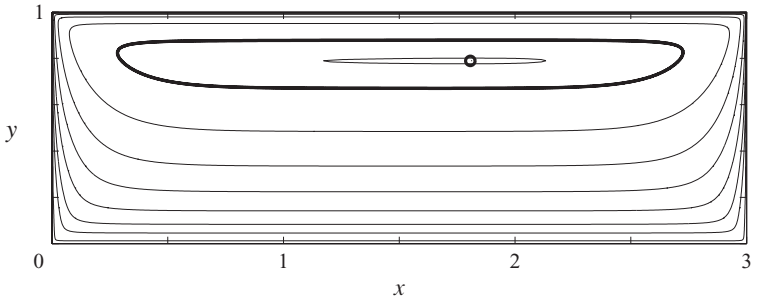

FIGURE 1. The set of trajectories of a point vortex in the uniform flow: $U(y) \equiv 1$, $\Gamma = 3.134$.

(ii) The simple and instructive example of the trapping of a point vortex can be seen for the infinite domain $\mathscr{D}$ in the form of a right angle: $\mathscr{D} = \{(x, y) : -\infty < x < 0,\ 0 < y < \infty\}$. It represents a 'semi-infinite channel' with $\partial\mathscr{D}^{out}$ ($x = 0$, $0 < y < \infty$) and a bottom solid wall ($y = 0$, $-\infty < x < 0$). The YBC remain the same (2.17), while some part of them is given at 'infinitely remote boundaries'. There are only three mirror vortices in this geometry, so all vortex trajectories can be expressed explicitly in elementary functions. It can be shown that in this case a vortex also cannot leave $\mathscr{D}$, however it can touch $\partial\mathscr{D}^{out}$ at $y \to \infty$.

(iii) It is worth to note that the trapping of a point vortex cannot be explained just by the luck of compliance between the given smooth normal velocity on $\partial\mathscr{D}^{out}$ and the singular velocity field of a point vortex. When the vortex Γ approaches $\partial\mathscr{D}^{out}$, the mirror image $-\Gamma$ approaches the same point of $\partial\mathscr{D}^{out}$ from the opposite side. If we assume that the vortex goes through $\partial\mathscr{D}^{out}$, then the instant of intersection corresponds to the collision between the vortex and its image, hence at this instant their singularities exactly cancel each other and the smoothness of BC is not violated.

Thus, we have discovered the trapping phenomenon for a point vortex. The generalization of this phenomenon to smooth perturbations and to more general basic flows is given in §§ 9 and 10. The next section is devoted to the phenomenon which is physically opposite to the trapping – the washout of perturbations.

4. The nonlinear stability and the washout property of channel flows

Let us consider the steady channel flow (defined in (2.7)) and its smooth perturbations that satisfy (2.15)–(2.17) and have finite enstrophy $\mathscr{I}$ (defined in (2.18)). Out target is to establish sufficient conditions for the nonlinear stability of this flow:

$$\mathscr{I}(t) \leqslant C\mathscr{I}(0), \quad C = \text{const}. \tag{4.1}$$

The stability criteria (4.1) of steady basic flows (2.7) with variable vorticity $\Omega(\boldsymbol{x})$ can be formulated in terms of the function $\Omega(\Psi)$ (2.8), its inverse $\Psi(\Omega)$, the derivative $\Psi'(\Omega) \equiv \mathrm{d}\Psi/\mathrm{d}\Omega$, a scalar parameter α ($\alpha = 1, 2$) and the notations:

$$\Psi^- = \min_{\boldsymbol{x}\in\mathscr{D}} \Psi(\boldsymbol{x}),\ \Psi^+ = \max_{\boldsymbol{x}\in\mathscr{D}} \Psi(\boldsymbol{x}); \quad \Omega^- = \min_{\boldsymbol{x}\in\mathscr{D}} \Omega(\boldsymbol{x}),\ \Omega^+ = \max_{\boldsymbol{x}\in\mathscr{D}} \Omega(\boldsymbol{x}).$$

The function $\Omega(\Psi)$ is completely determined on $\Psi^- \leqslant \Psi \leqslant \Psi^+$ by YBC for every non-separated flow (2.8).

PROPOSITION 2. *Let us consider a steady channel flow (see (2.7)) with the strictly monotonic function $\Omega(\Psi)$ (so $\Omega'(\Psi) \neq 0$). The inverse function $\Psi(\Omega)$ satisfies either*

of two conditions:

$$\alpha = 1 : 0 < c_1^- \leqslant -\Psi'(\Omega) \leqslant c_1^+ \quad \text{or} \quad \alpha = 2 : 1/\lambda < c_2^- \leqslant \Psi'(\Omega) \leqslant c_2^+, \tag{4.2}$$

where $\lambda \equiv \pi^2(1 + 1/L^2)$. *Then the flow is nonlinearly stable (see (4.1)) with the constants:*

$$\alpha = 1 : C = (c_1^+ + 1/\lambda)/c_1^-; \qquad \alpha = 2 : C = c_2^+/(c_2^- - 1/\lambda) \tag{4.3}$$

Moreover, $\mathscr{I}(t)$ *decreases unless* $\widetilde{\omega}$ *vanishes at* $\partial\mathscr{D}^{out}$.

Proof. We divide the proof into five steps.

Step 1: We use the functional introduced by Arnold (1966):

$$\left.\begin{aligned} &\mathscr{W}_\alpha[\Omega, \widetilde{\omega}, \widetilde{\psi}] \equiv (-1)^{\alpha+1} \int_{\mathscr{D}} W \, \mathrm{d}x \, \mathrm{d}y = \mathscr{W}_\alpha(t), \; W \equiv \widetilde{\boldsymbol{v}}^2/2 - \Phi(\Omega, \widetilde{\omega}), \; \alpha = 1, 2, \\ &\Phi(\Omega, \widetilde{\omega}) \equiv F(\Omega + \widetilde{\omega}) - F'(\Omega)\widetilde{\omega} - F(\Omega), \quad F(\omega) \equiv \int^{\omega} \widehat{\Psi}(\xi)\mathrm{d}\xi. \end{aligned}\right\} \tag{4.4}$$

The function $\widehat{\Psi}(\omega)$ represents a differentiable extension of $\Psi(\omega)$ (the latter is naturally defined for $\Omega^- \leqslant \omega \leqslant \Omega^+$ only) to all real axis $-\infty \leqslant \omega \leqslant \infty$, i.e.

$$\widehat{\Psi}(\omega) = \begin{cases} \Psi(\omega) & \text{if} \quad \omega \in (\Omega^-, \Omega^+), \\ \text{an arbitrary function} & \text{if} \quad \omega \notin (\Omega^-, \Omega^+), \end{cases} \tag{4.5}$$

where an arbitrary function matches $\Psi(\omega)$ together with the first derivative for $\omega = \Omega^+$ and $\omega = \Omega^-$. This definition shows that (4.4) represents not a single functional, but the infinite family of functionals corresponding to all possible differentiable extensions of $\Psi(\omega)$. The physical meaning of Φ can be clarified with the use of the remainder for Taylor's series in Lagrange's form

$$\Phi(\Omega, \widetilde{\omega}) = \widehat{\Psi}'(\Omega + \theta\widetilde{\omega})\,\widetilde{\omega}^2/2, \qquad 0 \leqslant \theta = \text{const} \leqslant 1 \tag{4.6}$$

that is valid for every real Ω, $\widetilde{\omega}$. One can see that Φ may be seen as the square of a vorticity perturbation taken with a variable amplitude.

Step 2: We choose an arbitrary element of (4.5) such that $\widehat{\Psi}'(\omega)$ admits the same bounds as those for $\Psi'(\Omega)$ in (4.2):

$$\alpha = 1 : \; 0 < c_1^- \leqslant -\widehat{\Psi}'(\omega) \leqslant c_1^+; \quad \alpha = 2 : \; 1/\lambda < c_2^- \leqslant \widehat{\Psi}'(\omega) \leqslant c_2^+. \tag{4.7}$$

From (4.6) and (4.7) we get:

$$c_\alpha^- \frac{\widetilde{\omega}^2}{2} \leqslant (-1)^\alpha \Phi(\Omega, \widetilde{\omega}) \leqslant c_\alpha^+ \frac{\widetilde{\omega}^2}{2}, \qquad \alpha = 1, 2. \tag{4.8}$$

Step 3: We recall that Arnold's functional (4.4) has been originally introduced as the combination of conserved quantities (or conservation laws) defined in closed flow domains or for spatially periodic flows. The related divergent form is

$$W_t = \operatorname{div} \boldsymbol{\Pi}; \quad \boldsymbol{\Pi} \equiv \Phi \boldsymbol{v} - \widetilde{b}\widetilde{\boldsymbol{v}}, \quad \widetilde{b} \equiv \widetilde{p} + \boldsymbol{V} \cdot \widetilde{\boldsymbol{v}} + \widetilde{\boldsymbol{v}}^2/2, \tag{4.9}$$

where $\widetilde{b}$ is the perturbation of Bernoulli's function $b \equiv p + \boldsymbol{v}^2/2$ (this divergent form is a novel result that requires rather cumbersome calculations). Hence:

$$\frac{\mathrm{d}}{\mathrm{d}t} \int_{\mathscr{D}} W \, \mathrm{d}x \, \mathrm{d}y = \int_{\partial\mathscr{D}} (\Phi(\Omega, \widetilde{\omega})\boldsymbol{v} \cdot \boldsymbol{n} - \widetilde{b}\widetilde{\boldsymbol{v}} \cdot \boldsymbol{n}) \, \mathrm{d}S.$$

Since $\tilde{\boldsymbol{v}}\boldsymbol{n} = 0$ on $\partial\mathscr{D}$, $\tilde{\omega} = 0$ on $\partial\mathscr{D}^{in}$ (2.17) and $\Phi(\Omega, 0) = 0$ (4.8), we conclude that the only non-zero part of the right-hand side is the surface integral over $\partial\mathscr{D}^{out}$:

$$\frac{\mathrm{d}}{\mathrm{d}t}\int_{\mathscr{D}} W \,\mathrm{d}x\,\mathrm{d}y = \int_0^1 u^{out}(y)\Phi(\Omega(L, y), \tilde{\omega}(L, y, t))\,\mathrm{d}y.$$

Using the definition of $\mathscr{W}_\alpha$ (4.4) we write

$$\frac{\mathrm{d}}{\mathrm{d}t}\mathscr{W}_\alpha = -\int_0^1 u^{out}(y)(-1)^\alpha\Phi(\Omega(L, y), \tilde{\omega}(L, y, t))\,\mathrm{d}y \tag{4.10}$$

where $u^{out}(y) \geqslant U^- > 0$ due to (2.6) and $(-1)^\alpha\Phi(\Omega, \tilde{\omega}(L, y, t)) > 0$ by (4.8). Hence:

$$\mathrm{d}\mathscr{W}_\alpha/\mathrm{d}t \leqslant 0, \quad \alpha = 1, 2. \tag{4.11}$$

Step 4: Let us choose $\alpha = 1$. Then Φ is always negative (4.8), hence $\mathscr{W}_1[\Omega, \tilde{\omega}, \tilde{\psi}]$ is always positive (4.4), and its time-derivative is non-positive by (4.11). Consequently, $0 < \mathscr{W}_1(t) \leqslant \mathscr{W}_1(0)$ and the upper bound for perturbations is

$$\int_{\mathscr{D}} (\tilde{\boldsymbol{v}}^2 + c_1^-\tilde{\omega}^2)\,\mathrm{d}x\,\mathrm{d}y \leqslant \int_{\mathscr{D}} (\tilde{\boldsymbol{v}}_0^2 + c_1^+\tilde{\omega}_0^2)\,\mathrm{d}x\,\mathrm{d}y, \tag{4.12}$$

where $\tilde{\boldsymbol{v}}_0 \equiv \tilde{\boldsymbol{v}}(\boldsymbol{x}, 0)$, $\tilde{\omega}_0 \equiv \tilde{\omega}(\boldsymbol{x}, 0)$. This inequality can be already considered as the mathematical definition of stability. However the use of well-known inequality

$$\lambda\int_{\mathscr{D}} \tilde{\boldsymbol{v}}^2 \,\mathrm{d}x\,\mathrm{d}y \leqslant \int_{\mathscr{D}} \tilde{\omega}^2 \,\mathrm{d}x\,\mathrm{d}y, \quad \lambda = \pi^2(1 + 1/L^2) \tag{4.13}$$

transforms (4.12) to (4.1) with $C = (c_1^+ + 1/\lambda)/c_1^-$, where λ is the minimal eigenvalue of Dirichlet's problem for the operator $-\Delta$ in $\mathscr{D}$ (this inequality follows from Rayleigh's principle for the eigenvalues of symmetric operators).

Let $\alpha = 2$. Then Φ is positive (again by (4.7)) and

$$c_2\,\mathscr{I}[\tilde{\omega}] \leqslant 2\mathscr{W}_2[\Omega, \tilde{\omega}, \tilde{\psi}] \leqslant c_2^+\mathscr{I}[\tilde{\omega}],$$

where $c_2 \equiv c_2^- - 1/\lambda > 0$ by assumption (4.2). Hence $\mathscr{W}_2$ is always positive and $\mathscr{W}_2(t) \leqslant \mathscr{W}_2(0)$ that yields (4.1) with $C = c_2^+/(c_2^- - 1/\lambda)$.

Step 5: Finally, (4.10) and (4.11) show the decrease of $\mathscr{W}_\alpha$ unless $\tilde{\omega} \equiv 0$ at $\partial\mathscr{D}^{out}$. The proof that the decrease of $\mathscr{W}_\alpha$ leads to the decrease of $\mathscr{I}(t)$ is omitted; that step completes the proof.

Proposition 3 in the case of the shear basic flow (2.11) takes an especially simple form since $\Psi'(\Omega) = -U(y)/U_{yy}(y)$ and $U(y)$ is always positive by (2.14).

PROPOSITION 2*a*. *A shear flow with*

$$\alpha = 1: \ 0 < d_1^- < U_{yy} < d_1^+ < \infty;, \qquad \alpha = 2: -\lambda U^- < d_2^- < U_{yy} \leqslant d_2^+ < 0$$

is nonlinearly stable in the sense of (4.1). *The relations between the constants* $d_\alpha^\pm$ *and* $c_\alpha^\pm$ (4.2) *can be obtained with the use of particular properties of* $U(y)$, *while the constant* C (4.3) *remains the same.*

The basic flows with constant vorticity represent a special (degenerated) case which should be treated separately:

PROPOSITION 3. *Any perturbation of a steady flow with constant vorticity* (3.1) *satisfies* (4.1) *with* $C = 1$. *Moreover,* $\mathscr{I}(t)$ *decreases unless* $\tilde{\omega}$ *vanishes at* $\partial\mathscr{D}^{out}$.

Proof. For $\Omega(\boldsymbol{x}) \equiv \text{const}$ in (2.16) $\widetilde{\omega}$ represents a 'passive admixture'. One can check the balance relation

$$\frac{\mathrm{d}\mathscr{I}}{\mathrm{d}t} = -\int_0^1 u^{out}(y)\widetilde{\omega}^2(L, y, t)\,\mathrm{d}y \leqslant 0 \tag{4.14}$$

that is valid by virtue of (2.16) and (2.17). Here the right-hand side represents the outflux of enstrophy through $\partial\mathscr{D}^{out}$. Clearly, $\mathrm{d}\mathscr{I}/\mathrm{d}t$ is non-positive due to $u^{out}(y) \geqslant U^- > 0$ (2.6) that immediately leads us to the required result.

The proofs of nonlinear stability in Propositions 2, 3 can be classified as applications of the direct Lyapunov method with the use of the Lyapunov functionals $\mathscr{I}$ and $\mathscr{W}_\alpha$. Both functionals are decreasing, unless $\widetilde{\omega} \equiv 0$ on $\partial\mathscr{D}^{out}$. The decreasing of $\mathscr{I}$ leads only to the stability of the flows with constant vorticity (3.1), while the use of $\mathscr{W}_\alpha$ produces the stability conditions for two broad classes of steady flows (4.2). The decreasing of $\mathscr{W}_\alpha$ is based on the explicit expression for the flux $\boldsymbol{\Pi}$ (4.9). Its inspection shows that YBC (2.4)–(2.5) or (2.17) are exceptional ones, since among all possible BC only they have two key properties: (i) they provide the decrease (non-increase) of Arnold's functional $\mathscr{W}_\alpha$ (4.4) and (ii) they are 'physically natural' as it is apparent that all other possible BC that enforce the decrease of Arnold's functionals contain rather artificial conditions for pressure. This observation links two directions of fluid mechanics previously separated from each other: Arnold's stability and Yudovich's existence theorems.

According to (4.14) and (4.10), the outflux (or the washout) of $\mathscr{W}_\alpha$ or $\mathscr{I}$ through $\partial\mathscr{D}^{out}$ represents the only reason for the decay of perturbations. Therefore, we use the term the washout of $\mathscr{W}_\alpha$ or $\mathscr{I}$ (or just the washout). The next section introduces a heuristic analogy based on the concept of the washout.

5. Analogy between inviscid channel flows, viscous flows and non-conservative dynamical systems

The analogy between the Navier–Stokes equations and finite-dimensional non-conservative dynamical systems is well known (Yudovich 1989). As $t \to \infty$, the trajectories of a finite-dimensional dissipative dynamical system can approach equilibria, limit cycles, or more complicated attractors. The tendency to approach an equilibrium is typical for purely dissipative systems, where energy is always decreasing. For such systems one can expect that an initial perturbation of a stable equilibrium can lead to two scenarios: (S1) return to the same equilibrium; (S2) transition to a different equilibrium. An additional scenario (S3) is available for more complex dynamical systems with the sources of energy when an initial perturbation can lead to self-oscillations (limit cycles). These three scenarios also appear in the solutions of Navier–Stokes equations, where viscosity plays two key roles: KROV1 – it provides the dissipation of energy; and KROV2 – it acts as a smoothing factor, which exhibits itself in the diffusion of vorticity and spreading of momentum (KROV stands for the key role of viscosity).

The qualitatively similar to KROV1 and KROV2 properties can be observed in the vorticity dynamics of channel flows with YBC: the washout represents an analogy to dissipation, while the trapping plays a part of a mixing and smoothing factor. Indeed, the decrease of $\mathscr{W}_\alpha$ or $\mathscr{I}$ represents the 'dissipation' of these functionals that is concentrated at $\partial\mathscr{D}^{out}$. In Propositions 2 and 3 we have shown that such dissipation takes place for generic perturbations, when $\widetilde{\omega}$ is not identically vanishing on $\partial\mathscr{D}^{out}$ (4.14), (4.10), (4.11). Physically, the key role of the trapping (KROT) is twofold:

KROT1 – it delays the washout due to the rejection of vorticity from $\partial\mathscr{D}^{out}$ back to $\mathscr{D}$; and *KROT2* – it introduces a strong mixing and smoothing property, due to the fact that the rejection of vorticity is always partial and always produces the intensive rearrangement of trapped vorticity and its spreading over a channel (see §§ 3 and 9). These qualitative ideas suggest that the washout and *KROT2* can play the roles similar to KROV1 and KROV2 correspondingly. On the basis of these very heuristic reasons, we propose to consider and exploit the analogy between the general properties of channel flows with YBC and Navier–Stokes equations (or dissipative dynamical systems).

Using this analogy one can expect the appearance of three scenarios (S1–S3) for the perturbations of a channel flow. The first two scenarios (S1 and S2) are expected to take place for the cases of Propositions 2 and 3, where we deal with the decreasing Lyapunov functionals $\mathscr{W}_\alpha$ and $\mathscr{I}$ (the analogies of purely dissipative systems). The third scenario (S3) is linked to the case when BC are chosen in such a way that $\mathscr{W}_\alpha$ fails to play a part of Lyapunov functional.

For the precise formulations of particular conjectures, we introduce the following definition: we say that BC are dissipative if all related flows admit positive and decreasing Lyapunov functionals. Proposition 2 shows that YBC are dissipative if: (D1) they admit at least one steady non-separated flow; and (D2) either inequality $\mathrm{d}\omega^{in}/\mathrm{d}\psi^{in} < 0$ or $0 < \mathrm{d}\omega^{in}/\mathrm{d}\psi^{in} < \lambda$ is valid for all $\psi^{in} : 0 \leqslant \psi^{in} \leqslant 1$. Here we use a scalar function

$$\omega^{in} = \omega^{in}(\psi^{in}) \equiv \omega^{in}(y(\psi^{in})), \qquad \psi^{in} \in (0, 1),$$

where $y(\psi^{in})$ is inverse to $\psi^{in}(y)$ (2.4); this function is constructed in the same way as (2.8) but it is related only to BC. If one non-separated flow does exist, then all other velocity fields can be considered as its perturbations, so they will be bounded from above as in Proposition 2. The existence of a non-separated flow entirely depends on the YBC; for example YBC (2.10) always admit shear flow solutions (2.11).

Proposition 3 states that YBC are always dissipative if (D3) the inlet vorticity is constant $\omega^{in} \equiv const$ while v_n can be arbitrary (satisfying (2.3) only). It is natural to expect that for the dissipative BC the flow dynamics follows the scenario of purely dissipative dynamical systems. Hence we propose the conjecture of global relaxation:

(C1) *Conjecture 1. Let YBC satisfy the conditions (D1), (D2) or (D3). Then as* $t \to \infty$ *an arbitrary perturbed initial flow converges (relaxes) to a steady flow.*

The conjecture (C1) contains conditions that are sufficient for the appearance of scenarios (S1) and (S2). In the following sections, we present a number of rigorous mathematical results as well as some computational results that support these conjectures. The formulation of the sufficient conditions that lead to the self-oscillations (S3) is less obvious. As we mentioned already, we expect that (S3) will take place when a basic flow is chosen in such a way that $\mathscr{W}_\alpha$ fails to play a part of Lyapunov functional:

(C2) *Conjecture 2. Let the function* $\omega^{in}(\psi^{in})$ *be non-monotonic on* $0 < \psi^{in} < 1$. *Then as* $t \to \infty$ *an arbitrary perturbed initial flow converges to a steady flow, self-oscillating flow, or a chaotic flow.*

One can also formulate a more general conjecture: (C3) Any dynamical system consisting of Euler's equations with YBC in a channel always possesses a non-trivial attractor.

It is clear that the non-monotonicity of $\omega^{in}(\psi^{in})$ leads to the non-monotonicity of $\Omega(\Psi)$ (2.8) in the corresponding non-separated steady flow. Physically that means that there is a vorticity extremum inside the flow. If this extremum is strong enough then the flow can be unstable by the Kelvin–Helmholtz mechanism. In § 11 we consider a computational example which demonstrates the appearance of self-oscillations (S3) under the condition related to (C2).

Conjecture 1 proposes that any perturbed stable basic flow must eventually (as $t \to \infty$) form a steady state. This relaxation of any initial conditions to a steady state is highly unusual for inviscid flows; it is the same as the existence of attractors for the solutions of Euler's equations. In such cases one may use the striking term conservative dissipation, as the entire unsteady part of perturbation is 'dissipated' or washed out by YBC at $\partial\mathscr{D}^{out}$. The idea of the existence of limit cycles (self-oscillations) C2 is well established for viscous flows but is also novel and highly unusual for inviscid flows. C1, 2 will be studied below both analytically and computationally. In §§ 6–8 we formulate sufficient conditions for C1 and justify them analytically; in §§ 9 and 10 we give supporting computational examples. In § 11 we provide the computational example illustrating C2.

6. The complete washout of fluid particles

We have established that the washout of $\mathscr{W}_\alpha$ or $\mathscr{I}$ to $\partial\mathscr{D}^{out}$ represents the only reason for the decay of perturbations. Therefore, the total decay of perturbations can reveal itself only as the complete washout of perturbations (CWOP). In turn, the availability of CWOP depends crucially on the replacing of old fluid particles (which present in $\mathscr{D}$ at $t=0$) with new ones (which enter $\mathscr{D}$ at $t>0$). Indeed, the full vorticity of each fluid particle is conserved. Therefore, the total decay of vorticity perturbations is linked (but not identical) to the full replacing of all old particles (that carry the initially perturbed vorticity) with new ones (that carry the 'basic' value of vorticity from inlet). We call this process the complete washout of fluid particles (CWOF). The most straightforward case corresponds to the constant inlet vorticity when the vorticity perturbation of each new particle is zero and CWOF can produce a non-separated flow with constant vorticity. The appearance of such a flow means that CWOP also has happened. The opposite possibility consists of the trapping of some old particles, so that they stay in $\mathscr{D}$ forever and keep initially perturbed vorticity in the flow. In the general case of variable inlet vorticity, the perturbation dynamics is more complex since vorticity perturbations can also appear due to the displacements of fluid particles from their undisturbed positions. As a result (it will be shown in § 7), the CWOP requires repeating CWOF many times. We came to a conclusion that CWOF is necessary but not sufficient for CWOP. Therefore, before studying CWOP, we must describe a simpler phenomenon of CWOF that implies that every fluid particle which is initially in $\mathscr{D}$ must leave it in finite time.

By definition CWOF always takes place for any steady non-separated flow with $\mathscr{D}^{tf} = \mathscr{D}$ (2.8). The problem of this section is: what conditions one should impose on the initial perturbations $\widetilde{\boldsymbol{v}}(\boldsymbol{x}, 0)$ of a given non-separated basic steady flow (2.7) in order to guarantee CWOF for a perturbed flow? We obtain the sufficient conditions that are based on two requirements: the basic flow is stable (4.1) and its initial perturbation must be small enough. The most difficult problem is to establish mathematically the smallness requirement.

The permanent appearance (the birth) of new material particles on $\partial\mathscr{D}^{in}$ is the striking feature of channel flows. Therefore, to introduce Lagrangian coordinates we

have to consider two classes of particles. Each fluid particle in $\mathscr{D}$ is either an old one (that is, in $\mathscr{D}$ at $t=0$) or a new one (that appears on $\partial\mathscr{D}^{in}$ at $t=t_0>0$). Lagrangian coordinates for old particles are $(a,b)\in\mathscr{D}\cup\partial\mathscr{D}^{in}$ and for new ones are (b,t_0), where $0\leqslant b\leqslant 1$, $0<t_0\leqslant t$. The trajectories are given as the solutions of Cauchy's problems:

$$\mathrm{d}\boldsymbol{x}/\mathrm{d}t=\boldsymbol{v}(\boldsymbol{x},t),\quad \boldsymbol{x}|_{t=0}=(a,b)\ \text{or}\ \boldsymbol{x}|_{t=t_0>0}=(0,b). \tag{6.1}$$

Then the trajectories of old and new particles are $\boldsymbol{x}=\boldsymbol{x}(a,b,t)$ and $\boldsymbol{x}=\boldsymbol{x}(b,t_0,t)$ correspondingly. In general, both these functions are not invertible since particles permanently appear on $\partial\mathscr{D}^{in}$ and disappear on $\partial\mathscr{D}^{out}$. The 'inverse' functions $\boldsymbol{a}=\boldsymbol{a}(\boldsymbol{x},t)$ and $t_0=t_0(\boldsymbol{x},t)$ can be better found as the solutions of hyperbolic problems with the initial conditions and BC:

$$\left.\begin{aligned}&(\partial/\partial t+\boldsymbol{v}\nabla)(\boldsymbol{a},t_0)=0;\quad \boldsymbol{x}\in\mathscr{D},\quad t\geqslant 0,\\ &\boldsymbol{a}(\boldsymbol{x},0)=\boldsymbol{x},\ \ \boldsymbol{a}(0,y,t)=(0,y);\qquad t_0(x,y,0)=0,\ \ t_0(0,y,t)=t.\end{aligned}\right\} \tag{6.2}$$

For a more general description, we consider three Lagrangian coordinates (a,b,t_0) where either $t_0=0$ or $a=0$. Then, any trajectory can be expressed as $\boldsymbol{x}=\boldsymbol{x}(\boldsymbol{a},t_0,t)$. For the particle $(\boldsymbol{a},t_0)$ the duration $\tau=\tau(\boldsymbol{x},t)$ of its stay in $\mathscr{D}$ (the age of a particle at the instant t) is

$$\tau=\tau(\boldsymbol{x},t)\equiv t-t_0(\boldsymbol{x},t)\geqslant 0. \tag{6.3}$$

Therefore,

$$\tau_t+J[\tau,\psi]=1,\quad J[\tau,\psi]\equiv\tau_x\psi_y-\tau_y\psi_x;\quad \boldsymbol{x}\in\mathscr{D},\quad t\geqslant 0, \tag{6.4}$$

$$\tau(0,y,t)=\tau(\boldsymbol{x},0)=0. \tag{6.5}$$

The required CWOF means that there exists the maximal lifespan of particles, i.e. the particle's 'age' admits an upper bound:

$$\max_{\boldsymbol{x}}\tau(\boldsymbol{x},t)\leqslant\tau^{+}=\mathrm{const}<\infty. \tag{6.6}$$

Now, we introduce a steady non-separated basic flow $\Psi(\boldsymbol{x})$ (2.7) with bounded vorticity:

$$\Psi(\boldsymbol{x}),\quad |\nabla\Psi(\boldsymbol{x})|\geqslant\mathrm{const}>0,\quad \max_{\boldsymbol{x}}|\Omega(\boldsymbol{x})|=|\Omega|^{+}<\infty\quad\text{in}\quad\mathscr{D}. \tag{6.7}$$

For this flow we formulate 'a steady version' of (6.4) and (6.5) for the function $\tau_0=\tau_0(\boldsymbol{x})$:

$$J[\tau_0,\Psi]=1;\qquad\text{and}\qquad\tau_0(0,y)=0. \tag{6.8}$$

Since $J[\tau_0,\Psi]$ represents a directional derivative along a streamline, (6.8) can be written as $\partial\tau_0/\partial s=|\nabla\Psi(\boldsymbol{x})|^{-1}$, where s is an arclength along a streamline; combining it with the inequalities (6.7) one can prove that

$$\tau_0(\boldsymbol{x})>0,\quad \max_{\boldsymbol{x}}\tau_0(\boldsymbol{x})=\tau_0^{+}<\infty,\quad \max_{\boldsymbol{x}}|\nabla\tau_0(\boldsymbol{x})|=(\nabla\tau_0)^{+}<\infty\quad\text{in}\quad\mathscr{D}. \tag{6.9}$$

For example, for the basic shear flow (2.11) we have

$$\begin{aligned}&\Psi=\Psi(y),\quad U^{-}=\min\Psi_y(y)>0,\quad |\Omega|^{+}=\max_{y}|\Psi_{yy}(y)|,\\ &\tau_0(\boldsymbol{x})=x/\Psi_y(y)\geqslant 0,\quad \nabla\tau_0=(1/\Psi_y(y))(1,-x\Psi_{yy}/\Psi_y),\\ &\tau_0^{+}=L/U^{-},\quad (\nabla\tau_0)^{+}=\frac{1}{U^{-}}\sqrt{1+(L|\Omega|^{+}/U^{-})^2}.\end{aligned}$$

Let us add the perturbation (2.15) with the bounded initial vorticity $\omega(\boldsymbol{x},0)=\Omega(\boldsymbol{x})+\widetilde{\omega}(\boldsymbol{x},0)$:

$$\psi(\boldsymbol{x},t)=\Psi(\boldsymbol{x})+\widetilde{\psi}(\boldsymbol{x},t);\quad |\widetilde{\omega}_0|^+\equiv\max_{\boldsymbol{x}}|\widetilde{\omega}(\boldsymbol{x},0)|<\infty,\quad \mathscr{I}_0\equiv\mathscr{I}(0)<\infty. \tag{6.10}$$

One can expect that the property of CWOF is preserved if the amplitude of velocity perturbations is small at any t. To show that the latter property can be controlled by the initial perturbation and to formulate a sufficient condition for CWOF (6.6) we introduce an auxiliary function $\mathscr{M}(a_1,a_2)$ of two scalar arguments a_1 and a_2 such that $0\leqslant a_1\leqslant a_1^+$, $0\leqslant a_2\leqslant a_2^+$ with positive constants a_1^+ and a_2^+:

$$\mathscr{M}(a_1,a_2)\equiv c\sqrt{a_1/L}\left(2+\sqrt{\ln^2\left(\frac{c_1a_2}{\sqrt{a_1/L}}\right)+4}\right), \tag{6.11}$$

$$c\equiv 4e\sqrt{\pi}(1+L^2)/\sqrt{L},\quad c_1\equiv 1+12\sqrt{6}(1+2\sqrt{3}). \tag{6.12}$$

The straightforward inspection of (6.11) shows that

$$\partial\mathscr{M}/\partial a_1>0,\ \partial\mathscr{M}/\partial a_2>0\quad\text{hence}\quad \mathscr{M}(a_1,a_2)\leqslant\mathscr{M}(a_1^+,a_2^+) \tag{6.13}$$

for all a_1 and a_2. It is clear that

$$\mathscr{M}\to 0\quad\text{as}\quad a_1\to 0\ \text{provided that}\ a_2<\infty. \tag{6.14}$$

Proposition 4. *Consider the steady non-separated flow (2.7), (6.7) that is nonlinearly stable in the enstrophy norm $\mathscr{I}(t)\leqslant\mathscr{I}^+\equiv C\mathscr{I}_0$(4.1). Assume that the initial perturbation $\widetilde{\omega}(\boldsymbol{x},0)$ is small enough to satisfy the condition*

$$J^+<1,\quad\text{where}\quad J^+\equiv\mathscr{M}(\mathscr{I}^+,|\widetilde{\omega}|^+)(\nabla\tau_0)^+, \tag{6.15}$$

$$|\widetilde{\omega}|^+=\begin{cases}|\widetilde{\omega}_0|^+ & \text{for the flows with}\ \ \Omega(\boldsymbol{x})\equiv\text{const},\\ 3|\Omega|^+ + |\widetilde{\omega}_0|^+ & \text{for the flows with}\ \Omega(\boldsymbol{x})\not\equiv\text{const}.\end{cases} \tag{6.16}$$

Then CWOF takes place in the perturbed flow $\psi(\boldsymbol{x},t)$ (defined in (6.10)) with the upper bound for 'the age of particles' (defined in (6.6)) given as

$$\tau^+\leqslant\tau_0^+/(1-J^+). \tag{6.17}$$

It is important that $J^+\to 0$ as $\mathscr{I}_0\to 0$ due to (6.14), provided that $|\widetilde{\omega}_0|^+$ remains bounded. Therefore, a sufficiently small initial perturbation satisfies $J^+<1$ (6.15), which makes (6.17) well defined.

The proof of this proposition is given in Appendix B.

The inequality (6.15) gives an unusual criterion of the smallness of initial perturbations which uses simultaneously two qualitatively different scales (norms): the mean-square value $\mathscr{I}_0$ of vorticity and the amplitude of vorticity $\widetilde{\omega}_0^+$. The appearance of $\widetilde{\omega}_0^+$ is required by the fact that the smallness of enstrophy does not imply the smallness of a velocity amplitude (see the proof).

Once CWOF takes place, the formation of recirculation zones is forbidden. However, initially introduced perturbations can still stay in $\mathscr{D}$ for indefinite time (say, in the form of internal waves that do not destroy the non-separated character of a basic flow). Therefore CWOP (that is the same as the asymptotic stability of a basic flow) represents a stronger result that should be addressed separately. In the next section we are establishing sufficient conditions for CWOP.

7. Asymptotic stability of quadratic basic flows

In this section, we justify C1 for the quadratic basic flows QBF (2.13)–(2.14). Let

$$\left.\begin{aligned} &U(y) = Q_u + 2Q_c y + 6Q_p(y - y^2), \quad U^- \equiv \min_y U(y) > 0, \\ &\Omega(y) = -2Q_c + 6Q_p(2y - 1), \quad \Omega_y(y) = -U_{yy}(y) = 12Q_p \equiv K. \end{aligned}\right\} \tag{7.1}$$

Geometrically, such profiles are convex forward if $K > 0$, and convex backward if $K < 0$. For example, the standard Poiseuille profile (2.12) is convex forward.

Since $\Psi'(\Omega) = U(y)/K$, constants in the nonlinear stability criteria (4.2) take the form:

$$\alpha = 1 : \; K < 0, \; c_1^+ = U^+/|K|, \; c_1^- = U^-/|K|, \tag{7.2}$$

$$\alpha = 2 : \; K > 0, \; c_2^+ = U^+/K, \; c_2^- = U^-/K > 1/\lambda, \tag{7.3}$$

where $U^+ = \max_y U(y)$. Therefore, all QBF for $\alpha = 1$, $K < 0$ are nonlinearly stable in the definition of stability (4.1). The related constant C can be specified with the use of (4.3) and (7.2). In the case of $\alpha = 2$, $K > 0$ (7.3) we have nonlinear stability if

$$\epsilon_n \equiv \frac{K}{U^-\lambda} < 1, \quad \lambda \equiv \pi^2(1 + 1/L^2), \tag{7.4}$$

where the subscript n in ϵ_n stands for nonlinear stability. Since convex forward flows are physically more natural than convex backward flows (e.g. the pressure-driven viscous flows in the limit of zero viscosity are always convex forwards), we will consider only QBF with $K > 0$. Moreover, we accept an extra restriction

$$\epsilon_a \equiv \epsilon_n L\sqrt{\lambda} = \frac{K\tau_0^+}{\sqrt{\lambda}} = \frac{KL}{U^-\sqrt{\lambda}} < 1 \quad \text{or} \quad \epsilon_n < 1/(L\sqrt{\lambda}) < 1/\pi, \tag{7.5}$$

where the subscript a in ϵ_a stands for asymptotic stability. Since $L\sqrt{\lambda} = \pi\sqrt{1 + L^2} > \pi$, the restriction (7.5) is stronger than (7.4). Therefore, every QBF satisfying (7.5) is nonlinearly stable

$$\mathscr{I}(t) \leqslant C\mathscr{I}(0), \quad C = U^+/[U^-(1 - \epsilon_n)], \tag{7.6}$$

where the expression for C follows directly from (4.3) and (7.3). Applying Proposition 4, we conclude that CWOF takes place for every QBF satisfying (7.5). The maximal 'particle's age' τ^+ and the smallness restriction (6.15) can be made more specific for each QBF. For example, if $Q_c = 0$, then

$$U^- = Q_u, \; U^+ = U^- + K/8, \; C = \frac{1 + K/(8U^-)}{1 - K/(\lambda U^-)}, \; \widetilde{\omega}^+ = \widetilde{\omega}_0^+ + \frac{3}{2}K, \tag{7.7}$$

$$\tau_0 = \frac{L}{U^-}, \quad (\nabla\tau_0)^+ = \frac{1}{U^-}\sqrt{1 + (\tau_0^+ K/2)^2}. \tag{7.8}$$

The substitution of (7.7) and (7.8) into (6.15) produces J^+ and τ^+ for a given flow. However, as we have already mentioned, CWOF does not mean CWOP. A sufficient condition for CWOP is given as follows.

PROPOSITION 5. *The QBF (7.1) with $\epsilon_a < 1$ (7.5) is asymptotically stable*

$$\mathscr{I}(t) \leqslant C\mathscr{I}_0 \text{ and } \mathscr{I}(t) \to 0 \text{ as } t \to 0$$

for every initial perturbation that obeys the smallness restriction for J^+ (6.15):

$$J^+ < 1 - \epsilon_a \tag{7.9}$$

The proof is given as the sequence of two steps.

Step 1 : CWOF takes place since $J^+ < 1$ by virtue of (7.9). The governing equation for vorticity perturbations (2.16) simplifies to

$$\widetilde{\omega}_t + \psi_y \widetilde{\omega}_x - \psi_x \widetilde{\omega}_y = K \widetilde{\psi}_x.$$

Its integration along a trajectory $\overline{\boldsymbol{x}} = \overline{\boldsymbol{x}}(\boldsymbol{x}, t, \bar{t})$ (cf. with (B 1) and (B 2)) gives

$$\widetilde{\omega}(\boldsymbol{x}, t) = \widetilde{\omega}(\boldsymbol{a}, t_0) + K \int_{t_0}^{t} \widetilde{\psi}_{\overline{x}}(\overline{\boldsymbol{x}}, \bar{t})\, \mathrm{d}\bar{t}. \tag{7.10}$$

Let us fix $t > \tau^+$. Then, a flow consists of the particles 'born' on $\partial\mathscr{D}^{in}$ with $t_0(\boldsymbol{x}, t) > 0$ and $\boldsymbol{a}(\boldsymbol{x}, t) \in \partial\mathscr{D}^{in}$ for every $\boldsymbol{x}$. Consequently, $\widetilde{\omega}_0(\boldsymbol{a}, t_0) = 0$ by virtue of BC, (2.5), (2.17) and (7.10) simplifies to

$$\widetilde{\omega}(\boldsymbol{x}, t) = K \int_{t_0}^{t} \widetilde{\psi}_{\overline{x}}(\overline{\boldsymbol{x}}, \bar{t})\, \mathrm{d}\bar{t}, \qquad \text{for } t > \tau^+.$$

Then,

$$\mathscr{I}(t) = K^2 \int_{\mathscr{D}} \left(\int_{t_0}^{t} \widetilde{\psi}_{\overline{x}}(\overline{\boldsymbol{x}}, \bar{t})\, \mathrm{d}\bar{t} \right)^2 \mathrm{d}\boldsymbol{x} \leqslant K^2 \int_{\mathscr{D}} \tau(\boldsymbol{x}, t) \int_{t_0(\boldsymbol{x},t)}^{t} \widetilde{\psi}_{\overline{x}}^2(\overline{\boldsymbol{x}}, \bar{t})\, \mathrm{d}\bar{t}\, \mathrm{d}\boldsymbol{x}, \tag{7.11}$$

where we use the definition of τ (6.3) and the inequality $(\int fg\ \mathrm{d}\bar{t})^2 \leqslant \int f^2\ \mathrm{d}\bar{t} \int g^2\ \mathrm{d}\bar{t}$ with $f \equiv 1$, $g \equiv \widetilde{\psi}_{\overline{x}}$. We note that $t - \tau^+ \leqslant \bar{t} \leqslant t$ by the definition of τ^+ ($t - \tau^+$ is 'the time of birth' of 'the oldest available particle'). Then, the change of the order of integration in the last integral (7.11) gives

$$\mathscr{I}(t) \leqslant \tau^+ K^2 \int_{t-\tau^+}^{t} \int_{\mathscr{D}_{\bar{t}}(t)} \widetilde{\psi}_{\overline{x}}^2(\overline{\boldsymbol{x}}, \bar{t})\, \mathrm{d}\boldsymbol{x}\, \mathrm{d}\bar{t},$$

where the domain $\mathscr{D}_{\bar{t}}(t)$ represents a part of $\mathscr{D}$ occupied at the instant t by the particles with 'the time of birth' $t_0(\boldsymbol{x}, t) < \bar{t}$. For every fixed $\bar{t}$ we consider the change of variables $\boldsymbol{x} \mapsto \overline{\boldsymbol{x}}$. Its determinant $\partial(x, y)/\partial(\overline{x}, \overline{y}) \equiv 1$ (due to the incompressibility of a fluid). Hence

$$\mathscr{I}(t) \leqslant \tau^+ K^2 \int_{t-\tau^+}^{t} \int_{\mathscr{D}_{\bar{t}}(\bar{t})} \widetilde{\psi}_{\overline{x}}^2(\overline{\boldsymbol{x}}, \bar{t})\, \mathrm{d}\overline{\boldsymbol{x}}\, \mathrm{d}\bar{t}, \tag{7.12}$$

where, in agreement with the above definition, $\mathscr{D}_{\bar{t}}(\bar{t})$ represents a part of $\mathscr{D}$ occupied at the instant $\bar{t}$ by the particles with 'the time of birth' $t_0(\boldsymbol{x}, t) < \bar{t}$.

Step 2 : Enlarging the integration area in (7.12) to the whole $\mathscr{D}$ and the use of (4.13) give us the inequality

$$\mathscr{I}(t) \leqslant \frac{\epsilon^2}{\tau^+} \int_{t-\tau^+}^{t} \mathscr{I}(\bar{t})\, \mathrm{d}\bar{t}, \qquad \epsilon \equiv \tau^+ K/\sqrt{\lambda}, \qquad t > \tau^+, \tag{7.13}$$

which, in turn, gives

$$\mathscr{I}(t) \leqslant \epsilon^2 \max_{\bar{t}} \mathscr{I}(\bar{t}), \qquad t - \tau^+ \leqslant \bar{t} \leqslant t, \qquad t > \tau^+. \tag{7.14}$$

Let us denote

$$\mathscr{I}_k^+ = \max_{k\tau^+ \leqslant t \leqslant (k+1)\tau^+} \mathscr{I}(t), \quad k = 0, 1, \ldots.$$

Then, (7.14) gives

$$\mathscr{I}_k^+ \leqslant \epsilon^2 \max(\mathscr{I}_k^+, \mathscr{I}_{k-1}^+),\ k = 1, 2, \ldots,$$

where k started from 1 since $t > \tau^+$ in (7.13). The use of (6.17) and (7.5) gives $\epsilon \leqslant \epsilon_a(1 - J^+)^{-1}$, so that by virtue of (7.9) we have $\epsilon < 1$. Consequently,

$$\mathscr{I}_k^+ \leqslant \epsilon^2 \mathscr{I}_{k-1}^+ \leqslant \epsilon^{2k} \mathscr{I}_0^+,\ k = 1, 2, \ldots.$$

Next, we estimate $\mathscr{I}_0^+$ with the use of (7.6) and then we arrive at the inequality

$$\mathscr{I}(t) \leqslant C\epsilon^{2[t/\tau^+]} \mathscr{I}_0 \to 0,\ \text{as } t \to +\infty,$$

where C is given in (7.6) and $[t/\tau^+]$ denotes the maximal integer that does not exceed t/τ^+. This estimate completes the proof.

Hence we have not only proven the asymptotic stability of forward-oriented QBF with $\epsilon_a < 1$ (see (7.5)) but also have shown that the decrease of perturbations is at least exponential. The obtained result once again emphasizes that CWOF is necessary for CWOP. In particular, the value of ϵ is proportional to the maximal lifespan of particles τ^+ while the exponent $[t/\tau^+]$ may be seen as the number of full replacements of fluid particles in $\mathscr{D}$ during the time interval t. One can see that CWOF requires finite time, while for CWOP we can guarantee the complete decay only in infinite time. In the next section we are considering one important exception from this rule: for the linear basic flows $\epsilon = 0$ and $I(t) = 0$ for $t > \tau^+$.

8. Washout of particles and perturbations in linear flows

For linear basic profiles $Q_p = 0$ in (2.13). Hence $Q_u + Q_c = 1$ and

$$\left.\begin{aligned} &U(y) = Q_u + 2yQ_c,\ \Omega \equiv -2Q_c = \text{const},\ \min(Q_u, 2 - Q_u) = U^- > 0, \\ &\tau_0^+ = L/U^-,\ U^-(\nabla\tau_0)^+ = \sqrt{1 + 4L^2Q_c^2/(U^-)^2}. \end{aligned}\right\} \tag{8.1}$$

PROPOSITION 6. *CWOF and CWOP take place provided that LBF (8.1) and its initial perturbation $\widetilde{\omega}_0$ obey the following inequality:*

$$Y < 1/(2 + \sqrt{4 + \ln^2 X}), \quad X \geqslant c_1, \tag{8.2}$$

where variables X and Y are

$$X \equiv c_1|\widetilde{\omega}_0|^+\sqrt{L/\mathscr{I}_0}, \quad Y \equiv C_0\sqrt{\mathscr{I}_0},\ C_0 \equiv 4e\sqrt{\pi}\frac{(1 + L^2)}{LU^-}\sqrt{1 + \frac{4L^2Q_c^2}{(U^-)^2}}. \tag{8.3}$$

There is a minor difference with the definition of X in (B 14); however, the inequality $X \geqslant c_1 > 1$ remains always valid due to (B 11) with $p = 1$.

Proof. Every LBF (8.1) is nonlinearly stable (4.1), (4.14) with $C = 1$. The vorticity perturbation represents a 'passive admixture', so $\widetilde{\omega}(\boldsymbol{x}, t) = \widetilde{\omega}_0(\boldsymbol{a}, t_0)$ that gives $|\widetilde{\omega}|^+ = |\widetilde{\omega}_0|^+$ and

$$\widetilde{\omega}(\boldsymbol{x}, t) = 0 \text{ for every } \boldsymbol{x} \text{ when } t > \tau^+,\ J^+ < 1 \tag{8.4}$$

as $\boldsymbol{a}(\boldsymbol{x}, t)$ belongs to $\partial\mathscr{D}^{in}$ for every $\boldsymbol{x}$ when $t > \tau^+$. The equality (8.4) immediately leads to the important conclusion that CWOP implies CWOF. More exactly, CWOP

takes place before CWOF or they happen simultaneously if the vorticity perturbation is non-zero in every old particle.

In this case, the expressions for J^+ (6.15) are simplified to

$$J^+ = \mathscr{M}(\mathscr{I}_0, |\widetilde{\omega}_0|^+)(\nabla\tau_0)^+ < 1. \tag{8.5}$$

Its further simplification with the use of (8.3) yields

$$J^+ = Y(2 + \sqrt{4 + \ln^2 X}) < 1, \quad X \geqslant c_1.$$

Hence (8.2) immediately follows from Proposition 4.

The established 'neutral curve' $J^+ = 1$ on the plane (X, Y) is

$$Y = 1/(2 + \sqrt{4 + \ln^2 X}), \quad X \geqslant c_1. \tag{8.6}$$

It represents a slowly (logarithmically) decreasing monotonic function $Y \to 0$ as $X \to \infty$. Its maximin value is $Y^+ = 1/(2 + \sqrt{4 + \ln^2 c_1})$. It allows us to calculate the 'threshold value' of enstrophy. For example,

$$\sqrt{\mathscr{I}_0^*} \approx 3.5 \times 10^{-3} \tag{8.7}$$

for the homogeneous profile $U(y) \equiv 1$ with $L = 3$, $Q_c = 0$; the options with $Q_c \neq 0$ give $\mathscr{I}_0^*$ of the same order. For $Q_c \neq 0$ and large L we have $J^+ \sim L^3$ (8.5), so for LBF in long channels one can obtain much lower threshold values of enstrophy. The same is true for small U^-, where $J^+ \sim (U^-)^{-2}$. Our theory guarantees both CWOF and CWOP for $\mathscr{I}_0 \leqslant \mathscr{I}_0^*$. Note that the washout condition (8.2) admits arbitrarily high values of X. It means that both CWOF and CWOP still take place when the absolute value of initial vorticity $\widetilde{\omega}_0^+ \to \infty$, if $\mathscr{I}_0 \to 0$ as fast as it is required by (8.2).

At the same time changing X along any line $Y = \text{const} < Y^+$ on the (X, Y)-plane shows that for fixed enstrophy 'more diffused' vortex patches (with lower $\widetilde{\omega}_0^+$) are washed away, while more concentrated ones (with higher $\widetilde{\omega}_0^+$) can be trapped. It complies with the proven fact that a point vortex is always trapped in $\mathscr{D}$. Of course, one should keep in mind that the neutral curve (8.6) corresponds to a rough sufficient condition that can be greatly improved. However, there is some ground which allows us to guess that the asymptotic estimate $Y \sim 1/\ln X$ as $X \to \infty$ represents a final result.

Hence, LBF and UBF give us the examples where we are able to prove analytically that CWOF and CWOP happen in finite time. It is important that we can estimate this time interval as well as calculate the restriction (upper bounds) for the amplitudes of perturbations.

At this point we finish our analytical studies; the rest of the paper contains computational results aimed to support C1 and C2. In the next section we study the vortex trapping phenomenon of § 3 in the cases of distributed vorticity perturbations and more general basic flows.

9. Counterbalance between washout and trapping

In this section, we study the transition from CWOF and CWOP to the vorticity trapping and examples of flows that appear as the result of trapping. The main target is to study the relaxation of generic initial data to steady flows as it is proposed by the conjecture C1.

9.1. *Numerical procedure*

The computational solution of the problem (2.1)–(2.6) or (2.15)–(2.17) is performed by the vortex particle-in-cells method (for the description and references, see Cottet & Koumoutsakos 1999) with the additional use of the results by Hald (1979), Liu & Xin (2000) and Vera & Rebollo (2001). Let us outline the numerical procedure used; its detailed description is given in Govorukhin & Ilin (2008). At $t=0$ the equal number of particles N_p/N_c is placed in each cell. We choose the coordinates of particles inside each cell as random independent uniformly distributed quantities. The vorticity of each particle is a constant that matches the given initial or boundary data at the initial location of a particle. The total number of particles N_p is varied from 30 000 to 200 000. The flow domain $\mathscr{D}$ (2.2) is divided into $N_c = n_x \times n_y$ cells of the same size. The equations of motion for particles are written in Hamiltonian form:

$$\dot{x}_i = \psi_y(x_i, y_i, t), \quad \dot{y}_i = -\psi_x(x_i, y_i, t);\ i = 1, \ldots, N_p, \tag{9.1}$$

where x_i, y_i are coordinates of ith particle; the Hamiltonian (that coincides with ψ) at every instant obeys the linear Dirichlet problem:

$$\begin{aligned} -\Delta\psi &= \omega, \\ \psi\,|_{y=1} &= 1,\ \psi\,|_{y=0} = 0, \\ \psi\,|_{x=0} &= \psi^{in},\ \psi\,|_{x=L} = \psi^{out}, \\ \psi^{in}(y) &\equiv \psi^{out}(y). \end{aligned}$$

This problem is solved by Galerkin's method where the approximation for the streamfunction

$$\psi^{appr}(x, y, t) = \psi^{in}(y) + \sum_{i=1}^{n_x}\sum_{j=1}^{n_y} \psi_{ij}(t) \sin\left(\frac{i\pi x}{l}\right) \sin(j\pi y) \tag{9.2}$$

contains unknown coefficients $\psi_{ij}(t)$ $(i=1, \ldots, n_x,\ j=1, \ldots, n_y)$. In computations, we take $n_x, n_y = 15$ and $n_x, n_y = 30$ that corresponds to the number of terms 225 and 900; the results for these two cases are the same, which indicate the high quality of computations. Vorticity in every cell is interpolated by a third-order polynomial that is constructed by the method of least squares with the use of the particles currently located in a cell. The resultant piecewise continuous polynomial approximation of vorticity is employed to derive Galerkin's system of equations for $\psi_{ij}(t)$. For integration (9.1) we use the pseudo-symplectic integrator by Aubry & Chartier (1998). When a particle leaves $\mathscr{D}$, a new particle with the vorticity equal to its boundary value (2.5) is introduced at $\partial\mathscr{D}^{in}$ (with the same y); thus the total number of particles remains constant. All results presented below are checked to be numerically convergent: they reproduce themselves when a time step is divided by two, and the numbers of cells and particles are doubled. The results reproduce themselves quantitatively when the parameters of a problem are not close to their critical values (such as thresholds, bifurcation points, etc.). If the parameters are close these values, we can achieve only the qualitative reproduction. For all our computations we take $L=3$ and $H=1$ in (2.2), which physically gives neither too short nor too long channel.

We will use two important time scales: the lifespan T of a perturbation and the lifespan $\widehat{T}$ of material particles. T is defined as the decay time of an initial perturbation below the level $\max|\widetilde{\omega}(x_i, y_i)| < \epsilon = 10^{-2}$, where the maximum is taken over all N_p

particles; while $\widehat{T}$ is introduced as the instant when all N_p particles, that are initially in $\mathscr{D}$, leave it. The comparison of $\widehat{T}$ with τ^+ (6.6) suggests that $\widehat{T} \leqslant \tau^+$. One can say that T and $\widehat{T}$ represent the minimal time intervals required for CWOP and CWOF correspondingly. Apparently, the rapid enlarging of $\widehat{T}$ can be seen as the indication of the transition to the vorticity trapping. One more notation $t = T^+$ denotes the instant when we stop our computations; we chose it differently for different cases in order to achieve a 'physically instructive' state.

9.2. *The initial Gaussian-2 perturbations*

In § 3 the trapping of a point vortex has been discovered and described. The next logical question is: does similar phenomenon exist for concentrated vortices with the finite sizes of vortex cores? To address this question we first consider the problem (2.1)–(2.6) for QBF with $\boldsymbol{Q} = (1/3, 0, 2/3)$ (9.9) and the initial Gaussian-2 perturbations (IG2P)

$$\widetilde{\omega}(x, y, 0) = \sum_k A_k \omega_k^g(x - x_k, y - y_k), \quad \omega_k^g(x, y) \equiv \exp\left[-\mu_k (x^2 + y^2)^2\right]. \tag{9.3}$$

We use the 'Gaussian-2 function' $\omega_k^g(x, y)$ in order to enhance the vorticity concentration near the given points (x_k, y_k). In particular, $\mu_k = \text{const} > 0$ is taken large enough to make the initial vorticity effectively vanishing at $\partial\mathscr{D}$; the amplitudes A_k are chosen sufficiently large to guarantee the well-developed trapping of perturbations. As the first representative example, we take the set of parameters: $A_1 = 83.3$, $\mu_1 = -300$, $x_1 = 0.4$, $y_1 = 0.6$; $A_2 = -85.7$, $\mu_2 = -200$, $x_2 = 1$, $y_2 = 0.4$; $A_3 = 77$, $\mu_3 = -200$, $x_3 = 1.7$, $y_3 = 0.6$; $A_4 = -87.7$, $\mu_4 = -300$, $x_4 = 2.5$, $y_4 = 0.6$, and $T^+ = 30$. This initial data are deliberately chosen in a generic form of different vortices with non-symmetrical initial positions; the aim is to demonstrate that the resulting steady flow does not necessarily possess the high degree of symmetry. The main result for this case is almost full trapping of vorticity and fast relaxation to a final steady state. The computations show that the major part of a vorticity perturbation is trapped in $\mathscr{D}$ and eventually (at $t = T^+$) it relaxes to four recirculation zones attached to $\partial\mathscr{D}^{\pm}$ (figure 2*a*). In figure 3(*c*), we present the trajectories of all four vorticity maxima as they move to their steady positions that become the centres of four recirculation zones. At the same time, figure 3(*a*, *b*) shows that the total amounts of vorticity $\Gamma(t)$ and enstrophy $\mathscr{I}(t)$ rapidly relax to their steady values (and finally perform small oscillations about these values). Also, we check the degree of steadiness of a vortex configuration in figure 2(*a*) by placing the computed pairs $(\Omega(x, y, T^+), \Psi(x, y, T^+))$ on the (Ω, Ψ) plane. For a steady flow such pairs must form a curve or a system of curves while our result in figure 2(*b*) displays a system of blurred curves. The thickness of each curve is of the order of several percents of the typical values of Ω or Ψ; this relative thickness can be considered as 'the measure of unsteadiness' that is likely to be produced the by errors of the used numerical method. For this example we can conclude that the relaxation to steady final positions and to the steady values of Γ and $\mathscr{I}$ is efficient and fast, while the final vorticity distribution inside a recirculation zone is only 'almost steady'. Studying the small-scale structure of the vorticity field in figure 2(*a*) shows that it gradually approaches the limiting steady states only for large scale motions, while small-scale motions form 'turbulent layers' around 'almost steady' vortex cores. However, one can consider that this result supports C1.

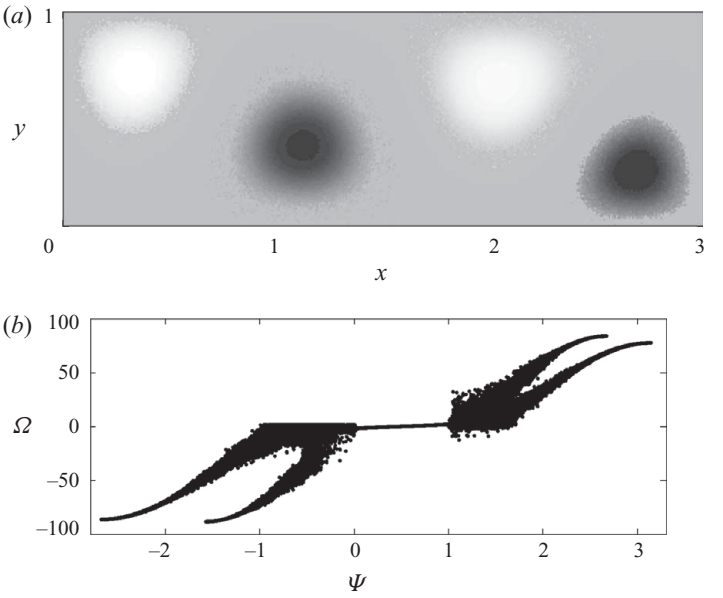

FIGURE 2. (*a*) 'Almost steady' vorticity distribution in QBF $\boldsymbol{Q} = (1/3, 0, 2/3)$ (9.9) where each vortex core is surrounded by a layer of small-scale 'turbulent' motions; here and in all similar figures below the intensity of grey colour reflects the value of vorticity: the darker (lighter) tones show more negative (positive) vorticity. (*b*) The computed pairs (Ψ, Ω) form blurred curves.

9.3. *The examples of a single vortex patch*

In the previous example we have considered a particular case of four concentrated vortices, where each vortex has a large amplitude and a small effective cross-section of a core. The natural question is: does similar phenomenon exist for a single vortex patch where vorticity is not necessarily high and the initial position can be varied within $\mathscr{D}$? To address this question we study the problem (2.1)–(2.6) for UBF with the initial perturbation in the form of a circular vortex core of radius r_0 centred at x_c, y_c:

$$U(y) \equiv 1, \tag{9.4}$$

$$\widetilde{\omega}_0(x, y) = \begin{cases} A \exp(-\gamma r^2) & \text{if } r < r_0 \\ 0 & \text{if } r > r_0 \end{cases}, \quad \mathscr{I}_0 = \frac{\pi A^2}{2\gamma}[1 - \exp(-2\gamma r_0^2)], \tag{9.5}$$

where A and γ are constants, $\mathscr{I}_0$ is initial enstrophy (2.18); $r^2 \equiv (x - x_c)^2 + (y - y_c)^2$. Usually vortex patches possess constant vorticity (Saffman 1992). However the numerical method we use generates maximal errors at the discontinuities of ω; therefore the distribution of ω inside the patches (9.5) is chosen to make those discontinuities small. We accept that an initial vortex core does not touch any part of $\partial\mathscr{D}$, which is $r_0 < x_c < L - r_0$, $r_0 < y_c < 1 - r_0$. We solve the problem (2.1)–(2.6), (2.16), (2.17), (9.4), (9.5) for the following values of parameters: $\gamma = 40$, $r_0 = 0.2$, $x_c = 0.3$, four selected amplitudes $A = 10, 20, 40, 50$ and a number of y_c obtained by the equipartition of the interval $0.21 < y_c < 0.79$. One can see that for the chosen parameters the perturbation (9.5) is not small: in terms of maximum velocity it is about ten times higher than the basic flow (9.4).

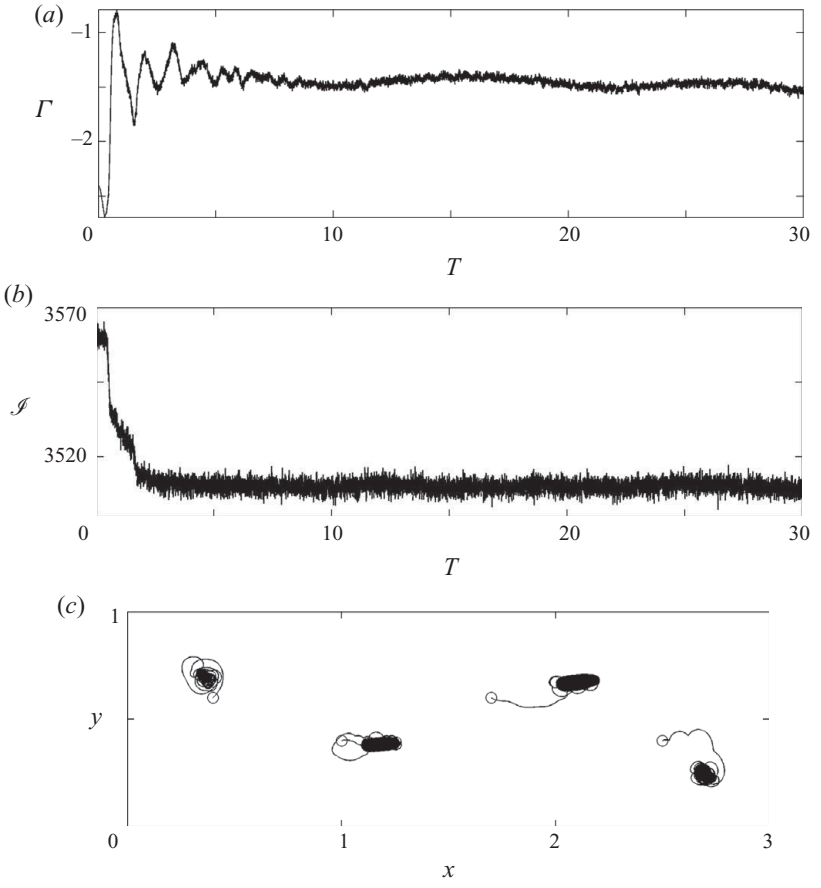

FIGURE 3. For the case of figure 2: (*a*) $\Gamma(t)$, (*b*) $\mathscr{J}(t)$, (*c*) the trajectories of four vorticity maxima as they move and become the centres of recirculation zones.

The main results are

(i) Our computations confirm the existence of the trapping of distributed vorticity which can manifest itself in many flow regimes ranging from the complete washout (figure 4) to almost complete trapping (figure 5). Figures 4 and 5 show the evolutions of streamlines and vorticity fields. For the chosen interval of parameters the trapping is always partial: a part of vorticity is washed away, while its remaining part is rejected from $\partial\mathscr{D}^{out}$ and moves back to $\mathscr{D}$.

(ii) In figure 4, $y_c = 0.4$, so the initial vortex is placed close to the middle of a channel. The result is a rapid CWOP ($T^+ = 2.3$) with a minor delay of vorticity just before $\partial\mathscr{D}^{out}$ as it is seen in the frame $t = 2.1$.

(iii) In figure 5, $y_c = 0.79$ the initial vortex with $r_0 = 0.2$ almost touches $\partial\mathscr{D}^+$. Computations show its rejection from $\partial\mathscr{D}^{out}$ and subsequent movement along a slowly converging trajectory (figure 6*a*), where the motion of the centre of vorticity is presented. The small-scale oscillations of the trajectory correspond to the rotational frequency of a vortex core. The total amount of vorticity Γ in $\mathscr{D}$ as a function of time is shown in figure 6(*b*). One can see that the vortex sheds a significant portion of vorticity during its first interaction (collision) with $\partial\mathscr{D}^{out}$, while the subsequent decrease of Γ is slow. Here $T^+ = 400$ is long enough to make visible the slow

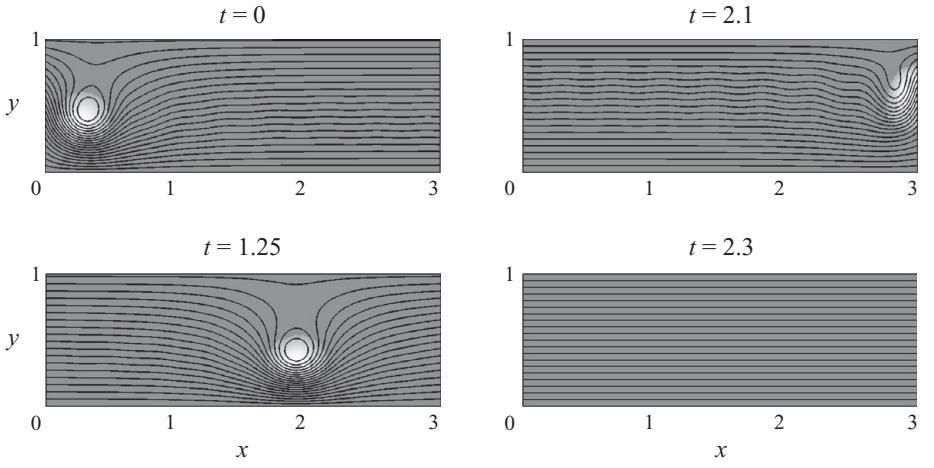

FIGURE 4. Developing CWOP for a vortex patch. The time-evolution of streamlines and vorticity for the vortex patch (9.5) with $r_0 = 0.2$, $A = 40$, $(x_c, y_c) = (0.3, 0.4)$ in UBF.

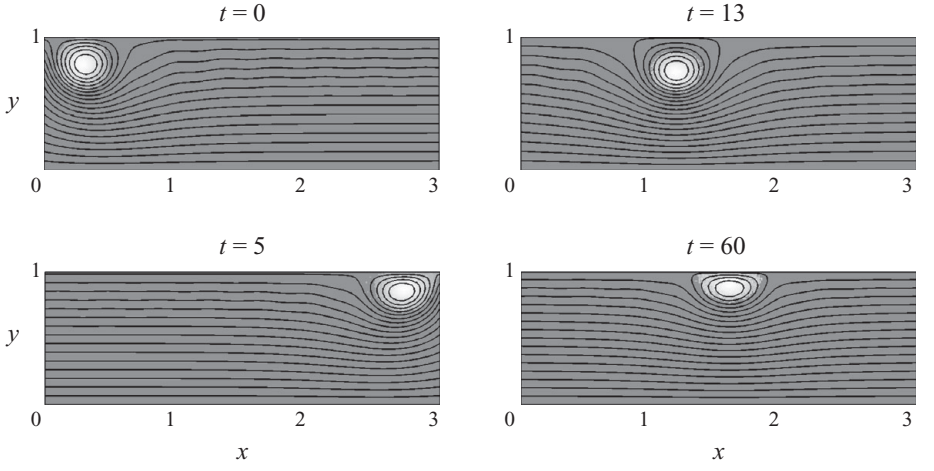

FIGURE 5. The 'almost complete' trapping of a vortex patch. The time evolution of streamlines and vorticity for the vortex patch (9.5) with $r_0 = 0.2$, $A = 50$, $(x_c, y_c) = (0.3, 0.79)$ in UBF.

convergence of the trajectory and the slow decrease of $\Gamma(t)$. It is instructive to note that the starting part of the trajectory in figure 6(*a*) is very close to the trajectory of the point vortex with the same Γ that is shown as the bold curve in figure 1.

(iv) The results for $A = 10$, 20, 40 and 50 are collected on the plane (y_c, T) (figure 7) where each point corresponds to full evolution from an initially perturbed flow (9.5) to UBF. The appearance of large $\widehat{T}$ and T indicates the transition to the vorticity trapping; $T < \widehat{T}$ since we consider UBF. The function $T(y_c)$ is monotonically increasing in all cases. All regimes for $A = 10$, 20 exhibit CWOP, while $A = A^* \backsimeq 40$ is the threshold value where the trapping appears for $y_c^* \simeq 0.79$. (We denote all threshold values of parameters with asterisks.) For $A = 50$, the trapping is well developed: T grows drastically when y_c^* approaches $y_c^* \simeq 0.63$. For $y_c > y_c^*$, we always observe the trapping. One can observe the fast decrease of y_c^* with the increase of A.

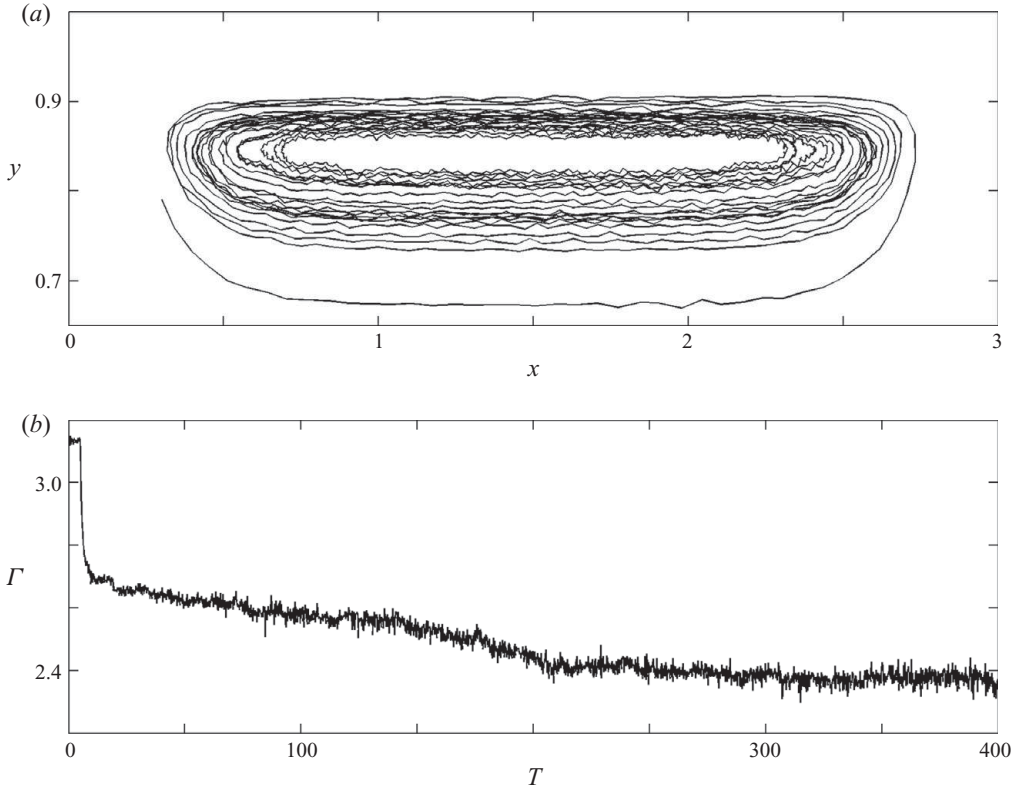

FIGURE 6. For the flow in figure 5: (*a*) the motion of the centre of vorticity along a slowly converging trajectory; (*b*) the total amount of vorticity $\Gamma(t)$ in $\mathscr{D}$.

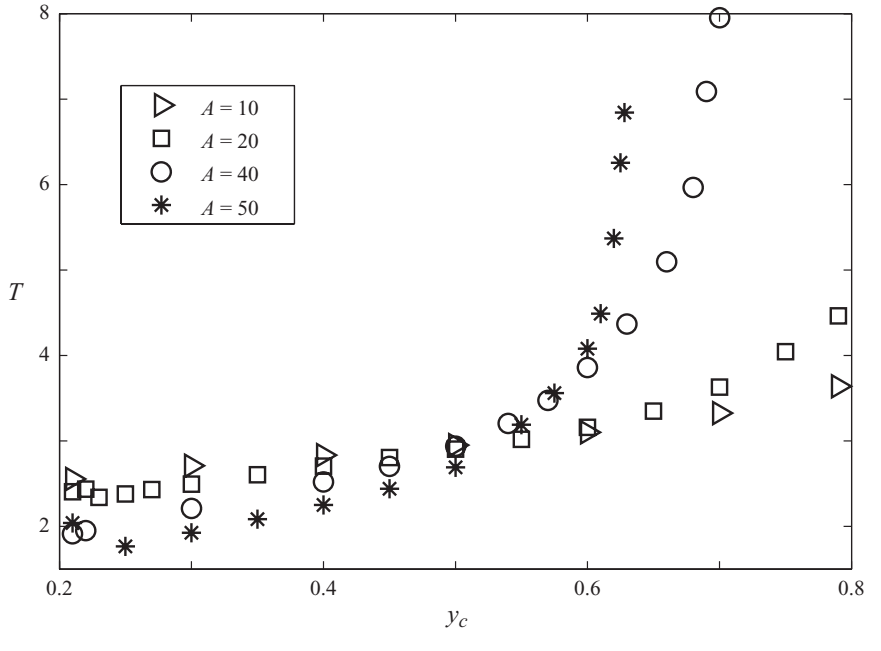

FIGURE 7. The lifespan $T(y_c)$ of the initially circular vortex patch (9.5) centred at $(0.3, y_c)$ with $r_0 = 0.2$, $A = 10, 20, 40$ and 50 in UBF.

(v) For $y_c = 1/2$, the lifespan $T \approx \tau_0^+ \equiv L/U_u = 3$ for all A (figure 7). It corresponds to the washout time for a passive admixture/tracer: indeed, in this case the distances to the nearest mirror images $-\Gamma$ across $\partial\mathscr{D}^{\pm}$ are approximately the same (see § 3). For $y_c < 0.5$ the patch is closer to the washing-oriented wall $\partial\mathscr{D}^+$ (3.2), hence $T < \tau_0^+$. On the contrary, $y_c > 0.5$ puts the vortex patch under the dominating influence from the trapping-oriented wall $\partial\mathscr{D}^-$ (3.2), hence $T > \tau_0^+$.

(vi) For $y_c = 0.79$, the threshold value is $A^* \backsimeq 40$ gives $\mathscr{I}_0^* \approx 6.84$ while computations of the full threshold curve $A^* = A(y_c^*)$ on the plane (A, y_c) is beyond the scope of this paper. One can see that this value of A^* is much greater than our analytical low bound (8.7). We are going to discuss this question later.

(vii) For $A > A^*(y_c^*)$, the amount of trapped vorticity rapidly increases with the growth of both A and y_c. One can evaluate the amount of trapped vorticity by the value

$$\delta\Gamma(T^+) = \Gamma(T^+)/\Gamma(0), \quad \delta\mathscr{I}(T^+) = \mathscr{I}(T^+)/\mathscr{I}(0); \quad \Gamma \equiv \int_{\mathscr{D}} \omega \, dx \, dy. \tag{9.6}$$

For the amplitudes $A = 10, 20, 40$, we choose $T^+ = T$, so at T^+ both $\delta\mathscr{I} = \delta\Gamma = 0$. For $A = 50$, $y_c = 0.79$ (the initial position closest to $\partial\mathscr{D}^+$), we choose $T^+ = 400$. Then we obtain $\delta\Gamma(400) \approx 0.812$, $\delta\mathscr{I}(400) \approx 0.915$. One can see that almost all vorticity is trapped for $A = 50$.

(viii) In the dynamics of vortex patches one can observe asymptotically stable flows that support C1. The relaxation to UBF is fast, while the cases of vorticity trapping show a slow relaxation. The variety of trapping regimes is very large and challenging to explain.

9.4. *The examples of initially harmonic perturbations*

The previous case of a vortex patch in a homogeneous flow (9.4) and (9.5) can be seen as the straightforward generalization of the motion of a point vortex (figure 1), hence the trapping can be expected. The next question arises: does the trapping take place for generic initial perturbations and for general basic flows? In order to address this question, we have computed three sets of examples of initially harmonic perturbations (IHP) in the basic flows (2.13):

$$U(y) = Q_p U_p(y) + Q_c U_c(y) + Q_u, \tag{9.7}$$

$$\widetilde{\omega}(x, y, 0) = A \sin(\pi k x/L) \sin(\pi m y), \quad \mathscr{I}_0 = LA^2/4, \tag{9.8}$$

where A is amplitude, (k, m) are two integer wavenumbers, and $\mathscr{I}_0$ is initial enstrophy. We have considered the following basic flows:

QBF: The symmetric 'forward-oriented' quadratic basic flow (7.7) with $\boldsymbol{Q} = (Q_p, Q_c, Q_u) = (1/3, 0, 2/3)$ in (2.13) and (9.7):

$$U(\hat{y}) = 7/6 - 2\hat{y}^2, \quad -1/2 \leqslant \hat{y} \equiv y - 1/2 \leqslant 1/2, \tag{9.9}$$

$$K = 4, \; U^- = 2/3, \; U^+ = 7/6, \; \Omega^{\pm} = \pm 2, \; \tau_0^+ = 9/2 = 4.5, \; \tau_0^- = 18/7, \tag{9.10}$$

where $\tau_0^{\pm}$ and $\Omega^{\pm}$ are the maxima and the minima of $\tau_0(L, y)$ (6.8) and $\Omega(y)$ over $0 \leqslant y \leqslant 1$.

UBF: The uniform basic flow $U(y) \equiv 1$, $\boldsymbol{Q} = (0, 0, 1)$.

LBF: Two linear basic flows $\boldsymbol{Q} = (0, Q_c, Q_u)$ (2.13) chosen as $(Q_c, Q_u) = (1/3, 2/3)$ and $(Q_c, Q_u) = (2/3, 1/3)$ with $-1/2 \leqslant \hat{y} \equiv y - 1/2 \leqslant 1/2$:

$$U_1(\hat{y}) = 1 + \tfrac{2}{3}\hat{y}, \quad U_2(\hat{y}) = 1 + \tfrac{4}{3}\hat{y}, \quad \widetilde{\omega}_0 = -A \sin\tfrac{3\pi x}{L} \sin 2\pi\hat{y}. \tag{9.11}$$

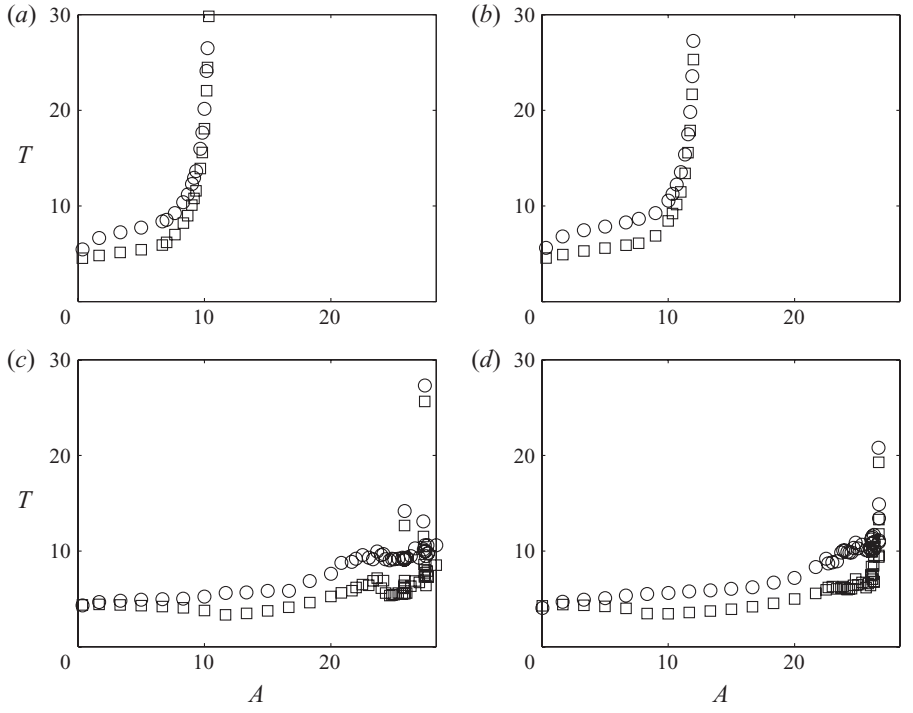

FIGURE 8. The lifespan $T(A)$ (circles) and the lifespan $\widehat{T}(A)$ of material particles (squares) for IHP+QBF with four different perturbations (9.8) with (k, m): (*a*) (1, 1), (*b*) (2, 1), (*c*) (2, 2), (*d*) (3, 2).

The main results are

(i) Figure 8(*a–d*) show $T(A)$ (circles) and $\widehat{T}(A)$ (squares) computed for IHP+QBF (9.9), (9.8) for four different pairs (k, m): (*a*) (1, 1), (*b*) (2, 1), (*c*) (2, 2), (*d*) (3, 2). One can see that for the amplitudes just below the thresholds $A < A^*$ both $T(A)$ and $\widehat{T}(A)$ drastically increase; this increase leads to the trapping for $A > A^*$ ((*a*) $A^* \approx 11$, (*b*) $A^* \approx 13$, (*c*) $A^* \approx 27$ and (*d*) $A^* \approx 28$).

(ii) To be more specific we consider the case figure 8(*c*) with $(k, m) = (2, 2)$ for four selected amplitudes $A = 35/3, 80/3, 84/3, 100/3$. For the smallest amplitude $A = 35/3$ the perturbation is rapidly and completely washed out, its lifespan T is only slightly longer then τ_0^-, so $\tau_0^- \leqslant T \approx 4.05 \leqslant \tau_0^+$ (9.10), so the complete washout is only slightly slower than for the case of a passive admixture. The second amplitude $A = 80/3$ (figure 9) is just below the threshold ($A^* \approx 81/3$). One can see that vorticity is drastically retarded near $\partial\mathscr{D}^{out}$, however the flow is eventually able to wash it out of $\mathscr{D}$ completely. The lifespan $T \approx 9.60$ is approximately twice as long as in the previous case. This time is already sufficient for the initially small (numerically introduced) asymmetry to grow up to noticeable asymmetric structures (we recall that the analytically prescribed functions (9.8) are symmetric or antisymmetric with respect to the reflections about two axes $x = L/2$, and $y = 1/2$, but in the computations these functions possess at $t = 0$ small asymmetries due to the random distribution of particles in each cell; since the cells are small, initial asymmetries are also small). The amplitude $A = 84/3$ is slightly above A^*, hence the trapping appears: $\partial\mathscr{D}^{out}$ partially rejects vorticity, it moves upstream and forms a single recirculation zone attached to

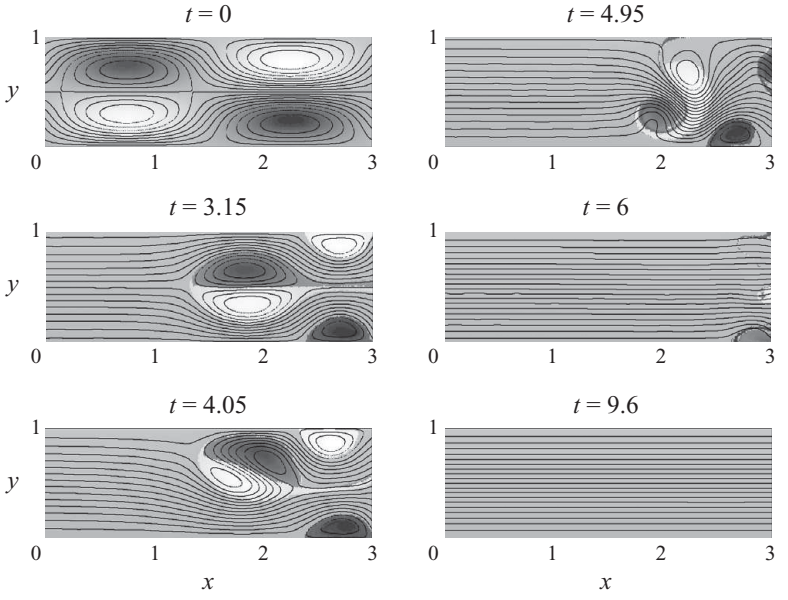

FIGURE 9. The process of CWOP for IHP+QBF just before the threshold. The evolution of streamlines and vorticity for the perturbation (9.8) with $(k, m) = (2, 2)$, $A = 80/3$.

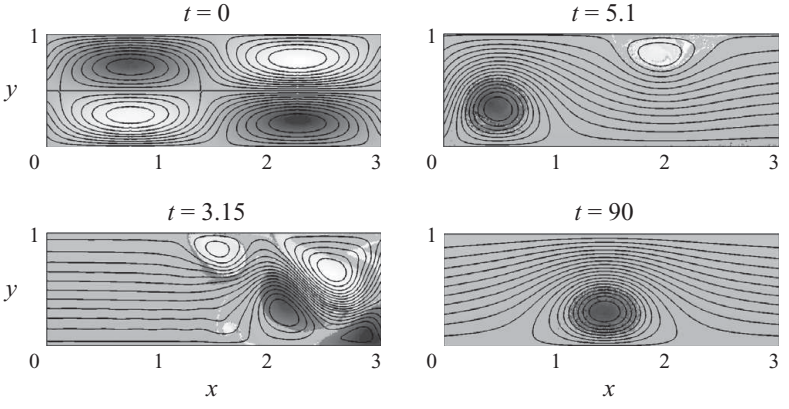

FIGURE 10. *The fully developed trapping for* IHP+QBF. The evolution of streamlines and vorticity for the perturbation (9.8) with $(k, m) = (2, 2)$, $A = 100/3$.

$\partial\mathscr{D}^-$. For the largest amplitude $A = 100/3$ (figure 10) the trapping is well developed; in order to illustrate it in detail we have chosen $T^+ = 100$. The trapped vorticity eventually relaxes to a single recirculation zone attached to $\partial\mathscr{D}^-$. Figure 11(a–c) shows the important characteristics of this relaxation process: figure 11(a, b) gives $\Gamma(t)$ and $\mathscr{I}(t)$, while figure 11(c) shows the trajectory of one vorticity maximum as it moves and becomes the centre of a single recirculation zone. Again, we check the degree of steadiness of this vortex by presenting the mapping $(x, y) \mapsto (\Psi, \Omega)(x, y, T^+)$ in figure 11(d). The image of the through-flow zone (where $0 \leqslant \Psi \leqslant 1$) represents a distinct line while the image of vortex core (where $\Psi \leqslant 0$) appears as a more general set. Hence only a partial relaxation takes place: the global parameters in figure 11(a, b) do relax to their steady values while vorticity in the core still undergoes an unsteady motion.

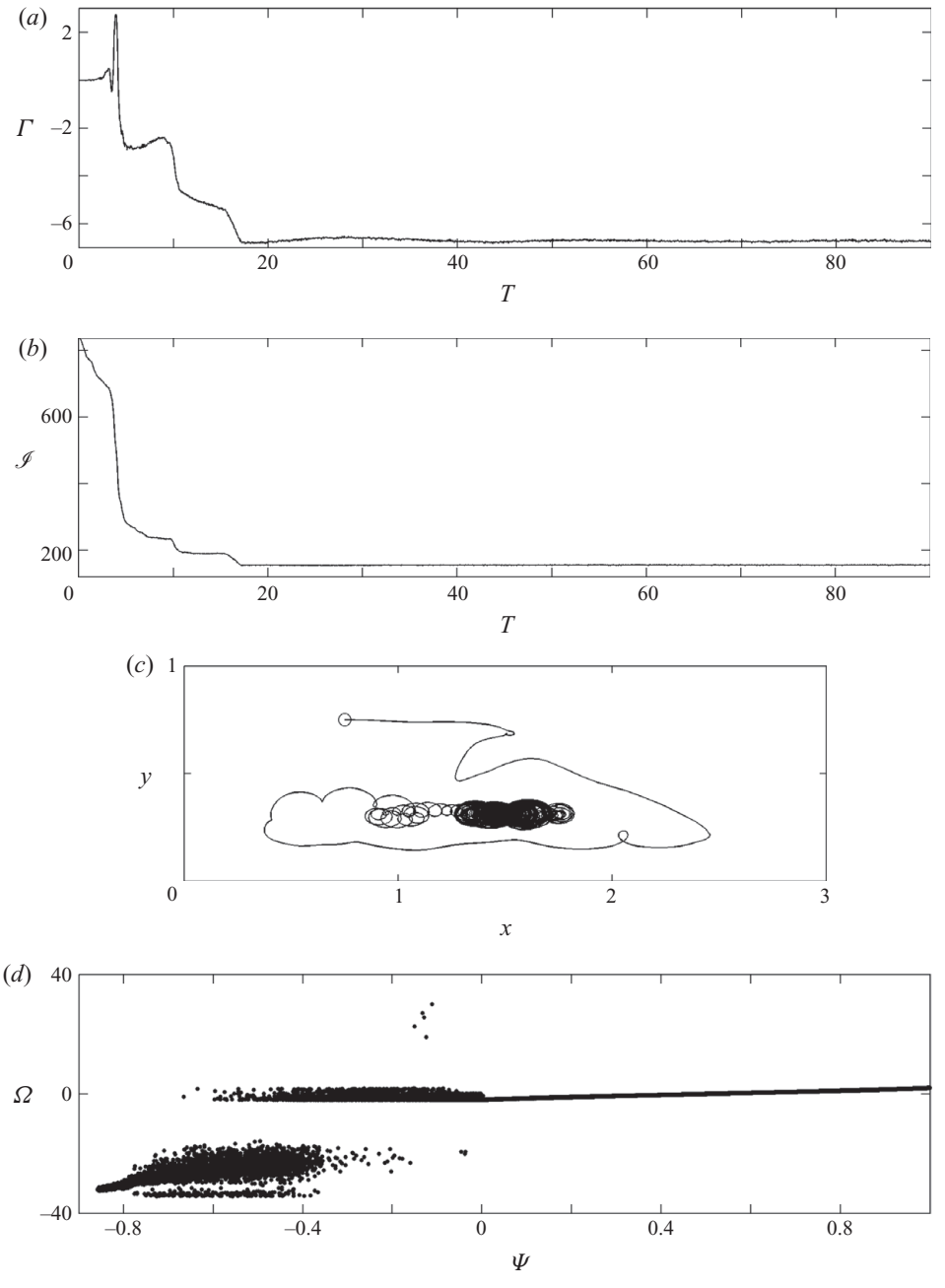

FIGURE 11. For the case of figure 10: (*a*) $\Gamma(t)$; (*b*) $\mathscr{I}(t)$; (*c*) the trajectory of one vorticity maximum as it moves and becomes a centre of a recirculation zone; (*d*) the computed pairs (Ψ, Ω) form a distinct curve in a through-flow zone and a 'cloud' of points in a recirculation zone.

(iii) The trapping of IHP represents the variety (depending on parameters) of partial trappings: the main part of vorticity is always washed out (figure 11*b*) and the trapping occurs in the vicinities of the outlet vertex points. The qualitative evolution of flows in these vicinities is described as the vortex-outlet-wall interaction in § 3. The final recirculation zones are always trapping-oriented (3.2), while washing-oriented

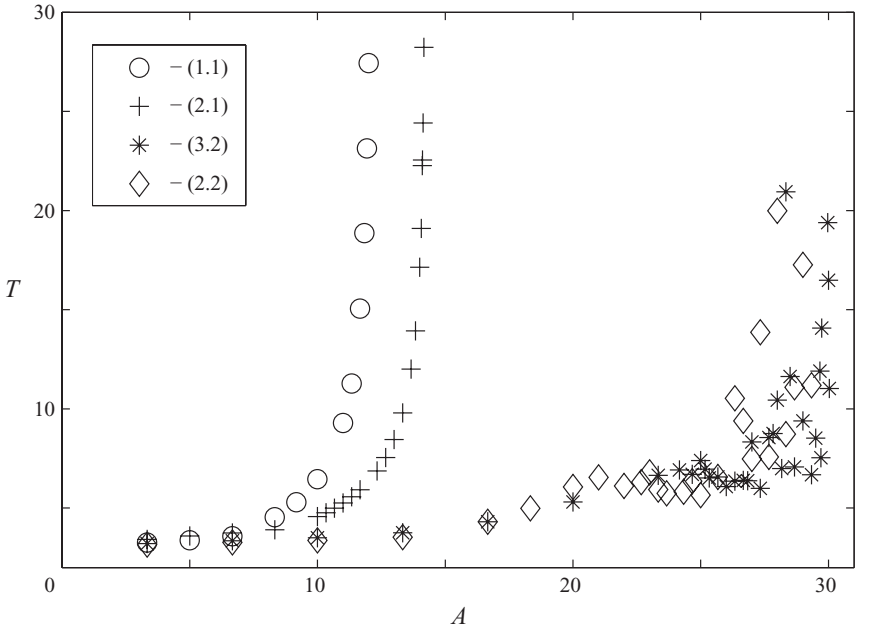

FIGURE 12. The lifespans $T(A)$ for IHP+UBF. The perturbations (9.8) have the wavenumbers $(k, m) = (1, 1)$, $(2, 1)$, $(2, 2)$ and $(3, 2)$.

vorticity (and all vorticity from the central part of the channel $\mathscr{D}$) is always washed out.

(iv) Figure 12 shows $T(A)$ for IHP+UBF with the same (k, m) as in IHP+QBF, figure 8. The modes are marked as: $(1, 1) \mapsto \circ$, $(2, 1) \mapsto +$, $(2, 2) \mapsto \diamond$, $(3, 2) \mapsto *$. There is a rapid growth of the perturbation lifespans for all modes as their amplitudes approach critical values. It shows how the increasing of lifespans leads to the vortex trapping.

(v) Figure 13 shows the lifespans $T(A)$ for IHP+LBF (9.11) for $(k, m) = (3, 2)$. We have chosen four selected initial flows that consist of the basic flows U_1, U_2 (see (9.11)) and the perturbations $\pm\widetilde{\omega}_0$:

$$\left.\begin{aligned} &(U_1, \widetilde{\omega}_0),\ (U_1, -\widetilde{\omega}_0),\ (U_2, \widetilde{\omega}_0),\ (U_2, -\widetilde{\omega}_0), \\ &\widetilde{\omega}_0 = -A \sin(3\pi x/L) \sin 2\pi\hat{y}; \quad -1/2 \leqslant \hat{y} \equiv y - 1/2 \leqslant 1/2, \end{aligned}\right\} \tag{9.12}$$

where $\widetilde{\omega}_0$ is antisymmetric in $\hat{y}$. In addition there are the asteriated points in figure 13 that repeat asterisks in figure 12 for UBF; they allow to compare the results for different profiles.

(vi) The qualitative behaviour of all functions $T(A)$ given in figures 8, 12 and 13 is similar to each other. All functions $T(A)$ are monotonically increasing (with some minor exceptions). Each graph $T(A)$ consists of two qualitatively different parts. The left part (the interval of linearity for relatively low A) represents the region of a slow growth; at $A \to 0$ the lifespan of perturbations $T \to \tau_0^- = L/U^-$ which corresponds to the advection of small vorticity perturbations as a passive admixture. It is physically natural that the value of T is linked to the minimal velocity $\min_y U(y) \equiv U^-$. Inside each interval of linearity the value of T increases slowly and (for example) can double its original value. The right part (a subcritical part, or the interval of nonlinearity)

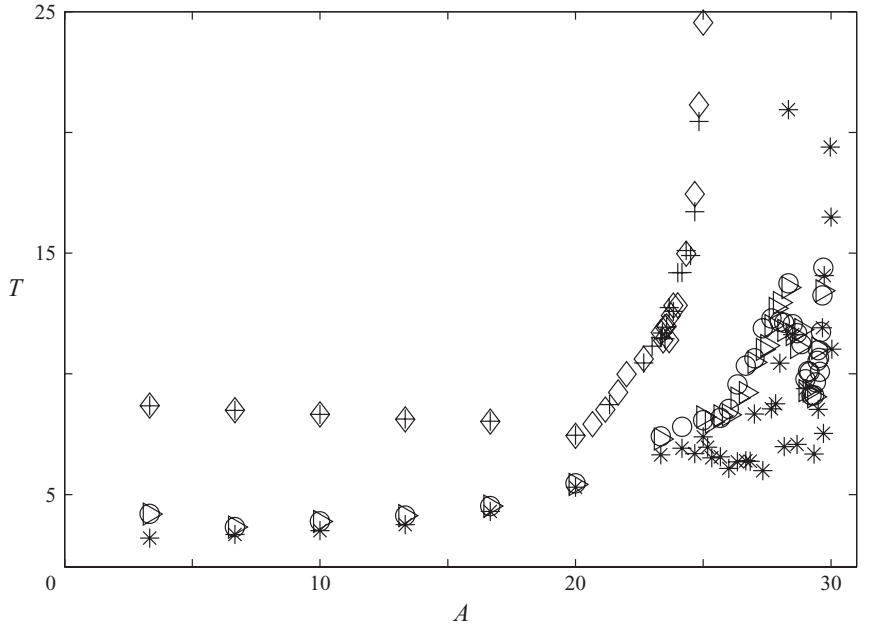

FIGURE 13. The lifespan $T(A)$ for IHP+LBF with the perturbations $\pm\widetilde{\omega}_0$ (9.12) and profiles $U_1(y)$ and $U_2(y)$ (9.11) for four selected flows shown as: $(U_1, \widetilde{\omega}_0) \mapsto \triangleright$, $(U_1, -\widetilde{\omega}_0) \mapsto \bigcirc$, $(U_2, \widetilde{\omega}_0) \mapsto +$, $(U_2, -\widetilde{\omega}_0) \mapsto \diamond$; the asteriated points repeat asterisks in figure 12.

shows the rapid increase of $T(A)$ that continues up to the threshold amplitude A^*, where formally $T \to \infty$.

(vii) For $A > A^*$ the amount of trapped vorticity rapidly increases with A–A^*. As an example one can evaluate $\delta\Gamma$ and $\delta\mathscr{I}$ (9.6) for IHP+QBF (figures 9 and 10). For the amplitudes $A = 35/3, 80/3$ we choose $T^+ = T$ so $\delta\Gamma = \delta\mathscr{I}(T) = 0$, while for $A = 84/3$ and $A = 100/3$ the results are $\delta\mathscr{I}(60) \approx 0.099$ and $\delta\mathscr{I}(60) \approx 0.186$ that reveal a rapid growth.

(viii) For IHP+QBF (figure 8) there is a systematic difference $T \geqslant \widehat{T}$, i.e. perturbations can stay in $\mathscr{D}$ (for finite time), while all initial material particles have been already washed out. To explain this feature, one should take into account that according to (2.16) the vorticity perturbations of both UBF and LBF are conserved in every material particle; therefore for these profiles always $T = \widehat{T}$. On the contrary, in (9.7) and (9.9) we deal with $\Omega_y \neq 0$, so vorticity perturbations in (2.16) can travel between particles as some vorticity waves and one can observe an upstream influence. Its mathematical description is still unknown since the related spectral theory is underdeveloped despite the progress made by Morgulis & Yudovich (2002). They have shown that the spectral theory for (2.16) and (2.17) is very different from the conventional theory for infinite channels.

(ix) In figure 8 one can also observe that the critical amplitudes A^* for the trapping of particles and for the trapping of perturbations coincide with each other. It shows that perturbations cannot be trapped unless there are some trapped material particles in $\mathscr{D}$ and vice versa.

(x) Figures 8 and 12 show that the value of A^*, considered as the function of wavenumbers (k, m) rapidly increases with m and not sensitive to k. It shows that the

washout of the larger (in y direction) vortices is much more difficult than the washout of the smaller ones. In particular in figures 8 and 12 one can see that the values of A^* for $m=1$ are two-three times lower than for $m=2$ and they do not depend on k.

(xi) Figure 13 shows that the function $T(A)$ most likely has the extended form

$$T = T(A, U^-, |\Omega|) \quad \text{with} \quad \partial T/\partial U^- < 0, \ \partial T/\partial |\Omega| > 0,$$

where the dependence T on U^- and the first inequality are mandatory, since for small perturbations ($A \to 0$) we always have $T \to \tau_0^- \equiv L/U^-$. As to the possible dependence of T on Ω, we can state here only the following: (i) it is clearly visible in figure 13 that mutually asymmetric perturbations $\pm\widetilde{\omega}_0$ (see (9.12)) produce the same T, therefore T can depend only on $|\Omega|$; (ii) this dependence is rather weak, since the asterisk, representing the results for UBF $|\Omega|=0$, are close to circles and triangles, which correspond to LBF with $|\Omega|=2/3$.

(xii) In figures 8 and 12 one can see that for all modes the threshold amplitudes A^* for UBF are systematically slightly higher than for QBF: they are approximately 12, 14, 27.5, 29 versus 11, 13, 27, 28. Since the Poiseuille part in the profile (defined in(9.9)) is relatively small (it is only 1/3 out of 1), it shows that a positive profile curvature enhances its trapping-efficiency. For the backward-oriented QBF (that we have also computed, but not presented here) the trapping-efficiency is lower then for UBF.

(xiii) For IHP+QBF with the lowest amplitude $A=35/3$ we have the rapid and complete washout. The corresponding initial enstrophy (9.8) $\sqrt{\mathscr{I}_0} \approx 18.32$ significantly exceeds the analytical estimation (8.7). In this connection we mention two facts: (*a*) A theoretical low bound have been obtained for arbitrary perturbations. The challenging problem to find the most dangerous perturbation among all possible perturbations with given $\mathscr{I}_0$ remains unsolved; (*b*) One can check that in our examples the trapping takes place when the basic flow is weaker than perturbations. For example, for IHP+QBF the ratio $|\widetilde{\omega}_0|^+/\Omega^+$ belongs to the interval from 2 to 10 with the similar ratio of velocities $|\widetilde{\boldsymbol{v}}_0^+|/U^+$. It shows that our computed examples are related to essentially nonlinear vortex dynamics, while the asymptotic stability theory in § 7 deals only with relatively weak nonlinearity, which corresponds to the smallness condition (6.15).

(xiv) We can conclude that all three examples: IG2P (9.3), the vortex patches (9.5) and IHP (9.8) support C1 and illustrate the variety of the relaxation processes.

10. Instantaneous filtration and steady separated flows

The computations of § 9 show that the obtaining of a high-quality steady separated solutions by the direct solving of Euler's equations is not feasible: a 'randomly' chosen initial datum ω_0 relax to steady states only partially. In contrast to these results the method of instantaneous filtration produces the quick convergence of numerical solutions to high-quality steady separated states. The first step of this method is solving an unsteady problem with given initial data until the instant $t_1 = T^+$ as in § 9. Then we take this solution at t_1 and perform instantaneous filtration of its vorticity distribution aimed to suppress the small-scale numerical noise. This filtration represents the sequence of three operations: (i) we average vorticity (that is originally given in the 'particles') over each cell with the use of a rectangular mesh (we use the cell size $h=0.01$); (ii) we reject the small spectral coefficients from the fast Fourier transformation (FFT)-image of averaged vorticity: the spectral coefficient $\widehat{\omega}_k$ is considered to be small if $|\widehat{\omega}_k/\widehat{\omega}_{max}| \leqslant 0.001$, where $\widehat{\omega}_{max}$ is the maximal

spectral coefficient; (iii) the inverse fast Fourier transformation (IFFT) is applied to reconstruct the improved field of vorticity. The filtrated vorticity field is taken as a new initial datum and the unsteady problem is computed (as in § 9) until $t_2 > t_1$, etc. In more detail: At $t = 0$ we chose a trial initial field $\omega_0 = \bar{\omega}_0$. Let ω_m be vorticity at the instant t_m that appears on the mth span of computations by the method of § 9.1 with the use of the initial datum $\omega|_{t=t_{m-1}} = \bar{\omega}_{m-1}$, where $\bar{\omega}_{m-1}$ is the smoothened field that appears as the result of filtrating ω_{m-1}. After few steps (say for $m = m_*$) we observe that $\omega_{m_*} = \bar{\omega}_{m_*} = \Omega$, where Ω is a high-quality approximation to a steady solution of Euler's equation with given YBC. It means that at the last span of our procedure we obtain the relaxation of the initial datum $\omega|_{t=t_{m-1}} = \bar{\omega}_{m-1}$ to a steady separated flow Ω. At the same time the dynamical link between Ω and ω_0 can be considered only as a reliable assumption. We emphasize that in all computations of this section we use only the method of § 9.1, i.e. we do not use any filtration procedure in solving unsteady Euler's equations. In all presented computations the required number of instantaneous filtrations $2 \leqslant m^* \leqslant 5$. The detailed description of the numerical procedures used in this section is given in Govorukhin & Ilin (2008).

In order to control the quality of our steady solutions we use three tests:

Test 1. The time-independence of all our solutions is controlled by the values of

$$\varepsilon_1 = \frac{\max_{s=t,\dots,t+\tau} \left| \int_{\mathscr{D}} (\omega(x, y, s) - \omega(x, y, t)) \, \mathrm{d}x \, \mathrm{d}y \right|}{\max_{s=t,\dots,t+\tau} \int_{\mathscr{D}} |\omega(x, y, s)| \, \mathrm{d}x \, \mathrm{d}y},$$

$$\varepsilon_2 = \left[\frac{\int_t^{t+\tau} \left(\int_{\mathscr{D}} (\omega(x, y, s) - \omega(x, y, t)) \, \mathrm{d}x \, \mathrm{d}y \right)^2 \mathrm{d}s}{\int_t^{t+\tau} \int_{\mathscr{D}} (\omega(x, y, s))^2 \, \mathrm{d}x \, \mathrm{d}y \, \mathrm{d}s} \right]^{1/2}.$$

We accept that our solution is 'computationally steady' after both ε_1 and ε_2 are less than 0.005 for $\tau = 10$. Once the procedure is completed we have the approximation for the steady solution that consists of the streamfunction $\Psi = \Psi(x, y)$ (in the Galerkin form (9.2)) and the vorticity $\Omega = \Omega(x, y)$ (which is given in 'particles'). Then we estimate the discrepancy of our solutions by one more parameter

$$\varepsilon_3 = \left[\frac{\sum_{i=1}^{n_x} \sum_{j=1}^{n_y} \left(\int_{\mathscr{D}} \left(\Psi_y \Delta\Psi_x - \Psi_x \Delta\Psi_y \right) \sin\left(\frac{i\pi x}{L} \right) \sin(j\pi y) \, \mathrm{d}x \, \mathrm{d}y \right)^2}{\sum_{i=1}^{n_x} \sum_{j=1}^{n_y} \left(\int_{\mathscr{D}} \Delta\Psi \sin\left(\frac{i\pi x}{L} \right) \sin(j\pi y) \, \mathrm{d}x \, \mathrm{d}y \right)^2} \right]^{1/2}$$

which is chosen to be less than 0.01 for all our solutions. Next, we employ two more tests; in both of them we require that relative errors are less than 0.01:

Test 2. There is always a functional dependence between Ω and Ψ for any planar steady inviscid flows; therefore all computed pairs $(\Psi(x, y), \Omega(x, y))$ must form a curve (or a system of curves) in the (Ω, Ψ)-plane. For our approximate steady solutions the pairs (Ψ, Ω) do form distinct (not blurred) curves with a high accuracy (figures 15 and 17).

Test 3. We have chosen $\psi^{in} \equiv \psi^{out}$ (2.10) and therefore in a numerical solution we must obtain $\omega^{in}(y) = \omega^{out}(y)$ for every $y \in (0, 1)$.

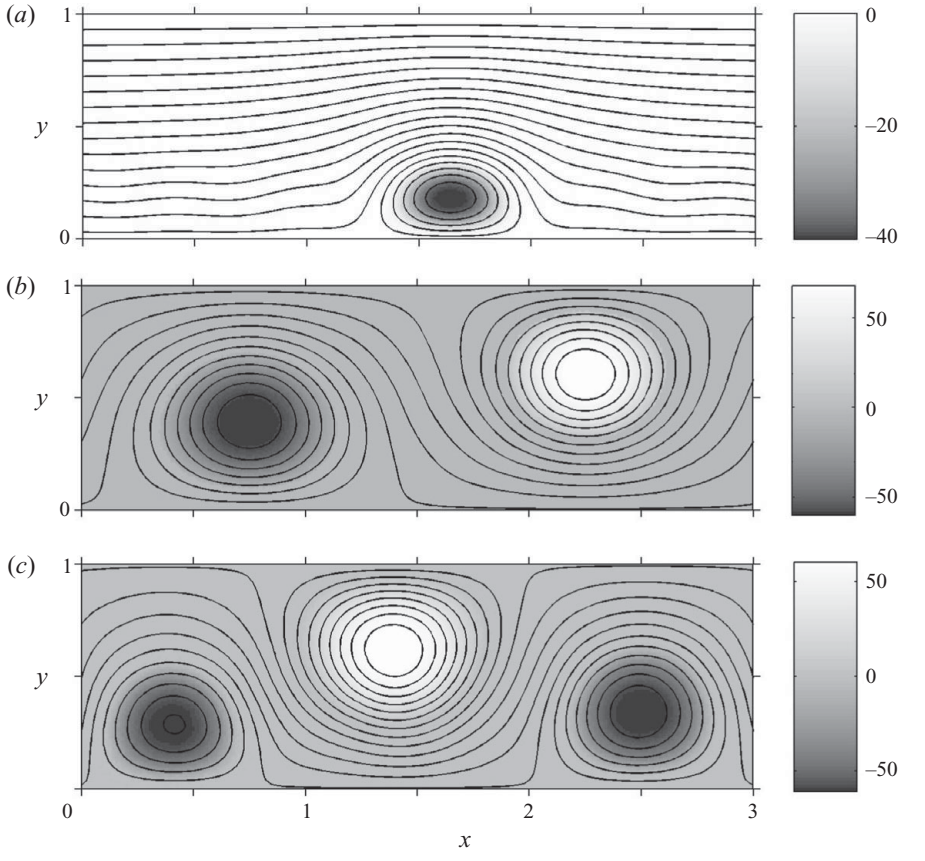

FIGURE 14. The streamlines and vorticity for three steady and stable separated flows which coexist with UBF $U(y) \equiv 1$: (*a*) one recirculation zone (single vortex); (*b*) two recirculation zones (dipole); (*c*) three recirculation zones (triple vortex).

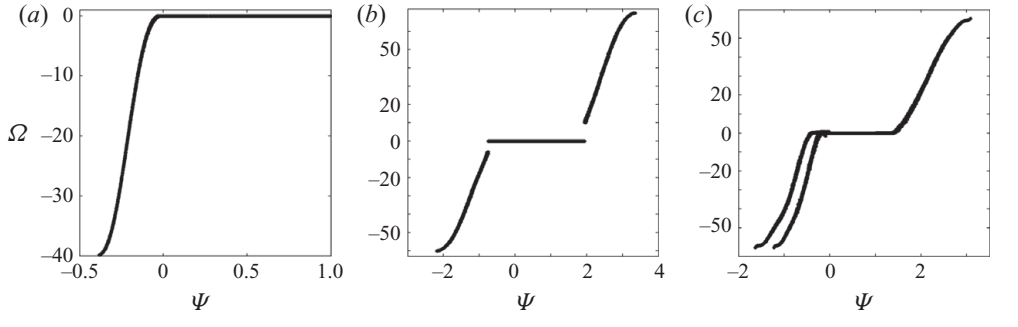

FIGURE 15. The function $\Omega(\Psi)$ for three steady and stable separated flows shown in figure 14.

The examples of steady solutions to the problem (2.1)–(2.6) obtained by the method of instantaneous filtration are shown in figures 14–17. These solutions correspond either to UBF or to QBF (9.9) with IG2P (9.3). Three steady flows co-existing with UBF and containing one, two and three vortices are shown in figures 14 and 15. One-, two-, three-, and four-vortex solutions co-existing with QBF are given in figures 16 and 17.

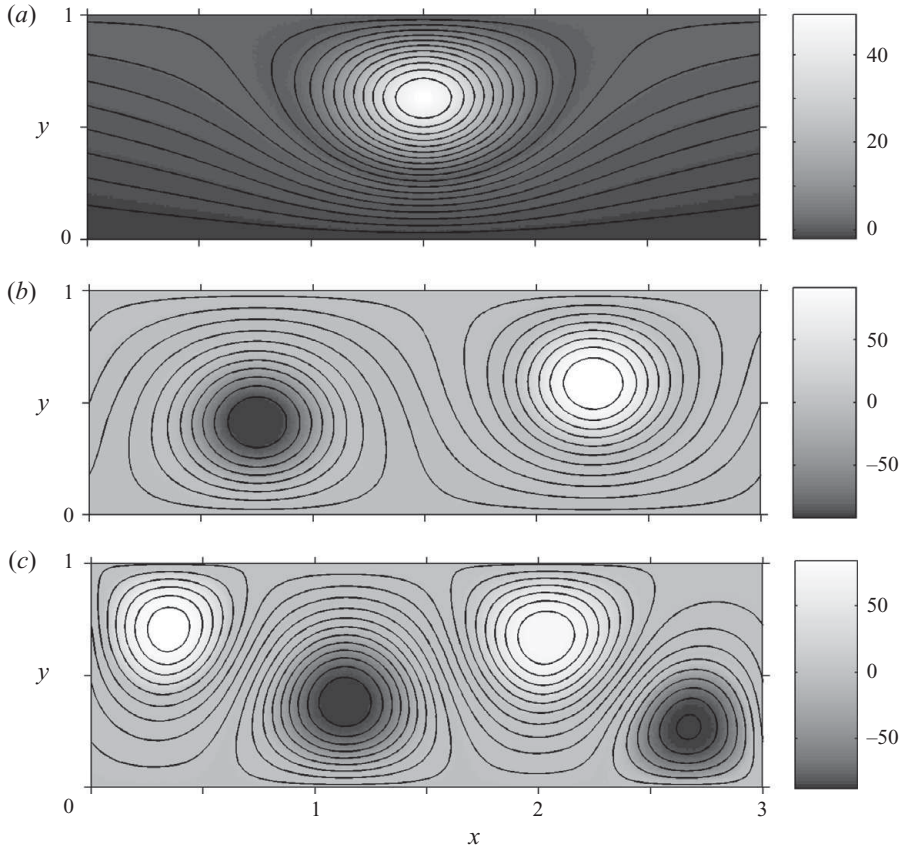

FIGURE 16. The streamlines and vorticity for steady and stable separated flows that coexist with QBF $\boldsymbol{Q} = (1/3, 0, 2/3)$: (a), (b) and (c) show one, two and four recirculation zones correspondingly.

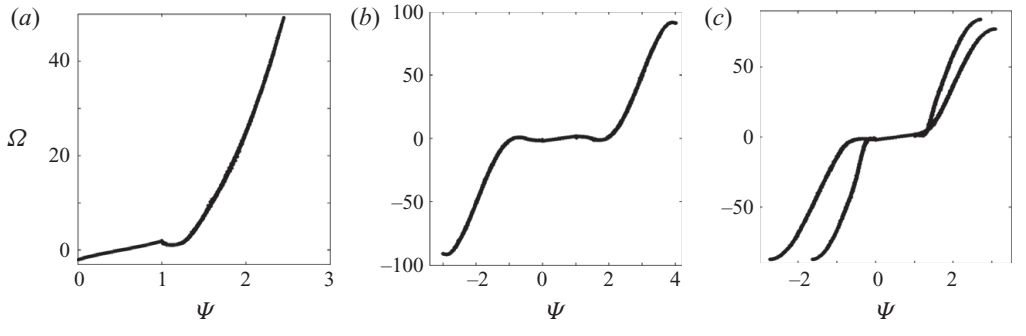

FIGURE 17. The function $\Omega(\Psi)$ for three steady and stable separated flows shown in figure 16.

Our comments on these results are

(i) The aim of the method of instantaneous filtration is to compute the high-quality steady solutions. The use of few instantaneous filtrations causes the loss of the direct link to initial data, and this is why we do not present these data explicitly. In order to ensure the rapid relaxation to the final states the parameters in (9.3) should match

the qualitative pattern of the final states. Naturally, the poor matching between initial conditions and the expected final states results in the longer time of relaxation or even in the relaxation to a different flow. If, say, we choose in (9.3) a wrong number of initial vortices then the relaxation pushes the excessive vortices out.

(ii) All three separated steady flows co-existing with UBF (figure 14) contain recirculation zones that are always attached to the trapping-oriented solid walls (3.2) and are separated by the irrotational through-flow zone (2.8). Figure 14(*a*) shows a single vortex, its $\Omega(\Psi)$ (figure 15*a*) is a single-valued and monotonic function. Figure 14(*b*) shows two vortices of different signs where $\Omega(\Psi)$ (figure 15*b*) is a single-valued and monotonic function that has discontinuities in the vorticity field. In this case we deliberately create the discontinuities by the cutting off the small values of $|\widetilde{\omega}|$ in the initial datum (9.3). The flow with three recirculation zones (bearing vorticity of alternating signs) is shown in figure 14(*c*). The corresponding $\Omega(\Psi)$ is multi-valued (figure 15*c*): it is different in two zones with negative vorticity and is monotonic inside each vortex core.

(iii) Figure 16(*a*, *b*) show one- and two-vortex flows co-existing with QBF (9.9) with $\Omega(\Psi)$ shown in figure 17(*a*, *b*). These results are qualitatively similar to that for UBF (figures 14 and 15). In addition, in figure 16(*c*) one can see the street of four vortices of alternating signs; their functions $\Omega(\Psi)$ (figure 17*c*) are again monotonic inside each vortex core. Figures 16(*c*) and 17(*c*) represent the improved version of figure 2, as it is obtained by the method of instantaneous filtration.

(iv) The graphs of $\Psi(\Omega)$ in figure 15(*b*, *c*) clearly show that vorticity cores occupy only the central parts of recirculation zones. It is well visible from the fact that in the through-flow zones $\mathscr{D}^{tf}$ (2.8) the values of a streamfunction are $0 \leqslant \Psi \leqslant 1$. Therefore all regions with $\Psi > 1$ and $\Psi < 0$ in figure 15(*b*, *c*) correspond to the interior of recirculation zones. For example in figure 14(*b*) the region $\Omega = 0$ covers almost all interval $-1 \leqslant \Psi \leqslant 2$; it shows that there are thick potential layers that surround the vortex cores inside each recirculation zone.

(v) In all cases figures 15 and 17 the functions $\Omega(\Psi)$ inside vortex cores are very close to the case $\alpha = 2$ (4.2) that is $0 < \epsilon \leqslant \mathrm{d}\Omega/\mathrm{d}\Psi \leqslant \lambda$ with $\lambda \approx 10$ and with any fixed ϵ. One can see that there are always regions with $\Omega = 0$ or points with $\mathrm{d}\Omega/\mathrm{d}\Psi = 0$ outside vortex cores. It means that all flows are only 'close to stable', so our sufficient stability criteria of Proposition 3 (see (4.2)) do not work. In order to prove the stability of the observed flows one should generalize Proposition 3 to the basic flows which contain: (i) discontinuous fields of $\Omega(\boldsymbol{x})$ (or its first derivatives); (ii) the large values of derivative $\mathrm{d}\Omega/\mathrm{d}\Psi > \lambda$; (iii) potential zones, where $\Psi(\Omega)$ mathematically is not defined. All these generalizations are very challenging. However the presented steady flows are stable with respect to the perturbations caused by unavoidable numerical errors. Indeed, all these flows are obtained as the steady time-limits of unsteady solutions. When we take these steady solutions as the initial data for an unsteady problems their further solving shows that they do not change over a long period of time.

(vi) We have analytically proven that the monotonicity of $\Omega(\Psi)$ (4.2) provides a sufficient condition for stability. This result generalizes the classical theorem by Arnold (1966) and its subsequent developments by Burton (1987), Vladimirov (1987), Vladimirov (1988), Morgulis & Yudovich (2002) and Shnirelman (1993). However, there are known 'counterexamples' to the Rayleigh–Arnold condition (see Rosenbluth & Simon 1964; Vladimirov 1978, 1979), which show the broad classes of linearly stable flows with $\Omega'(\Psi) = 0$ at an internal point. Our computational results indicate that there is another class of stable steady flows with $\Omega'(\Psi) = 0$ at least at two internal points (such as in figure 17*b*, *c*).

(vii) The computed steady regimes with vortex cores always coexist with the non-separated basic flows, which satisfy the same BC. Here we deal with the nonuniqueness of steady flows in a finite channel. The continuous changes of the parameters of initial data produce two types of results: the slow changes of final solutions and the jumps in final solutions. The slow changes lead to the appearance of the families of flows with similar to each other properties while the jumps exhibit themselves as the sudden appearance of qualitatively different flow regimes with the different number of trapped vortices. As it often happens, the jump changes are linked to hysteresis and non-uniqueness. Hence the most challenging problems for the studies of steady multi-vortex solutions are: (i) to describe the non-uniqueness of solutions; (ii) to find the multi-parametric family of steady separated solutions; and (iii) to predict which solution appears at $t \to \infty$ for the given initial datum. Hopefully these problems can be approached within the cosymmetry theory that has successfully solved similar problems for convective flows in a porous medium (Yudovich 1995).

(viii) It is interesting to compare the ratio of kinetic energies $\mathscr{K}_s/\mathscr{K}_n$ for the coexisting separated and non-separated flows. For the flows in figure 14 this ratio is: (*a*) 1.44, (*b*) 19.06, (*c*) 17.86, and for figure 16 it is: (*a*) 5.32, (*b*) 28.40, (*c*) 33.84. One can see that separated flows can accumulate much higher energy than basic flows (so one can think that separated flows can be used as 'a storage of energy'). Similar figures and trends also appear for the values of enstrophy.

(ix) Steady planar multi-vortex solutions play important part in vortex dynamics (Saffman 1992; Meleshko & Konstantinov 1993; Borisov, Mamaev & Sokolovsky 2003; Kozlov 2003). One can find a number of recently discovered solutions (mainly for unbounded and/or rotating flows) in the papers by Aref (1979), Carton, Flierl & Polvani (1989), Orlandi & van Heijst (1992), Morel & Carton (1994) and Kizner & Khvoles (2004), which are partially inspired by the experiments of van Heijst & Kloosterziel (1989) and Vladimirov & Tarasov (1980). The near-wall vortex structures in the flows around obstacles or cavities have been studied by Chernyshenko (1988), Fornberg (1993), Elcart *et al.* (2000). The papers by Goldstik (1963), van Geffen, Meleshko & van Heijst (1996), Stremler & Aref (1999) and Elcart & Miller (2001) consider finite channels but in a different from our context. For example, Elcart & Miller (2001) use the reduction of the governing equations to Dirichlet's problem for the equation $-\Delta\Psi = \Omega(\Psi)$ with a non-decreasing positive function $\Omega(\Psi)$ that can be discontinuous; their result predicts a steady monopole vortex in a finite channel with the inflow of an irrotational fluid. It should be mentioned that our numerical solutions for multi-vortex configurations in a straight finite channel with YBC add a new class of solutions to the range of well-known results.

11. The example of self-oscillatory flow

Here we present the example of nonlinear self-oscillations that supports *C2*. To ensure the supply of energy for the maintenance of self-oscillations we choose the basic flow which has a point with $\mathrm{d}\Psi/\mathrm{d}\Omega = 0$, that violates the sufficient stability condition (4.2). We take YBC:

$$\psi^{in}(y) = \psi^{out}(y) = y, \quad \omega^{in}(y) = A/[1 + \sigma(2y-1)^2], \tag{11.1}$$

where A, σ are two positive parameters. In (11.1) the condition $\omega^{in}(y) = -\psi^{in}_{yy}(y)$ (2.10) is violated, hence these YBC do not correspond to any basic shear flow. These YBC give the uniform profiles of the horizontal velocity component at both $\partial\mathscr{D}^{in}$ and $\partial\mathscr{D}^{out}$ but the vertical velocity at $\partial\mathscr{D}^{in}$ is more complicated since it provides the inlet

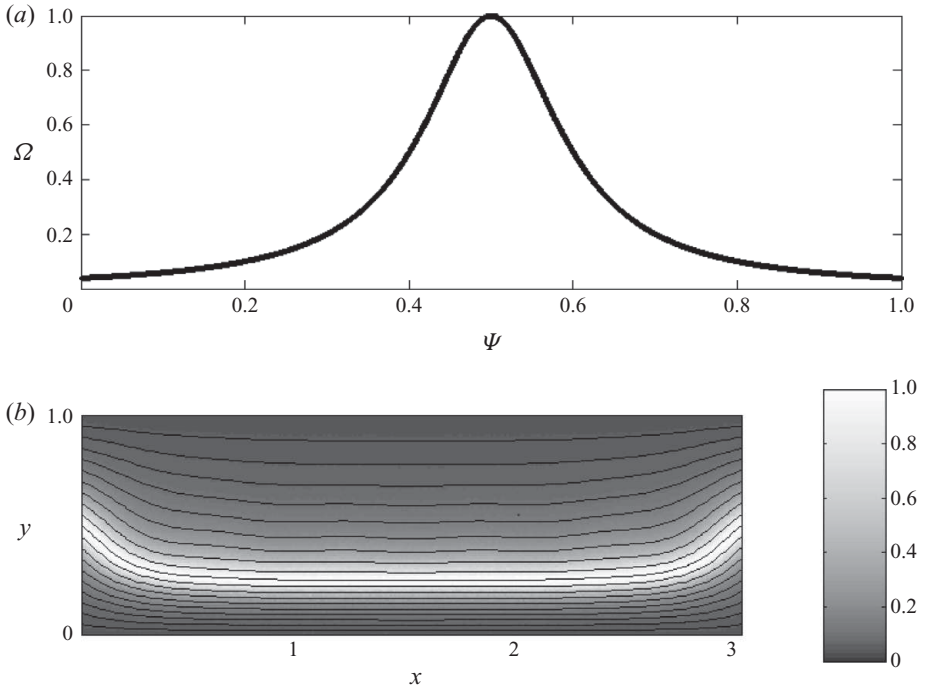

FIGURE 18. (*a*) $\Omega(\Psi)/A$ for (11.1) with $\sigma = 25$; (*b*) The streamlines and vorticity field for the steady flow with $A = 8$.

vorticity (11.1). The graph $\omega^{in}(\psi^{in})/A$ for $\sigma = 25$ in figure 18(*a*) shows the vorticity maximum at the point $y = 1/2$. For the large enough A and σ a vorticity profile forms a strong shear layer near $y = 1/2$, so that short-wave Kelvin–Helmholtz instability can be expected.

In order to obtain the expected unstable regimes we organize the following iteration process. For $A = 0$, the data (11.1) gives us UBF $U(y) \equiv 1$. It is proven by Morgulis & Yudovich (2002) that the YBC (11.1) for a sufficiently small A produce a non-separated steady flow that is linearly asymptotically stable. We find this flow by solving the unsteady problem (2.1)–(2.5), (11.1) with a very small amplitude $A = a_1$ and UBF $U(y) \equiv 1$ taken as an initial condition in $\mathscr{D}$: for large t this unsteady flow evolves to a steady flow with $A = a_1$ that is taken as an initial state for a slightly larger value $A = a_2$ etc. The same procedure is repeated many times. At the first stage of this iteration process we obtain the family of steady flows with $\Omega(\Psi)$ the same as $\omega^{in}(\psi^{in})$ for the set of increasing values of A. A sample from this family is shown in figure 18(*b*).

At the threshold value $A^* \approx 9$ we find that for $A < A^*$ a flow evolves to a steady one, while for $A > A^*$ we obtain an oscillating flow. The sample data for the obtained oscillating flows are given in figures 19 and 20, where we use the 'normalized' velocity circulation $\Gamma(t) \equiv \int_{\mathscr{D}} \omega(x, y, t)\, dx\, dy/AL$. We have observed that the oscillations of Γ are time-periodic for a small $A - A^* > 0$, quasi-periodic (with two independent frequencies) for a moderately supercritical A, and (possibly) chaotic with the continuous spectrum of frequencies for a significantly supercritical A (see figure 20). We have also observed that if $A - A^*$ is large enough then a wavy shear layer clearly tends to form a vortex street.

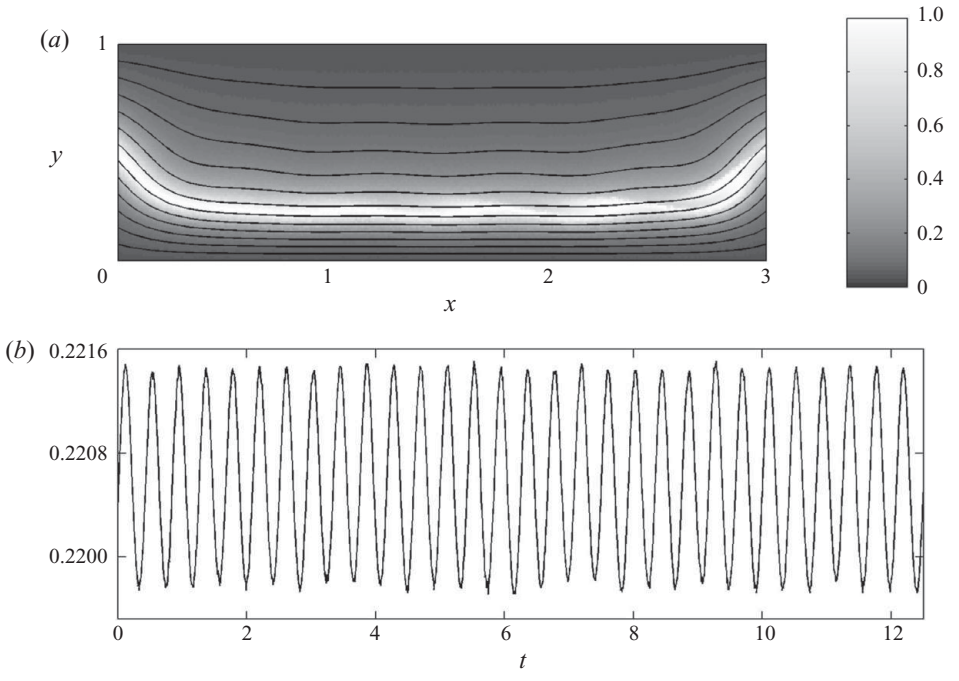

FIGURE 19. (*a*) The streamlines and vorticity field for a secondary oscillating flow; (*b*) The normalized velocity circulation (the averaged vorticity) as the function of time for $\sigma = 25$, $A = 10$.

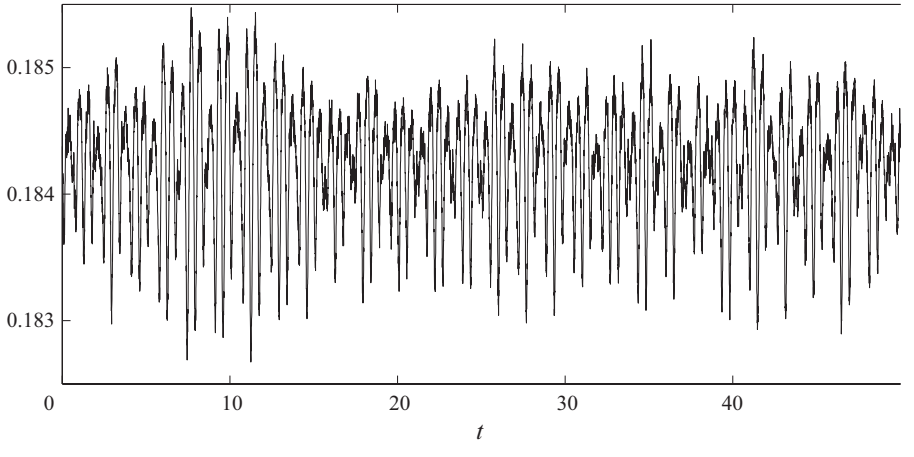

FIGURE 20. The 'chaotic oscillations' of the averaged vorticity for $\sigma = 25$, $A = 20$.

The observation of self-oscillatory flows shows how BC on $\partial\mathscr{D}^{out}$ control instability of an incoming flow. Physically, YBC on $\partial\mathscr{D}^{in}$ produce an unstable shear flow; the unstable modes grow downstream and then adjust themselves to BC on $\partial\mathscr{D}^{out}$. This adjustment does not alow the instability to grow further (it works as a damping), that leads to self-oscillations. In sharp contrast to the self-oscillations of planar viscous Poiseuille flows in infinite channels or Taylor–Couette flows between cylinders (Drazin & Reid 1981; Chossat & Iooss 1994) our example shows that the self-oscillations of an incompressible flow in finite channels can be generated and

maintained merely by the inlet and outlet BC in the absence of any viscous dissipation (i.e. for arbitrary high Reynolds numbers). The relevant example of the time-periodic regime in the vortex breakdown was reported by Lopez & Perry (1992). This area certainly requires further studies.

12. Discussion

(i) A natural question is: are YBC 'correct' physically? Another way to ask the same question is: are YBC the 'most reasonable' physically and can they be created, say, in laboratory conditions? The frequent appearance of such a question reflects the current unsatisfactory situation in the studies of flows with inlets and outlets. This research direction is so underdeveloped and skated over that one may think that the only available options are infinite channels or periodic BC. Therefore the first step here is to understand in which general terms one can think about BC. We have outlined some related issues in the questions Q1–Q5 at the beginning of the Introduction. In contrast to a looking for a single 'correct' BC it is important to recognize that there are many (but still unknown how many) possible BC for inlets and outlets. Different types of BC diversify physically due to various methods of blowing a fluid into a channel at an inlet and its suction off an outlet. Indeed one can imagine different systems of fans, filters, honeycombs, pumps, magnetohydrodynamics (MHD) and electrohydrodynamics (EHD) devices, etc. For example, a relevant EHD method of creating controlled vorticity in small fluid volumes is given in Shiriaeva, Vladimirov & Zhukov (2009). Hence the correct approach is to classify various BC and to find which types of BC produce the problems that are relevant physically and well posed mathematically. A short review of the latter BC can be found in Morgulis & Yudovich (2002).

(ii) Popular BC different from YBC are 'soft' BC at $\partial\mathscr{D}^{out}$ when $\psi = \psi^{out}$ at $x = L$ in (2.4) is replaced with $\psi_x^{out} = 0$, $\psi_y^{out} > 0$. The aim is to enforce the 'horizontal pattern' of streamlines at $\partial\mathscr{D}^{out}$. However the condition $\psi_y^{out} > 0$ makes this problem so difficult that this formulation has not been mathematically analysed yet. If we require only $\psi_x^{out} = 0$ (and do not require $\psi_y^{out} > 0$) then there is a possibility of the inflow through the cross-section $x = L$ and the mathematical problem becomes ill-posed (underdetermined). At the same time, the point-vortex model of § 3 can be conditionally modified to the soft boundary condition. In this case the nearest mirror image across $\partial\mathscr{D}^{out}$ must have the same sign as the original vortex. A simple qualitative consideration shows that (in sharp contrast to the motion of a vortex described in § 3) a point vortex will be deviated towards the washing-oriented wall and eventually will leave $\mathscr{D}$ through the vertex point $(x, y) = (L, 0)$ or $(L, 1)$. Here one can use the solutions for the collision and annihilation of point vortices which are known since Gröbli (1877). Such a drastic difference in the behaviour of a point vortex suggests that the trapping of distributed vorticity in this case should be very different from one observed under YBC.

(iii) The first attempt to formulate an extra inlet BC in terms of vorticity can be traced back to Kochin (1956) who considered three-dimensional Euler equations and proposed to specify v_n everywhere at $\partial\mathscr{D}$ and the vector of vorticity $\boldsymbol{\omega}$ at $\partial\mathscr{D}^{in}$. However these BC produced an overdetermined problem, that gave an example of the difficulties and possible errors mentioned in the § 1. For planar flows Kochin's BC coincide with YBC; this case was singled out and developed mathematically by Yudovich (1963).

(iv) Some problems of this paper were previously studied for linear perturbations by Morgulis & Yudovich (2002) who introduced the decreasing Lyapunov functionals and proved the linear asymptotic stability for a wide class of non-separated steady flows.

(v) The conjecture C1 proposes that any flow with the dissipative YBC must eventually (for $t \to \infty$) form a steady state. This idea of relaxation of any initial conditions to a steady state is of the same nature as the existence of attractors for the solutions of Euler's equations. One may also use a frantic term conservative dissipation, as the entire unsteady part of a flow is dissipated by YBC. Of course some dissipative BC are well known, say in acoustics, where they have a simple physical meaning of the dissipation of energy due to the negative work of surface forces or radiative BC. In our case the physical meaning of 'dissipation' of Arnold's functional or enstrophy functional by YBC requires further studies. However our explanation of the computationally observed relaxation to steady flows (§ 9) is purely physical: it is based on the mixing, smoothing, and dissipative properties of the trapping and the washout.

(vi) The motion of a point vortex inf § 3 does not show any relaxation, which may be seen as a contradiction to C1 and C2. However the case of a point vortex is too degenerated: it does not possess any internal structure, therefore it is unable to undergo the relaxation. Also the energy, Arnold's functional, and enstrophy are infinite in this case. Therefore it is certainly out of the framework of our theory and must be treated as an exception.

(vii) The conjecture C2 is even more radical than C1. The underpinning assumption is: any YBC which do not admit the decreasing Lyapunov functional must eventually produce steady, time-periodic or chaotic flows. In other words all YBC eventually produce dynamical systems whose attractors are points, limit cycles, or more complicated sets that bear chaotic dynamics. The existence of limit cycle attractors is well known for viscous flows but it is novel and highly unusual for inviscid flows. The only reason to expect them is the analogy of § 5. We should add here that we have not proven the non-existence of any decreasing Lyapunov functionals (this problem is most likely unsolvable). Hence the fulfilment of condition C2 is supported only by the failure of Arnold's functional to play a part of Lyapunov functional and by the results of computations of § 11

(viii) The relation between materials of §§ 4, 6–8 should be explained in more details. In § 4 we have introduced Arnold's Lyapunov functionals and enstrophy Lyapunov functional and have used them for the proof on nonlinear stability. At the same time we have shown that (for generic perturbations) both these functionals are decreasing. However the decreasing of these functionals cannot be directly used for the proofs of CWOF and CWOP. The key mathematical difficulty is: the dissipation is concentrated at the outlet $\partial\mathscr{D}^{out}$, while the functionals themselves are defined as integrals over the whole channel $\mathscr{D}$. Hence the mathematical deriving of *a priori* upper bounds is not feasible. As the result, both Lyapunov functionals do allow us to formulate the Conjectures, but they are insufficient for obtaining upper bounds and for the clarification of the conditions to manifest three scenarios. To resolve this difficulty we have additionally employed the integration along trajectories.

(ix) The existence of three key scenarios (S1–S3 in § 5) of dynamics is a grand result of the dynamical system theory. However from any book on dynamical systems one can see that (even for simple dynamical systems) the conditions under which each scenario is manifesting depend in a very complicated manner on the initial data. If the asymptotic behaviour of the channel flows (which represents more complex dynamical

system than one-dimensional equations) also exhibits the same three scenarios, then it would be also a grand result. Due to the difficulty of the problem we give only a few rough estimations of the conditions related to each scenario; we also study these conditions qualitatively in the computational part. For the self-oscillations (§ 11) we are able only to indicate the general nature of the conditions.

(x) In §§ 6–9 we have presented substantial information on the lifespans of both perturbations and particles. These lifespans are important theoretically: they give us basic information about the flow stability, vortex dynamics, and the Lagrangian dynamics of particles. For example the finite time required for CWOF is a phenomenon of Lagrangian dynamics that excludes the formation of recirculation zones and hence underlies the CWOP in finite time. Such decay represents the strong case of the asymptotic stability (nilpotent stability, Morgulis & Yudovich 2002). The existence of nilpotent stability for fluid flows is in strong contrast with finite-dimensional results, where the total decay of perturbations always takes infinite time. It is also important that the gradual increasing of the lifespans of both perturbations and particles finally leads to the trapping: hence we know why and how the trapping develops gradually; it can be seen in details and explained (both physically and mathematically) at all its stages. The lifespans also appear in many important practical applications, e.g. in the weather forecast and in the dynamics of pollution.

(xi) The washout and trapping of vorticity represent exciting and challenging problems of vortex dynamics. Our computational solutions show that the collision of a vortex patch with $\partial\mathscr{D}^{out}$ leads to the partial shedding of vorticity from a vortex core through $\partial\mathscr{D}^{out}$ while the remaining part of the patch drastically changes its size and geometry and moves back towards $\partial\mathscr{D}^{in}$. Neither the velocity circulation nor the effective distance from the trapping-oriented wall for this backward motion can be theoretically predicted yet. This vortex–outlet–wall interaction exhibits the complex dynamics of vorticity and certainly deserves further studies. The most interesting question is how to control the trapping of vorticity. Our computations show that the amount of trapped vorticity and the structure of a trapped vortex strongly depend on the changing of BC on $\partial\mathscr{D}^{out}$. At the same time these results are not sensitive to the changes of BC on $\partial\mathscr{D}^{in}$. This property has a clear physical explanation: the changing of BC on $\partial\mathscr{D}^{in}$ brings changes only to the basic flow. In contrast, the changing of BC on $\partial\mathscr{D}^{out}$ produces drastic changes in the amount and structure of trapped vorticity during the described above collision.

(xii) From the viewpoint of vortex dynamics the most classical version of the problem (2.16), (2.17) is to consider UBF combined with the initial perturbation $\widetilde{\omega}_0(\boldsymbol{x}) = \omega_0 = \text{const}$. This problem possesses only two dimensionless parameters: ω_0 and L. In the process of evolution such a flow divides itself into two parts: with $\omega = 0$ and $\omega = \omega_0$. The interface dynamics between these parts can be rather complex, however the main interest is to determine the universal limiting flows as $t \to \infty$ and to make their classification in the plane (ω_0, L). These flows are expected to be stable, since they are obtained by the relaxation process; the analytical stability criteria can be obtained by the generalization of Vladimirov (1988). One may also introduce the idea of the vortex capacity of $\mathscr{D}$ defined as the maximal amount of vorticity that can be trapped. We do not study this topic due to two reasons: (*a*) our numerical method generates the maximal errors at the jumps of ω, therefore, for example, the distribution of ω inside the patches (9.5) has been chosen Gaussian to make those jumps small; (*b*) we deliberately restrict ourselves with the study of generic perturbations.

(xiii) There are two highly unusual elements in the nonlinear asymptotic stability results of §§ 7 and 8: (i) we simultaneously use two norms to measure 'the smallness'

of vorticity perturbations: $\widetilde{\omega}^+$ (C-norm) and $\mathscr{I}$ (L_2-norm); (ii) in contrast to the widespread mathematical statements about the stability with respect to finite but sufficiently small (unknown how small) perturbations, we are able to evaluate the thresholds values of amplitudes explicitly.

(xiv) The justification of any results for an inviscid fluid is often understood as solving similar problems for a viscous fluid with vanishing viscosity. We can mention here only the first studies of inlet and outlet boundary layers by Temam & Wang (2002) and Ilin (2008). Such boundary layers can be very different from the conventional ones. This direction of research is very promising, for example, Doering, Spiegel & Worthing (2000) have obtained the non-zero rate of energy dissipation in the limit of vanishing viscosity for the flows with the suction through a wall.

(xv) This paper can be also considered as a preparatory stage for the further studies of the vortex breakdown theory with various BC, which have been started by Wang & Rusak (1997) and Gallaire & Chomaz (2004). The linear axisymmetric modes in swirling flows (subject to different BC) were studied by Gallaire & Chomaz (2004) who discovered that kinetic energy of perturbations could not increase, provided v_n was given on $\partial\mathscr{D}$ and the azimuthal velocity was given on $\partial\mathscr{D}^{in}$. Therefore, any linear instability is impossible and the concept of the incipient vortex breakdown by Wang & Rusak (1997) cannot be used in this situation. However, a vortex breakdown can be caused by a nonlinear mechanism similar to the trapping of perturbations. Although, the BC of Wang & Rusak (1997) are sometimes considered as more physically realistic than YBC, it should be mentioned that their generalization to non-axisymmetric flows is conceptually unknown, while YBC are well formulated both in two and three dimensions. At the same time the similar studies of flow regimes have not yet been started for Kazhikhov's BC (Antontsev *et al.* 1990) that prescribe the full velocity vector at $\partial\mathscr{D}^{in}$. It is proven that Kazhikhov's BC, as well as YBC, lead to a well-posed problem for three-dimensional Euler equations, hence they simultaneously allow us to approach both two- and three-dimensional vortex breakdown problems.

(xvi) It is a challenging problem to study the limit of zero minimal horizontal velocity $U^- \to 0$ on $\partial\mathscr{D}^{in}$ and/or $\partial\mathscr{D}^{out}$ in (2.6). This limit appears as singular in our theory, since the expressions we use (such as (7.4)–(7.7)) contain U^- in denominators. However we do not consider this case as being untractable; it should be treated separately and one can expect here much stronger trapping of vorticity.

(xvii) An interesting generalization of the problem (2.1)–(2.5) is to prescribe the time-oscillations of velocities at $\partial\mathscr{D}^{in}$ and $\partial\mathscr{D}^{out}$. The studies of such a generalization have already been started by Morgulis (2005), Vladimirov (2005) and Morgulis & Vladimirov (2008) for an inviscid fluid and by Vladimirov (2008) for a viscous fluid. Here one can find important links to the steady streaming theory (Stuart 1966; Batchelor 1987; Riley 2001) and to biological applications for time-periodic flows (Pedley 1980).

(xviii) The divergent form (4.9) and the related fluxes of Arnold's functional $\mathscr{W}_\alpha$ can be generalized to all known cases of Arnold's stability, for example to various MHD flows such as the flows studied by Moffatt (1985, 1986), Vladimirov & Moffatt (1995) and Vladimirov, Moffatt & Ilin (1996) and to a broad variety of geophysical flows (see e.g. Swaters 1992).

This research is supported by EPSRC grants GR/S96616/01, GR/S96616/02 and EP/D035635/1. The authors thank: the Department of Mathematics of the University of York for providing excellent working conditions, the Hull Institute of Mathematical Sciences and Applications (HIMSA) where this research was initiated, the Department

of Computer Sciences of the University of Hull and Professor R.Phillips for the given access to the computer cluster in the HIVE Laboratory. The part of the team from the Southern Federal University is partially supported by CRDF RUMI-2842-RO-06, RFBR-08-01-00895-a, by the programme for development of high school research potential (Russia) nos. 2.1.1/554 and 2.1.1/6095, and by the research environment of the European group in Regular and Chaotic Hydrodynamics. The authors are grateful to Profsessors K. I. Ilin, H. K. Moffatt, T. J. Pedley, H. Aref and V. L. Berdichevsky for useful discussions.

Appendix A. Proof of Proposition 1

We divide the proof into five steps.

Step 1: The stream function of the perturbed flow is

$$\left.\begin{aligned} &\psi(\boldsymbol{x},t)=\Psi(\boldsymbol{x})+\Gamma G(\boldsymbol{x}-\boldsymbol{x}_0(t)),\\ &-\Delta G(\boldsymbol{x},\boldsymbol{x}_0)=\delta(\boldsymbol{x}-\boldsymbol{x}_0),\quad \text{when } \boldsymbol{x},\boldsymbol{x}_0\in\mathscr{D},\\ &G(\boldsymbol{x},\boldsymbol{x}_0)=0,\ \text{when } \boldsymbol{x}\in\partial\mathscr{D}, \end{aligned}\right\} \tag{A 1}$$

where $\boldsymbol{x}_0(t)=(x_0(t),y_0(t))$ is the current position of a vortex, G is Green's function for Dirichlet's problem in $\mathscr{D}$, and δ is the delta function. The 'reflected' part of G is

$$g(\boldsymbol{x},\boldsymbol{x}_0)=G(\boldsymbol{x},\boldsymbol{x}_0)+(2\pi)^{-1}\ln|\boldsymbol{x}-\boldsymbol{x}_0|, \tag{A 2}$$

where for any $\boldsymbol{x}_0\in\mathscr{D}$ function g is the solution of Dirichlet's problem:

$$\Delta g(\boldsymbol{x},\boldsymbol{x}_0)=0,\ \boldsymbol{x}\in D;\quad g(\boldsymbol{x},\boldsymbol{x}_0)=(2\pi)^{-1}\ln|\boldsymbol{x}-\boldsymbol{x}_0|,\ \boldsymbol{x}\in\partial D. \tag{A 3}$$

If $\boldsymbol{x}_0\in\mathscr{D}$, then BC for g represents a smooth function, hence g is also smooth everywhere in $\mathscr{D}$. However the smoothness of BC in (A 3), and consequently the smoothness of g in $\mathscr{D}$, are deteriorating as $\boldsymbol{x}_0\to\partial\mathscr{D}$.

The equations of motion for a vortex

$$\mathrm{d}\boldsymbol{x}_0/\mathrm{d}t=\nabla^{\perp}|_{\boldsymbol{x}=\boldsymbol{x}_0}\left(\Psi(\boldsymbol{x})+\Gamma g(\boldsymbol{x},\boldsymbol{x}_0)\right),\quad \nabla^{\perp}\equiv(\partial/\partial y,-\partial/\partial x) \tag{A 4}$$

represent a Hamiltonian system with the Hamiltonian function

$$\mathscr{H}(\boldsymbol{x})=\Psi(\boldsymbol{x})+\Gamma\hat{\mathscr{H}}(\boldsymbol{x}),\quad \hat{\mathscr{H}}(\boldsymbol{x})\equiv g(\boldsymbol{x},\boldsymbol{x})/2,$$

where we used the well-known symmetry of g:

$$g(\boldsymbol{x},\boldsymbol{x}_0)=g(\boldsymbol{x}_0,\boldsymbol{x}),\quad 2\nabla^{\perp}|_{\boldsymbol{x}=\boldsymbol{x}_0}\,g(\boldsymbol{x},\boldsymbol{x}_0)=(\nabla^{\perp}g(\boldsymbol{x},\boldsymbol{x}_0)+\nabla_0^{\perp}g(\boldsymbol{x},\boldsymbol{x}_0))|_{\boldsymbol{x}=\boldsymbol{x}_0}$$

with $\nabla_0^{\perp}\equiv(\partial/\partial y_0,-\partial/\partial x_0)$. One can see that all possible trajectories of a vortex lie on the level curves

$$\mathscr{H}(\boldsymbol{x})=\text{const}<\infty \tag{A 5}$$

for the different values of a constant.

Step 2: For the rectangular domain $\mathscr{D}$ (defined in (2.2)), Green's function G can be written explicitly as a double series over all mirror reflections of the point vortex with respect to all sides of the domain (Villat 1930):

$$G(\boldsymbol{x},\boldsymbol{x}_0)=\frac{1}{4\pi}\sum_{\boldsymbol{p}}\ln\frac{|\boldsymbol{x}-\overline{\boldsymbol{x}}_0-\boldsymbol{p}|^2|\boldsymbol{x}+\overline{\boldsymbol{x}}_0-\boldsymbol{p}|^2}{|\boldsymbol{x}-\boldsymbol{x}_0-\boldsymbol{p}|^2|\boldsymbol{x}+\boldsymbol{x}_0-\boldsymbol{p}|^2},\ \overline{\boldsymbol{x}}_0=(x_0,-y_0),$$

where $\boldsymbol{p}=(2kL,2m)$ and the summation is performed over all $k,m=0,\pm1,\ldots$. The sum of this series can be expressed with the use of Weierstrass' function $\wp$ (Villat

1930); however, the explicit presentation is more instructive for our purposes. The original vortex contributes the unique term $(k, m) = (0, 0)$ with a singularity inside $\mathscr{D}$; removing this term gives the formula for g (see (A 2)):

$$g(\boldsymbol{x}, \boldsymbol{x}_0) = \frac{1}{4\pi} \ln \frac{|\boldsymbol{x} - \overline{\boldsymbol{x}}_0|^2 |\boldsymbol{x} + \overline{\boldsymbol{x}}_0|^2}{|\boldsymbol{x} + \boldsymbol{x}_0|^2} + \frac{1}{4\pi} \sum_{\boldsymbol{p} \neq 0} \ln \frac{|\boldsymbol{x} - \overline{\boldsymbol{x}}_0 - \boldsymbol{p}|^2 |\boldsymbol{x} + \overline{\boldsymbol{x}}_0 - \boldsymbol{p}|^2}{|\boldsymbol{x} - \boldsymbol{x}_0 - \boldsymbol{p}|^2 |\boldsymbol{x} + \boldsymbol{x}_0 - \boldsymbol{p}|^2}.$$

Hence,

$$\hat{\mathscr{H}}(\boldsymbol{x}) = \frac{1}{8\pi} \ln \frac{4x^2 y^2}{x^2 + y^2} + \frac{1}{8\pi} \sum_{k^2 + m^2 \neq 0} \ln \frac{((x - kL)^2 + m^2)((y - m)^2 + k^2 L^2)}{(m^2 + k^2 L^2)((y - m)^2 + (x - kL)^2)}. \tag{A 6}$$

The series in the right-hand side of (A 6) converges in the following sense: the partial sums over the 'squares' $|k| \leqslant N$, $|m| \leqslant N$ have well-defined limit values for $N \to \infty$ and for every $\boldsymbol{x}$ inside $\mathscr{D}$ (see the proof of this statement in step 5). However, the terms with $(k, m) = (1, 0)$, $(0, 1)$ and $(1, 1)$ have singularities on the boundary. These terms relate to the collisions of the original vortex with its nearest reflections. We denote the sum of all these singular terms as $\hat{\mathscr{H}}_s(\boldsymbol{x})$:

$$\hat{\mathscr{H}}_s(\boldsymbol{x}) = \frac{1}{8\pi} \ln \left(\frac{x^2 y^2 (L - x)^2 (1 - y)^2}{(x^2 + y^2)((1 - y)^2 + x^2)(y^2 + (L - x)^2)((1 - y)^2 + (L - x)^2)} \right).$$

The sum of all other terms in (A 6) (which are regular in $\mathscr{D}$ with $\partial\mathscr{D}$) is denoted as $\hat{\mathscr{H}}_r(\boldsymbol{x}) = \hat{\mathscr{H}}(\boldsymbol{x}) - \hat{\mathscr{H}}_s(\boldsymbol{x})$. This regularized sum converges uniformly in $\boldsymbol{x} \in \mathscr{D}$ with $\partial\mathscr{D}$. Consequently, $\hat{\mathscr{H}}_r(\boldsymbol{x}) = O(1)$ as $\boldsymbol{x} \to \partial\mathscr{D}$.

Step 3: Let $\rho \equiv \min(x, L - x, y, 1 - y)$ be the distance between $\boldsymbol{x} \in \mathscr{D}$ and $\partial\mathscr{D}$. Let us take $\rho = x$ (all other cases can be treated similarly). Then

$$\begin{aligned} \hat{\mathscr{H}}_s(\boldsymbol{x}) = {} & \frac{1}{8\pi} \ln \frac{\rho^2 (L - \rho)^2}{[y^2 + (L - \rho)^2][(1 - y)^2 + (L - \rho)^2]} \\ & + \frac{1}{8\pi} \ln \frac{y^2 (1 - y)^2}{(\rho^2 + y^2)[(1 - y)^2 + \rho^2]} = \frac{1}{4\pi} \ln \rho + O(1), \quad \text{as } \rho \to 0. \end{aligned} \tag{A 7}$$

The regular part $\hat{\mathscr{H}}_r(\boldsymbol{x}) = O(1)$ and $\Psi(\boldsymbol{x}) = O(1)$ as $\rho \to 0$. Consequently,

$$\mathscr{H}(\boldsymbol{x}) = \frac{\Gamma}{4\pi} \ln \rho + O(1) \quad \text{as } \rho \to 0.$$

As one can see $\mathscr{H} \to -\infty$ as $\rho \to 0$ (for $\Gamma > 0$), hence a vortex cannot approach the boundary along any available trajectory $\mathscr{H}(\boldsymbol{x}) = \text{const}$ (A 5). It proves that the vortex is trapped inside the channel $\mathscr{D}$.

Step 4: It is clear from (A 7) that $\hat{\mathscr{H}}_s(\boldsymbol{x})$ is bounded from above; hence $\mathscr{H}$ is also bounded from above. Therefore $\mathscr{H}$ always attains its maximum in $\mathscr{D}$. It proves that there is always at least one vortex equilibrium in $\mathscr{D}$.

Step 5: The convergence of the series (A 6) has been essentially used above. Let us prove it now. An arbitrary term of (A 6) contains the function

$$\ln(1 + R(k, m)), \quad R(k, m) \equiv yx \frac{4mkL - 2(Lky + mx) + yx}{(m^2 + k^2 L^2)((y - m)^2 + (x - kL)^2)},$$

where $(x, y) \in \mathscr{D}$. One can notice that

$$R(k, m) = \frac{4mkL}{(m^2 + k^2 L^2)^2} + O((m^2 + k^2 L^2)^{-3}) \quad \text{as } k^2 + m^2 \to \infty. \tag{A 8}$$

Let S_N be a partial sum of (A 6) over $|k| \leqslant N$, $|m| \leqslant N$. Using the symmetry $k \to -k$, $m \to -m$ we rewrite it as

$$S_N = \sum_{k>0,\, m>0} \ln\{(1+R(k,m))(1+R(-k,m))(1+R(k,-m))(1+R(-k,-m))\}.$$

Now (A 8) yields

$$(1+R(k,m))(1+R(-k,m))(1+R(k,-m))(1+R(-k,-m)) \\ = 1 + O((m^2+k^2L^2)^{-3}),\ \ k^2+m^2 \to \infty.$$

That gives us the convergence of the series (A 6). Since the number of singular terms at $\partial\mathscr{D}$ in series (A 6) is finite, their omitting does not change the convergence of (A 6). It means that the function $\hat{\mathscr{H}}_r(\boldsymbol{x})$ is well defined and the convergence of the corresponding series is uniform in $\boldsymbol{x} \in \mathscr{D}$ with $\partial\mathscr{D}$. Hence the proposition is proven.

Appendix B. Proof of Proposition 4

We divide the proof into five steps.

Step 1: Equations (6.4) and (6.5) yield

$$\left.\begin{aligned} &\widetilde{\tau}_t + \psi_y\widetilde{\tau}_x - \psi_x\widetilde{\tau}_y = \widetilde{\psi}_x\tau_{0y} - \widetilde{\psi}_y\tau_{0x} \equiv \widetilde{J}_0(\boldsymbol{x},t), \\ &\widetilde{\tau}(0,y,t) = 0,\ \ \widetilde{\tau}(\boldsymbol{x},0) = -\tau_0(\boldsymbol{x}), \end{aligned}\right\} \tag{B 1}$$

where $\widetilde{\tau}(\boldsymbol{x},t) \equiv \tau(\boldsymbol{x},t) - \tau_0(\boldsymbol{x})$. In (B 1) the left-hand side represents the full (material) time-derivative along the trajectory of exact motion. Let $\overline{\boldsymbol{x}} = (\overline{x},\overline{y})$ be the current (intermediate) Cartesian coordinates and and $\overline{t}$ $(t_0 \leqslant \overline{t} \leqslant t)$ be the current time on the trajectory which starts at the point $(\boldsymbol{a},t_0)$ and passes through the point $(\boldsymbol{x},t)$. Then the integration of (B 1) along the trajectory $\overline{\boldsymbol{x}} = \overline{\boldsymbol{x}}(\boldsymbol{a},t_0,\overline{t}) = \overline{\boldsymbol{x}}(\boldsymbol{x},t,\overline{t})$ (6.1), (6.2) gives

$$\widetilde{\tau}(\boldsymbol{x},t) - \widetilde{\tau}(\boldsymbol{a},t_0) = \int_{t_0}^{t} \widetilde{J}_0(\overline{\boldsymbol{x}},\overline{t})\,\mathrm{d}\overline{t},$$

where the integration is performed for fixed $\boldsymbol{x}$ and t in $\overline{\boldsymbol{x}}(\boldsymbol{x},t,\overline{t})$. Since by definition $\widetilde{\tau}(\boldsymbol{a},t_0) = \tau(\boldsymbol{a},t_0) - \tau_0(\boldsymbol{a})$ and $\tau(\boldsymbol{a},t_0) = 0$, we arrive at

$$\widetilde{\tau}(\boldsymbol{x},t) = -\tau_0(\boldsymbol{a}) + \int_{t_0}^{t} \widetilde{J}_0(\overline{\boldsymbol{x}},\overline{t})\ \mathrm{d}\overline{t}. \tag{B 2}$$

The function τ_0 is everywhere positive (6.9) and $\tau \equiv t - t_0$, hence we obtain that

$$\left.\begin{aligned} &\tau(\boldsymbol{x},t) = \tau_0(\boldsymbol{x}) + \widetilde{\tau}(\boldsymbol{x},t) \leqslant \tau_0(\boldsymbol{x}) + \widetilde{J}_0^{+}(t)\tau(\boldsymbol{x},t), \\ &\widetilde{J}_0^{+}(t) \equiv \max_{\overline{\boldsymbol{x}},\overline{t}} |\widetilde{J}_0(\overline{\boldsymbol{x}},\overline{t})| \quad \text{where} \quad \overline{\boldsymbol{x}} \in \mathscr{D},\ 0 \leqslant \overline{t} \leqslant t, \end{aligned}\right\} \tag{B 3}$$

where the dependence of $\widetilde{J}_0^{+}(t)$ on t appears due to the fact that t represents the upper value of $\overline{t}$. With the use of (6.9) we derive

$$\widetilde{J}_0^{+}(t) \equiv \max_{\boldsymbol{x},\overline{t}} |\widetilde{\psi}_x(\boldsymbol{x},\overline{t})\tau_{0y}(\boldsymbol{x}) - \widetilde{\psi}_y(\boldsymbol{x},\overline{t})\tau_{0x}(\boldsymbol{x})| \leqslant \max_{\boldsymbol{x},\overline{t}} |\nabla\widetilde{\psi}(\boldsymbol{x},\overline{t})| \max_{\boldsymbol{x}} |\nabla\tau_0(\boldsymbol{x})| \\ = \max_{\boldsymbol{x},\overline{t}} |\widetilde{\boldsymbol{v}}(\boldsymbol{x},\overline{t})| (\nabla\tau_0)^{+} \quad \text{where} \quad \boldsymbol{x} \in \mathscr{D},\ 0 \leqslant \overline{t} \leqslant t. \tag{B 4}$$

We strengthen the inequality in (B 4) by the extension of the interval of evaluation of the maximum over $0 \leqslant \bar{t} < \infty$:

$$\widetilde{J}_0^+(t) \leqslant J^+ \equiv \widetilde{q}^+(\nabla\tau_0)^+ \quad \text{where } \widetilde{q} \equiv |\widetilde{\boldsymbol{v}}(\boldsymbol{x},t)| \leqslant \widetilde{q}^+ \quad \text{for } \boldsymbol{x} \in \mathscr{D} \quad \text{and} \quad t > 0. \tag{B 5}$$

Here the upper bound $\widetilde{q}^+$ for the absolute value of velocity is unknown. We are going to estimate it to provide $J^+ < 1$; after that (B 3) will lead to the required result (6.17).

Step 2: We employ two auxiliary inequalities which we accept without proof. They represent the special cases of much more general inequalities given in Lemmas 7.16 and 7.12 of Gilbarg & Trudinger (1983). The first one is valid for any differentiable in $\mathscr{D}$ function $\boldsymbol{f} = \boldsymbol{f}(\boldsymbol{x})$:

$$|\boldsymbol{f}(\boldsymbol{x}) - \boldsymbol{f}^{aver}| \leqslant \frac{1+L^2}{2L} \int_{\mathscr{D}} \frac{|\widehat{\nabla} \bigotimes \boldsymbol{f}(\widehat{\boldsymbol{x}})|}{|\boldsymbol{x} - \widehat{\boldsymbol{x}}|}\, \mathrm{d}\widehat{\boldsymbol{x}}, \quad \boldsymbol{f}^{aver} \equiv \frac{1}{L} \int_{\mathscr{D}} \boldsymbol{f}(\boldsymbol{x})\, \mathrm{d}\boldsymbol{x}, \quad \boldsymbol{x} \in \mathscr{D}, \tag{B 6}$$

where $\nabla \bigotimes \boldsymbol{f}$ is the tensorial derivative with the components $\partial f_i/\partial x_k$ with $i, k = 1, 2$ and $\boldsymbol{f}^{aver}$ is the average value of $\boldsymbol{f}$ over $\mathscr{D}$. The absolute value of matrix m_{ik} is defined as $|m_{ij}|^2 = m_{kl}m_{kl}$, where the summation convention is employed. The second inequality

$$\left| \int_{\mathscr{D}} \frac{g(\widehat{\boldsymbol{x}})}{|\boldsymbol{x} - \widehat{\boldsymbol{x}}|}\, \mathrm{d}\widehat{\boldsymbol{x}} \right| \leqslant \sqrt{\pi} \left(2\frac{p-1}{p-2} \right)^{1-1/p} L^{1/2-1/p} \|g\|_p\,; \quad \|g\|_p \equiv \left(\int_{\mathscr{D}} |g(\boldsymbol{x})|^p\, \mathrm{d}\boldsymbol{x} \right)^{1/p} \tag{B 7}$$

is valid for every $\boldsymbol{x} \in \mathscr{D}$, for any real number $p > 2$, and for an arbitrary (even for a non-differentiable) function $g(\boldsymbol{x})$. We take $\boldsymbol{f} = \widetilde{\boldsymbol{v}}$, $g = |\nabla \bigotimes \widetilde{\boldsymbol{v}}|$ (this g is non-differentiable), then we apply (B 6) and (B 7) one after another, and use $\widetilde{\boldsymbol{v}}^{aver} = 0$ that follows from the incompressibility of a fluid and the YBC (2.17). The result is

$$|\widetilde{\boldsymbol{v}}(\boldsymbol{x},t)| \leqslant c_0 \left(\frac{p-1}{p-2} \right)^{1-1/p} L^{-1/p} \left\| \nabla \bigotimes \widetilde{\boldsymbol{v}} \right\|_p; \quad c_0 \equiv \sqrt{\frac{\pi}{L}}(1+L^2); \quad p > 2. \tag{B 8}$$

Step 3: We need to obtain an upper bound for $\|\nabla \bigotimes \widetilde{\boldsymbol{v}}\|_p$, $p \geqslant 2$ in the terms of vorticity perturbation $\widetilde{\omega}$. For $p = 2$ instead of an upper bound one can get an exact expression via enstrophy:

$$\left\| \nabla \bigotimes \widetilde{\boldsymbol{v}} \right\|_2^2 = \|\widetilde{\omega}\|_2^2 = \mathscr{I}[\widetilde{\omega}] \tag{B 9}$$

that can be proven with the use of Fourier's presentation

$$\widetilde{\omega}(\boldsymbol{x},t) = \sum_{k,m=-\infty}^{\infty} \widetilde{\omega}_{k,m} \mathrm{e}^{\mathrm{i}(k\alpha x + \pi m y)}, \ \alpha = \pi/L.$$

Here $\widetilde{\omega}_{k,m} = -\widetilde{\omega}_{-k,m} = -\widetilde{\omega}_{k,-m} = \widetilde{\omega}_{-k,-m}$ so that the Fourier series represents the odd periodic extension of $\widetilde{\omega}$. Then the Fourier coefficients for $\widetilde{\psi}$ are $\widetilde{\psi}_{k,m} = -[(\alpha k)^2 + (\pi m)^2]^{-1}\widetilde{\omega}_{k,m}$ hence the Fourier coefficients for $\nabla \bigotimes \widetilde{\boldsymbol{v}}$ are

$$\left(\nabla \bigotimes \widetilde{\boldsymbol{v}} \right)_{k,m} = \widetilde{\omega}_{k,m} M_{km}, \quad M_{km} \equiv \frac{1}{\alpha^2 k^2 + \pi^2 m^2} \begin{pmatrix} \pi\alpha mk & \pi^2 m^2 \\ -\alpha^2 k^2 & -\pi\alpha mk \end{pmatrix},$$

and (B 9) follows from this expression, $|M_{km}| = 1$, and Parseval's theorem.

The case $p > 2$ is more complicated; the related theory gives only a well-known inequality that we also accept without proof (one can find it in Stein & Weiss 1971,

chapter 7; Stein 1986, chapter 2):

$$\left\|\nabla \bigotimes \widetilde{\boldsymbol{v}}\right\|_p \leqslant c_1 p \, \|\widetilde{\omega}\|_p, \quad p > 2. \tag{B 10}$$

Here a constant c_1 is independent of both p and L. The explicit expression for c_1 taken from Yudovich (1989, § 1) is already given in (6.12).

Step 4: The use of (B 8)–(B 10) allows us to estimate $\widetilde{q}(\boldsymbol{x}, t) \equiv |\widetilde{\boldsymbol{v}}(\boldsymbol{x}, t)|$ in terms of $\mathscr{I}$ and $\widetilde{\omega}$ only. For $p > 2$ we write

$$|g|^p = |g|^{\overline{p}} |g|^{p-\overline{p}}, \ \overline{p} = p/(p-1); \ g \equiv \left|\nabla \bigotimes \widetilde{\boldsymbol{v}}\right|.$$

The estimation of $\|g\|_p$ obtained with the use of the Hölder inequality with the conjugated exponents $2/\overline{p}$, $2/(2-\overline{p})$ is

$$L^{-1/p} \|g\|_p \leqslant \left(L^{-1/2p} \|g\|_{2p}\right)^{(p-2)/(p-1)} (L^{-1/2} \|g\|_2)^{1/(p-1)}.$$

This inequality together with (B 10), (B 9), and (B 8) yields

$$|\widetilde{\boldsymbol{v}}(\boldsymbol{x}, t)| \leqslant c_0 \left(\frac{p-1}{p-2}\right)^{1-1/p} \left(2c_1 p \, L^{-1/2p} \|\widetilde{\omega}\|_{2p}\right)^{(p-2)/(p-1)} (\sqrt{\mathscr{I}/L})^{1/(p-1)}.$$

An additional simple inequality follows directly from the definition of $\|\cdot\|_{2p}$ (B 7):

$$L^{-1/2p} \|\widetilde{\omega}\|_{2p} \leqslant |\widetilde{\omega}|_{\boldsymbol{x}}^+, \quad \text{where } |\widetilde{\omega}|_{\boldsymbol{x}}^+ \equiv \max_{\boldsymbol{x}} |\widetilde{\omega}(\boldsymbol{x}, t)|. \tag{B 11}$$

It gives

$$|\widetilde{\boldsymbol{v}}(\boldsymbol{x}, t)| \leqslant c_0 \left(\frac{p-1}{p-2}\right)^{1-1/p} \left(2p \, c_1 |\widetilde{\omega}|_{\boldsymbol{x}}^+\right)^{(p-2)/(p-1)} (\sqrt{\mathscr{I}/L})^{1/(p-1)}. \tag{B 12}$$

The increase of the right-hand side in (B 12) gives a more compact inequality

$$|\widetilde{\boldsymbol{v}}(\boldsymbol{x}, t)| \leqslant 4c_0 \sqrt{\mathscr{I}/L} \frac{X^\sigma}{\sigma(1-\sigma)}, \tag{B 13}$$

$$X \equiv c_1 |\widetilde{\omega}|_{\boldsymbol{x}}^+ \sqrt{L/\mathscr{I}} \geqslant c_1 > 1, \quad \sigma = \frac{p-2}{p-1} \in (0, 1), \tag{B 14}$$

where the bound $X \geqslant c_1 > 1$ follows from (B 11) at $p = 1$. The inequality (B 13) is valid for every $\sigma \in (0, 1)$; therefore the next step is to choose the value of σ that minimizes the right-hand side. The calculation of the minimizer yields:

$$\sigma^- = \frac{2}{2 + \chi + \sqrt{\chi^2 + 4}}, \quad \text{where } \chi \equiv \ln X > 0.$$

It is easy to see that $\sigma^- < 1/2$ for every positive χ. The minimal value of the right-hand side of (B 13) is

$$4c_0 \sqrt{\mathscr{I}/L} \exp\left(\frac{1-2\sigma^-}{1-\sigma^-}\right) (2 + \sqrt{\chi^2+4}) \leqslant 4ec_0 \sqrt{\mathscr{I}/L} (2 + \sqrt{\chi^2+4}).$$

Thus we arrive to the estimate

$$\widetilde{q}_{\boldsymbol{x}}^+ \equiv \max_{\boldsymbol{x}} |\widetilde{\boldsymbol{v}}(\boldsymbol{x}, t)| \leqslant \mathscr{M}(\mathscr{I}, |\widetilde{\omega}|_{\boldsymbol{x}}^+)$$

with the function $\mathscr{M}$ given in (6.11).

Step 5: Our final aim in this proof is to obtain the upper bound $\widetilde{q}_x^+ \leqslant \widetilde{q}^+$ in order to use it in (B 5). By virtue of (6.13) we obtain

$$\widetilde{q}_x^+ \leqslant \mathscr{M}(\mathscr{I}^+, |\widetilde{\omega}|^+) \tag{B 15}$$

provided that we have the upper bounds $\mathscr{I}(t) \leqslant \mathscr{I}^+$ and $|\widetilde{\omega}|_x^+ \leqslant |\widetilde{\omega}|^+$ for every $t > 0$. To obtain these bounds we use the fact that our basic flow (6.7) is nonlinearly stable, hence by virtue of (4.1) we have $\mathscr{I}^+ = C\mathscr{I}_0$. To find the upper bound $|\widetilde{\omega}|^+$ for vorticity perturbations we use the conservation of full vorticity in each material particle $\omega(\boldsymbol{x}, t) = \omega_0(\boldsymbol{a}, t_0)$. It gives $|\omega(\boldsymbol{x}, t)| \leqslant \max(|\omega(\boldsymbol{x}, 0)|, |\omega(0, y, t)|)$ where the maximum of two functions is taken over x, y, t. Physically it means that the maximum of vorticity can appear either in initial data or in an inlet condition. Since the basic flow (6.7) is non-separated we get $\max_y |\omega(0, y, t)| = \max_{\boldsymbol{x}} |\Omega(\boldsymbol{x})| = |\Omega|^+$; therefore $|\omega(\boldsymbol{x}, t)| \leqslant \max(|\omega(\boldsymbol{x}, 0)|, |\Omega|^+) \leqslant |\omega_0|^+ + |\Omega|^+$. The use of this inequality and the definition of perturbations gives

$$|\widetilde{\omega}| = |\omega - \Omega| \leqslant |\omega| + |\Omega| \leqslant |\omega_0|^+ + 2|\Omega|^+ = |\Omega + \widetilde{\omega}_0|^+ + 2|\Omega|^+ \leqslant |\widetilde{\omega}_0|^+ + 3|\Omega|^+,$$

hence one can take $|\widetilde{\omega}|^+ = 3|\Omega|^+ + |\widetilde{\omega}_0|^+$ as it stated in (6.16). For the perturbations with continuous $\widetilde{\omega}(\boldsymbol{x}, t)$ this value can be lowered to $|\widetilde{\omega}|^+ = 2|\Omega|^+ + |\widetilde{\omega}_0|^+$. We keep the consideration so general that it includes the perturbations with the finite jumps of vorticity. In the case $\Omega \equiv \text{const}$ the vorticity perturbation represents a passive admixture, so that $|\widetilde{\omega}|^+ = |\widetilde{\omega}_0|^+$ as it is also stated in (6.16). Hence (B 15) is justified. Moreover, since both arguments in (B 15) represent the maxima valid for any instant $t > 0$ we derive that $\widetilde{q}_x^+ \leqslant \widetilde{q}^+ = \mathscr{M}(C\mathscr{I}_0, \widetilde{\omega}^+)$. Now the use of (B 5) gives (6.15) that completes the proof.

REFERENCES

Alekseev, G. 1972 On vanishing viscosity in the two dimensional steady problems of dynamics of an incompressible fluid. *Dyn. Continuous Media (Dinamica Sploshnoy Sredy)*, **10**, 5–28, Novosibirsk (in Russian).

Antontsev, S., Kazhikhov, A. & Monakhov, V. 1990 *Boundary Value Problems in Mechanics of Inhomogeneous Fluids*. Studies in Mathematics and Applications, vol. 22. North-Holland.

Aref, H. 1979 Motion of three vortices. *Phys. Fluids*, **22**, 393–400.

Arnold, V. I. 1966 On an a priori estimate in the theory of hydrodynamical stability. *Izvestiya Visshikh Uchebnikh Zavedevniy, Matematika* **5**, 3–5 (in Russian); English translation in 1969 *Am. Math. Soc. Trans.* II **79**, 267–269.

Aubry, A. & Chartier, P. 1998 A note on pseudo-symplectic Runge–Kutta methods. *BIT* **38** (4), 802–806.

Batchelor, G. K. 1987 *An Introduction to Fluid Dynamics*. Cambridge University Press.

Beavers, G. S. & Joseph, D. D. 1967 Boundary conditions at a naturally permeable wall. *J. Fluid Mech.* **30**, 197–207.

Benjamin, T. B. 1967 Some developments in the theory of vortex breakdown. *J. Fluid Mech.* **28**, 65–84.

Berdichevskiy, V. L. 1983 *Variational Principles in the Continuous Mechanics*. Nauka (in Russian).

Borisov, A. B, Mamaev, I. S. & Sokolovsky, M. A (ed.) 2003 *Fundamental and Applied Problems of Vortex Dynamics*. Institute of Computational Research Press (in Russian).

Brown, G. L. & Lopez, J. M. 1990 Axisymmetric vortex breakdown. Part II. Physical mechanisms. *J. Fluid Mech.* **221**, 553–576.

Burton, G. R. 1987 Rearrangements of functions, maximization of convex functionals, and vortex rings. *Math. Annu.* **276**, 225–253.

Carton, X. J., Flierl G. R. & Polvani, L. M. 1989 The generation of tripoles from unstable axisymmetric isolated vortex structures. *Europhys. Lett.* **9**, 339–345.

Chernyshenko, S. 1988 The asymptotic form of a stationary separated flow around a solid at high Reynolds numbers. *Appl. Math. Mech.* **52**, 746–753.

Chossat, P. & Iooss, G. 1994 *The Couette–Taylor Problem*. Applied Mathematical Sciences, vol. 102. Springer.

Chwang, A. T. 1983 A porous-wavemaker theory. *J. Fluid Mech.* **132**, 395–406.

Cottet, G.-H. & Koumoutsakos, P. 1999 *Vortex Methods: Theory and Practice*. Cambridge University Press.

Cox, S. 1991 Two-dimensional flow of a viscous fluid in a channel with porous walls. *J. Fluid Mech.* **227**, 1–33.

Doering, C. R., Spiegel, E. A. & Worthing, R. A. 2000 Energy dissipation in a shear layer with suction. *Phys. Fluids* **12** (8), 1955–1968.

Drazin, P. G. & Reid, W. H. 1981 *Hydrodynamic Stability*. Cambridge University Press.

Elcart, A., Fornberg, B., Horn, M. & Miller, K. 2000 Some steady vortex flows past a circular cylinder. *J. Fluid Mech.* **409**, 13–27.

Elcart, A. & Miller, K. 2001 A monotone iteration for concentrated vortices. *Nonlinear Anal.* **44**, 777–789.

Fornberg, B. 1993 Computing of steady incompressible flows past a blunt bodies – a historical overview. In *Numerical Method for Fluid Dynamics* (ed. M. J. Baines & K. W. Morton), vol. 4, pp. 115–135. Oxford University Press.

Gallaire, F. & Chomaz, J.-M. 2004 The role of boundary conditions in a simple model of incipient vortex breakdown. *Phys. Fluids* **16** (2), 274–286.

van Geffen, J. H. G. M., Meleshko, V. V. & van Heijst, G. J. F. 1996 Motion of a two-dimensional monopolar vortex in a bounded rectangular domain. *Phys. Fluids* **8** (9), 2393–2399.

Gilbarg, D. & Trudinger, N. 1983 *Elliptic Partial Differential Equations of Second Order*. 2nd edn. Springer.

Goldstik, M. 1963 A mathematical model of separated flow in an incompressible fluid. *Sov. Phys. Dokl.* **7**, 1090–1093.

Goldshtik, M. & Javorsky, N. 1989 On the flow between a porous rotating disk and a plane. *J. Fluid Mech.* **207**, 1–28.

Goldshtik, M. & Hussain, F. 1998 Analysis of invicsid vortex breakdown in a semi-infinite pipe. Inviscid separation in steady planar flows. *Fluid Dyn. Res.* **23** (4), 189–266.

Govorukhin, V. N. & Ilin, K. I. 2008 Numerical study of an inviscid incompressible fluid through a channel of finite length. *Intl J. Numer. Methods Fluids* **60** (12), 1315–1333.

Gröbli, W. 1877 Specialle Probleme über die Bewegung geredliniger parallierer Wirbelfäden. *Vierteljahrsch. d. Nat.forsch. Geselsch. Zürich* **22** (37–81), 129–165.

Hald, O. 1979 Convergence of vortex methods. Part II. *SIAM J. Numer. Anal.* **16**, 726–755.

Haltiner, G. J. & Williams, R. T. 1980 *Numerical Prediction and Dynamic Meteorology*. 2nd edn. Wiley.

van Heijst, G. J. F. & Kloosterziel, R. 1989 Tripolar vortices in a rotating fluid. *Nature* **338**, 569–570.

Ilin, K. I. 2008 Viscous boundary layers in flows through a domain with permeable boundary. *Eur. J. Mech.* B *Fluids* **27**, 514–538.

Kazhikhov, A. 1981 Note on the formulation of the problem of flow through a bounded region using equations of perfect fluid. *Appl. Math. Mech.* **44**, 672–674.

Kizner, Z. & Kholves, R. 2004 The tripolar vortex: experimental evidence and explicit solutions. *Phys. Rev.* E **70**, 016307.

Kochin, N. 1956 On the existence theorem in hydrodynamics. *Appl. Math. Mech. (Prikl. Mat. Mekh.)* **20** (2), 153–172 (in Russian).

Kozlov, V. V. 2003 *General Theory of Vortices. Dynamical Systems X*. Encyclopedia of Mathematical Sciences, vol. 67. Springer.

Liu, J.-G. & Xin, Z. 2000 Convergence of Galerkin method for 2-D discontinuous Euler flows. *Commun. Pure Appl. Math.* **53** (6), 786–798.

Lopez, J. M. 1990 Axisymmetric vortex breakdown. Part I. Confined swirling flow. *J. Fluid Mech.* **221**, 533–552.

Lopez, J. M. & Perry, A. D. 1992 Axisymmetric vortex breakdown. Part III. Onset of periodic flow and chaotic advection. *J. Fluid Mech.* **234**, 449–471.

Martemianov, S. & Okulov, V. L. 2004 On heat transfer enhancement in swirl pipe flows. *Intl J. Heat Mass Transfer* **47**, 2379–2393.

Meleshko, V. V. & Konstantinov, M. Yu. 1993 *Dynamics of Vortex Structures*. Naukova Dumka (in Russian).

Moshkin, N. & Mounnamprang, P. 2003 Numerical simulation of vortical ideal fluid flow through curved channel. *Intl J. Numer. Methods Fluids* **41**, 1173–1189.

Moffatt, H. K. 1985 Magnetostatic equilibria and analogous Euler flows of arbitrarily complex topology. Part. I. Fundamentals. *J. Fluid Mech.* **159**, 359–378.

Moffatt, H. K. 1986 On the existence of localized rotational disturbances which propagate without change of structure in an inviscid fluid. *J. Fluid Mech.* **173**, 289–302.

Morel, Y. G. & Carton, X. J. 1994 Multipolar vortices in two-dimensional incompressible flows. *J. Fluid Mech.* **267**, 23–39.

Morgulis, A. B. 2005 High-frequency asymptotic for the forced periodical flows of an inviscid fluid through a given domain. *J. Math. Fluid Mech.* **7**, S94–S109.

Morgulis, A. B. & Vladimirov, V. A. 2008 Dynamics of a solid affected by a pulsating point source of fluid. In *Hamiltonian Dynamics, Vortex Structures, Turbulence*. IUTAM Bookseries, vol. 6, 135–150. Springer.

Morgulis. A. & Yudovich, V. 2002 Arnold's method for asymptotic stability of steady inviscid incompressible flow through a fixed domain with permeable boundary. *Chaos* **12** (2), 356–371.

Orlandi, P. & van Heijst, G. J. F. 1992 Numerical simulations of tripolar vortices in 2D flows. *Fluid. Dyn. Res.* **9**, 1147–1159.

Pedley, T. J. 1980 *The Fluid Mechanics of Large Blood Vessels*. Cambridge University Press.

Riley, N. 2001 Steady streaming. *Annu. Rev. Fluid Mech.* **33**, 43–65.

Rosenbluth, N. M. & Simon, A. 1964 Necessary and sufficient condition for the stability of plane parallel inviscid flow. *Phys. Fluids* **7** (4), 557–558.

Rusak, Z., Wang, S. & Whiting, S. H. 1998 The evolution of a perturbed vortex in a pipe to axisymmetric vortex breakdown. *J. Fluid. Mech.* **366**, 211–237.

Saffman, P. G. 1992 *Vortex Dynamics*. Cambridge University Press.

Shiriaeva, E. V., Vladimirov, V. A. & Zhukov, M. Yu. 2009 Theory of rotating electrohydrodynamic flows in a liquid film. *Phys. Rev.* E **80** (4), 041603.

Shnirelman, A. I. 1993 Lattice theory and flows of ideal incompressible fluid. *Russ. J. Math. Phys.* **1**, 105–113.

Stein, E. M. 1986 *Singular Integrals and Differentiability Properties of Functions*. Princeton Mathematical Series, vol. 30. Princeton University Press.

Stein, E. M. & Weiss, G. 1971 *Introduction to Fourier Analysis on Euclidian Spaces*. Princeton Mathematical Series, vol. 32. Princeton University Press.

Stremler, M. A. & Aref, H. 1999 Motion of three point vortices in a periodic parallelogram. *J. Fluid Mech.* **392**, 101–128.

Stuart, J. T. 1966 Double boundary layers in oscillatory viscous flow. *J. Fluid Mech.* **24**, 673–687.

Stuart, J. T. 1971 Stability problems in fluids. In *Mathematical Problems in Geophysical Science*, Lecture Notes in Applied Math. Series (ed. W. H. Reid), vol. 13, pp. 139–145. American Mathematical Society, Providence, RI.

Swaters, G. E. 2000 *Introduction to Hamiltonian Fluid Dynamics and Stability Theory*. Chapman & Hall/CRC.

Temam, R. & Wang, X. M. 2002 Boundary layers associated with incompressible Navier–Stokes equations: the noncharacteristic boundary case. *J. Differ. Equ.* **179** (2), 647–686.

Vera, E. C. & Rebollo, T. C. 2001 On cubic spline approximations for the vortex patch problem. *Appl. Numer. Math.* **36**, 359–387.

Villat, H. 1930 *Lecons sur la theorie des tourbillons*. Gauthier-Villars.

Vladimirov, V. A. 1978 Stability of a tornado type flow. *Dyn. Continuous Media* **37**, 50–62, Lavrentyev Institute for Hydrodynamics Press, Novosibirsk (in Russian).

Vladimirov, V. A. 1979 Stability of ideal incompressible flows with circular streamlines. *Dyn. Continuous Media* **42**, 103–109. Lavrentyev Institute for Hydrodynamics Press, Novosibirsk (in Russian).

Vladimirov, V. A. 1987 Application of conservation laws for obtaining conditions of stability for steady flows of an ideal fluid. *J. Appl. Mech. Tech. Phys.* **28** (3), 351–358 (translated from Russian).

Vladimirov, V. A. 1988 Stability of the flows with discontinuities in vorticity field. *J. Appl. Mech. Tech. Phys.* **29** (1), 77–83 (translated from Russian).

Vladimirov, V. A. 2005 Vibrodynamics of pendulum and submerged solid. *J. Math. Fluid Mech.* **7**, S397–S412.

Vladimirov, V. A. 2008 Viscous flows in a half space caused by tangential vibrations on its boundary. *Stud. Appl. Math.* **121** (4), 337–367.

Vladimirov, V. A. & Moffatt, H. K. 1995 On general transformations and variational principles for the magnetohydrodynamics of ideal fluids. Part I. Fundamental principles. *J. Fluid Mech.* **283**, 125–139.

Vladimirov, V. A., Moffatt, H. K. & Ilin, K. I. 1996 On general transformations and variational principles for the magnetohydrodynamics of ideal fluids. Part II. Stability criteria, for two-dimensional flow. *J. Fluid Mech.* **329**, 187–205.

Vladimirov, V. A. & Tarasov, V. F. 1980 Formation of a system of vortex filaments in a rotating liquid. *Fluid Dyn.* **15** (1), 34–40 (translated from Russian).

Wang, S. & Rusak, Z. 1997 The dynamics of a swirling flow in a pipe and transition to axisymmetric vortex breakdown. *J. Fluid. Mech.* **340**, 177–223.

Wei, Q. 2004 Bounds on convective heat transport in a rotating porous layer. *Mech. Res. Commun.* **31** (3), 269–276.

Yudovich, V. 1963 Flows of an inviscid incompressible liquid through a given domain. *Sov. Phys. Dokl.* **7**, 789–791 (in Russian).

Yudovich, V. I. 1989 *Linearization Method in Hydrodynamical Stability Theory*. AMS Translations of Mathematical Monographs, vol. 74. American Mathematical Society.

Yudovich, V. I. 1995 Secondary cycle of equilibria in a system with cosymmetry, its creation by bifurcation and impossibility of symmetric treatment of it. *Chaos* **5** (2), 402–411.